UNCLASSIFIED

AD 422945

DEFENSE DOCUMENTATION CENTER

FOR

SCIENTIFIC AND TECHNICAL INFORMATION

CAMERON STATION, ALEXANDRIA, VIRGINIA

UNCLASSIFIED

REPRODUCTION QUALITY NOTICE

This document is the best quality available. The copy furnished to DTIC contained pages that may have the following quality problems:

- Pages smaller or larger than normal.
- Pages with background color or light colored printing.
- Pages with small type or poor printing; and or
- Pages with continuous tone material or color photographs.

Due to various output media available these conditions may or may not cause poor legibility in the microfiche or hardcopy output you receive.

☐ If this block is checked, the copy furnished to DTIC contained pages with color printing, that when reproduced in Black and White, may change detail of the original copy.

Technical Report No. 323

J. L. Allen

The Theory of Array Antennas

(with Emphasis on Radar Applications)

25 July 1963

Lincoln Laboratory

MASSACHUSETTS INSTITUTE OF TECHNOLOGY

MASSACHUSETTS INSTITUTE OF TECHNOLOGY

LINCOLN LABORATORY

THE THEORY OF ARRAY ANTENNAS
(with Emphasis on Radar Applications)

J. L. ALLEN

Group 44

TECHNICAL REPORT NO. 323

25 JULY 1963

ABSTRACT

This report is a thorough summary of the theory of large array antennas, with emphasis on electronic scanning ("phased array") radar applications. It was originally prepared as one of the chapters for a radar text, but is being issued in this form due to the current lack of any comprehensive treatise on arrays that emphasizes the large-number-of-radiators case and electronic scanning effects. The treatment is comprehensive, covering the theory of error-free arrays of isotropic radiators, arrays of real radiators, and the effects of errors on array patterns and properties. The report concludes with a survey of methods of feeding and phasing large arrays. The understanding and presentation of useful, approximate results is emphasized, with all but the most vital or simple derivations referenced to an extensive bibliography.

LEXINGTON MASSACHUSETTS

TABLE OF CONTENTS

LIST OF SYMBOLS

Numbers in parentheses ( ) indicate the defining equation.

$A(\varphi, \Theta)$	Array factor of planar array
$A(\xi)$, $A(0)$	Array factor of linear array
$A(\tau, \mu)$	Array function of planar array
$A(\upsilon)$	Array function of linear array
A	Area of antenna
a_{mn}, a_n	Amplitude taper coefficients of mn^{th} element of planar array, n^{th} element of linear array
a'_n	a_n in the presence of random errors (76)
a(x, y), a(z)	Equivalent continuous illumination: $a_{mn} = a(mD_x, nD_y)$; $a_n = a(nD)$
b	Number of beamwidths; pointing angle from broadside in beamwidths (38)
c	Velocity of light in free space
D	Regular spacing interval between elements of a linear array; projected spacing between planar array elements
D_x	Regular spacing interval between elements in x-direction of planar array
D_y	Regular spacing interval between elements in y-direction of planar array
d_n	Amplitude taper coefficient of difference beam illumination for monopulse operation (29)
d(z)	Equivalent continuous illumination for difference beam
$d(z)$	Density function of a density-tapered array (22)
$\mathcal{E}$	Ratio of effective receiving aperture to array area (84)
$\mathcal{E}_e(\varphi_o, \Theta_o)$	Ratio of element aperture in the direction φ_o, Θ_o to the area allotted the element D_xD_y (85); i.e., the value of the normalized element gain function in the direction φ_o, Θ_o
$F(\varphi, \Theta)$	Far-field pattern of an array [either E- or H-field, commensurate with $f(\varphi, \Theta)$] (62)
$f_{mn}(\varphi, \Theta)$	mn^{th} element pattern (E- or H-field) in its array environment, with all other elements passively terminated in their usual generator impedance
$f(\varphi, \Theta)$	The "element factor," a "typical" (or average) $f_{mn}(\varphi, \Theta)$ (64)
$G(\varphi_o, \Theta_o)$	Gain of array for a pointing angle φ_o, Θ_o (65)
$g(\varphi_o, \Theta_o)$	Gain function of a typical element in its array environment at angles φ_o, Θ_o (65)

$g_i(\varphi, \theta)$	Gain function of a fictional "constant impedance" element (67)
h(t)	Impulse response of antenna (40)
I_{mn}, I_n	Total current that actually flows in the feed of the mn^{th} element of a planar array, n^{th} element of a linear array (68)
$I_n(x)$	Bessel function of first kind of order n of imaginary argument
$J_n(x)$	Bessel function of first kind of order n
j	$\sqrt{-1}$
K	Beamwidth constant relating broadside beamwidth Θ (half-power beamwidth if subscripted by a zero) to antenna dimension L: $\Theta = K/(L/\lambda)$
K_1	Constant relating array gain to beamwidth $G = K_1(4\pi/\Theta_o\Phi_o)$ (84)
k	$2\pi/\lambda$, the free-space wave number (2); Boltzmann's constant (84); beam index number (89)
L	Distance across an antenna
ℓ	Beam index number (91); distance between elements measured in the feed line (88)
M	Number of elements in x-direction of rectangular planar array; composite beam index number (93)
m	x-direction index for planar array elements; beam index number (90); z-direction index for linear array elements
N	Number of elements in y-direction of rectangular planar array; total number of elements in an array; composite beam index number (93)
N_T	Total number of elements required to fill an array grid
N_a	Number of active elements ($a_n \neq 0$) (23)
n	y-direction index for planar array elements; z-direction index for linear array
P	Probability that an element is operating; hence, expected fraction of elements operating (77); point; peak fractional density of density-tapered array
P_{AV}	Total average power of array (84)
$\bar{p}$	Average power of highest-power element of array
R	Radial distance; range; sidelobe ratio
S/N	Signal-to-noise power ratio (84)
s_n	Amplitude taper coefficient of sum beam illumination (28)
s(z)	Equivalent continuous illumination for sum beam
T	Effective temperature referred to antenna (84)

T_s	Time allotted to search a solid angle Ω_s (84)
t	Time
$U(\varphi_o, \theta_o)$, $U(\xi_o)$, $U(\nu_o)$, U	Directivity of array factor or function for pointing angle φ_o, θ_o, etc.
U'	Directivity in the presence of random errors (81)
U_d	Directivity of density-tapered array (26)
$Z_D(\varphi_o, \theta_o)$	Apparent driving point impedance of an element imbedded in a large array, linearly phased (70)
α	Phase increment between elements in x-direction of a planar array, also between elements in z-direction of linear array
β	Phase increment between elements in y-direction of planar array; difference between pointing angle and signal arrival angle in broadside beamwidths
Γ	Voltage reflection coefficient
Δ_n	Random fractional amplitude error of n^{th} element (74)
δ_n	Random phase error of n^{th} element (75)
ϵ	Total rms illumination error (78)
η	Taper efficiency (14); usually amplitude taper efficiency (27)
Θ	Beamwidth (degrees or radians, as indicated)
Θ_o	Half-power beamwidth of beam for broadside pointing angle
Θ_s	"Standard" beamwidth $1/(L/\lambda)$
θ	Colatitude angle of spherical coordinates
θ_o	Beam pointing angle θ
λ	Wavelength in free space
λ_L	Wavelength in a transmission line
μ	Sin θ sin φ
μ_o	$-\beta/kD_y$
ξ	Complement of θ
ξ_o	Beam pointing angle ξ
ρ	Far-field amplitude in presence of errors (79)
$\bar{\rho}$	"No-error" far-field amplitude (79)
σ	Radar cross section (84)
σ_a	rms amplitude error (78)

σ_φ	rms phase error (78)
σ_R	Normalized rms error in far field (80)
τ	Sin Θ cos φ; also time delay
τ_o	$-\alpha/kD_x$
u	Sin ξ
u_o	$-\alpha/kD$
φ	Longitudinal angle of spherical coordinates
φ_o	Beam pointing angle φ
ψ_n	Phase of n^{th} element of a linear array
Ω	Solid angle
Ω_s	Solid angle to be searched (84)
ω	Angular frequency $2\pi f$

PREFACE

This report is a thorough summary of the theory of large array antennas, with emphasis on electronic scanning ("phased array") radar applications. It was originally prepared as one of the chapters for a radar text, but is being issued in this form due to the current lack of any comprehensive treatise on arrays that emphasizes the large-number-of-radiators case and electronic scanning effects. The treatment is comprehensive, covering the theory of error-free arrays of isotropic radiators, arrays of real radiators, and the effects of errors on array patterns and properties. The report concludes with a survey of methods of feeding and phasing large arrays. The understanding and presentation of useful, approximate results is emphasized, with all but the most vital or simple derivations referenced to an extensive bibliography.

The text was originally written in early 1961, and materially revised in 1962 after its presentation as part of an M.I.T. summer lecture series. Only minor revisions and additions, reflecting results deemed to be of unusual significance, have been inserted since that time.

The author would like to acknowledge the contributions of the other members of the Lincoln Laboratory Phased Array Project who, by virtue of the alphabet, became the "et al." of the frequently cited "Allen, et al."

THE THEORY OF ARRAY ANTENNAS
(with Emphasis on Radar Applications)

I. INTRODUCTION

Whenever more than a single radiating source is used in an antenna, the collection of radiators or "elements" is generally referred to as an "array." The use of multiple discrete sources provides more degrees of freedom in antenna design, permitting more control over the radiation pattern of the antenna, than can be conveniently obtained with a continuous source. Further, the circuitry that interconnects the antennas may contain time-varying components, so that a time-varying antenna pattern may be generated. In particular, if the element excitation amplitudes are held fixed and the element phase is varied in a simple manner, the beam from the antenna can be moved rapidly without bulk physical motion of the antenna. Such an antenna is commonly referred to as a "phased array." The concept of such arrays predates World War II; an early example was the MUSA (multiple unit steerable antenna) system.[1†] By the use of low-inertia mechanical phase shifters, rapid scanning can be obtained and, if electronic phase shifters are used, so-called "inertialess scanning" or "electronic scanning" results and beams can be pointed in a random manner over wide angles in times of the order of a microsecond. ESAR,[2] an example of an electronic scanning array radar, is shown in Fig. 1.

The scanning flexibility of phased arrays can be profitably utilized in radar to achieve increased detection and parameter estimation performance[3] for a given power level. In addition, some array configurations may conveniently use multiple power sources, driving separate elements or groups of elements to achieve tremendous peak powers. This high peak power capability can lead to enhanced radar range resolution in confusing multiple target situations and may also provide "burn-through" capability in a jamming situation.

It is the use of array antennas as phased arrays that will be the principal subject of this report, although the treatment will not be completely divorced from other applications of arrays useful in radar.

Since it has been pointed out that the term "array" can encompass everything from a two-horn monopulse feed to an "acreage" of hundreds or thousands of antennas and associated electronic components (Fig. 2), a wide choice of array techniques exists to help the system designer meet his radar problems. Arriving at the best compromise of all the conflicting requirements demands: (a) familiarity with the many configurations that arrays can assume, (b) knowledge of the limitations and complexities of arrays in general and of specific configurations, and (c) knowledge of the requirements that the array configuration places on individual component performance and utilization.

† Sequential numbers are assigned for the References on pp. 93 through 96.

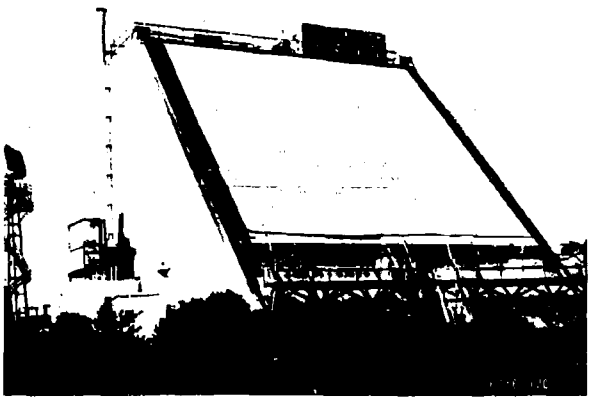

Fig. 1. ESAR – electronic scanning array radar. The sloping face contains approximately eight thousand antennas imbedded in plastic. (Courtesy of the Bendix Corporation.)

Fig. 2. Antenna "farm." 38-Mcps dipole array for Lincoln Laboratory solar radar (El Campo, Texas).

Consequently, in this report, we shall attempt to set forth some of the theoretical and practical considerations involved in the design of radar systems that use arrays. Primary attention will be directed toward arrays of large numbers of elements, and useful approaches to this case will be emphasized.

The first part of the report will deal with the theory of array antennas, since it is the behavior of the array as an antenna that dictates the electronic component requirements peculiar to array radar systems. The performance of the array antenna will be examined in terms of the exciting currents in the elements of the array, with attention to the way in which such currents are physically achieved left to the second part of the report. The emphasis in the theory section will be on obtaining useful and approximate results, with detailed derivations given in the References.

Following the theoretical section, techniques for realizing the drive circuits for arrays will be examined, with some of the merits and potential pitfalls of various techniques briefly discussed. Attention will be directed toward a few selected basic techniques, since space does not allow us to pursue the many interesting variations that are possible.

We shall not include a discussion of the properties of specific types of the various classes of components (i.e., types of radiators, phase shifters, transmitters, receivers, etc.) for array use. The present total experience in this area is both limited and rudimentary, and any discussion would be doomed to early obsolescence. Reference to components will consequently be limited to examining the general requirements that the array configuration dictates.

II. SURVEY OF THE THEORY OF ARRAY ANTENNAS

We shall begin the discussion of array theory with the simplest configuration possible: arrays of isotropic radiators equally spaced along a line (linear in a geometric sense). It will be seen that most of array theory can be framed as an extension of this simple case, and from linear arrays we shall proceed to two- and three-dimensional arrays. The theory of arrays of isotropic radiators will then be extended and modified to apply to arrays of real elements. The survey concludes with an examination of the effects of errors on array performance.

To simplify and contain the material presented, a few restrictions in scope and principal assumptions will be adhered to in this report:

(a) For practical radar purposes, targets of interest will lie in the "far-field" region of the antenna, commonly defined by ranges R satisfying

$$R \geq 2\,\frac{L^2}{\lambda} \quad , \tag{1}$$

where L is the greatest dimension of the antenna, and λ is the operating wavelength. It is this region to which attention will be directed in most of this report. In this region, the antenna pattern is insensitive to range except for a scale factor of $1/R^2$ in power, which will usually be ignored.

(b) The reciprocity theorem[4] will be used extensively to justify analysis of array far fields from either the transmitting or receiving viewpoint, as convenient at the moment, and usually without explicit mention. By virtue of this theorem, the pattern will be the same in either case if no nonreciprocal devices are used. Where such devices are used, one can usually perform pattern analysis neglecting their presence.

(c) For simplicity, interest will be restricted to response of arrays to continuous wave (CW) signals in most sections, with discussion of transient phenomena confined to the last part of Sec. II-A-3.

A. Linear Arrays of Isotropic Radiators

The predominant factor in array pattern behavior is the placement of the individual antenna elements and the manner in which they are interconnected. The characteristics of the individual elements, assuming they are nominally identical, have a secondary effect. Thus a study of arrays of isotropic radiators produces useful results for later extension to more realistic cases without undue complication.

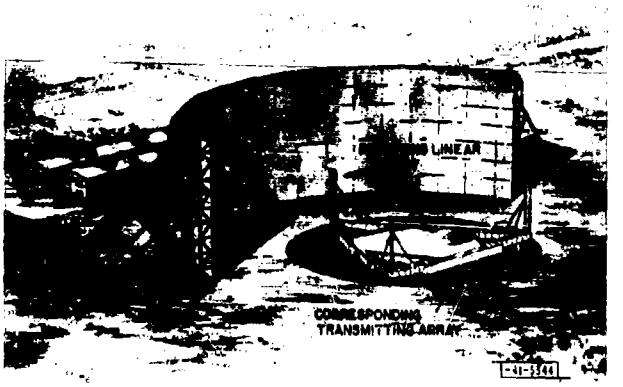

Fig. 3. Radar configuration using linear arrays for both transmission and reception.

The simplest geometric configuration is the linear array which, in addition to serving as a study vehicle for two- and three-dimensional array behavior, often constitutes a useful antenna concept in its own right. For example, Fig. 3 illustrates a radar concept using linear arrays in two different ways. For transmission, arrays of shaped radiators are used to provide the desired coverage in elevation, with high radiated power attained by the use of multiple transmitting tubes driving the transmitting arrays. The receiving arrays, in conjunction with the reflector, form a "stack" of "pencil" beams in elevation. Each beam has the sensitivity associated with a single-beam array.

Furthermore, since linear arrays are easier to fabricate as well as to analyze, two- and three-dimensional arrays are often constructed of interconnected linear arrays. Consequently, this section will be devoted exclusively to a study of linear arrays.

1. Linear Array Factors and Array Functions

Let us consider the elementary array of Fig. 4, consisting of four isotropic radiators, equally spaced a distance D apart. If a plane wave is incident upon the array from a direction making an angle ξ with the x-y plane, the current in the n^{th} element will be of the form†

$$i'_n = E \exp[jnkD \sin \xi] \quad , \tag{2}$$

† The real part of this expression and those that follow is to be implicitly understood.

where E is a complex constant related to the instantaneous amplitude and phase of the wave, and k is the wave number

$$k = \frac{\omega}{c} = \frac{2\pi}{\lambda} \quad ,$$

where c is the velocity of light.

The verbal statement of Eq. (2) is that the current in the n^{th} element leads that in the $n-1$ element by a phase shift due to the difference in time of arrival τ of a reference "point" on the plane wave of

$$\tau = \frac{D}{c} \sin\xi \quad .$$

If we place a "box" behind the n^{th} antenna, as indicated in the figure, with a transfer coefficient for the n^{th} box of

$$\frac{i_n''}{i_n'} = a_n \exp[j\psi_n] \quad ,$$

where a_n and Ψ_n are the real current gain and phase shift of the box, the summing network produces an output

$$A(\xi) = \sum_{n=0}^{3} a_n \exp[j(\psi_n + nkD \sin\xi)] \quad , \tag{3}$$

where we now neglect the constant E of Eq. (2). This relationship gives the response of the array of Fig. 4 to a signal arriving from a direction ξ in terms of the set of a_n's and ψ_n's. A similar analysis would show that the same expression, except for constants and factors of 1/R, gives the far-field radiated pattern at an angle ξ when the array transmits.

Consequently, for either transmission or reception, we can extend the above reasoning to write the angular variation of the far field of any N-element linear array of the geometry of Fig. 5 as

$$A(\xi) = \sum_{n=0}^{N-1} i_n \exp[jnkD \sin\xi] \quad , \tag{4a}$$

where the complex current

$$i_n = a_n \exp[j\psi_n] \tag{4b}$$

is the current flowing into the n^{th} antenna (the i_n' of Fig. 4) when the array is transmitting, and the current flowing into the n^{th} input of the adder circuit (i_n'' of Fig. 4) when receiving. Note that $A(\xi)$ does not depend on the angle φ, since we have assumed that the radiators are isotropic.

The expression of Eq. (4) is a basic relationship of array theory and is called the "array factor."† The set of coefficients a_n are usually called the array amplitude "taper," while the ψ_n's are the phase taper. The combined results (the i_n's) are often referred to as the array "illumination."

† This terminology is by no means universal. Schelkunoff (Ref. 5) and Silver (Ref. 4, p. 260) call $A(\xi)$ the "space factor" and reserve the term "array factor" for the power pattern, $|A(\xi)|^2$. However, precedence exists for our choice [see King (Ref. 6, pp. 579-580)].

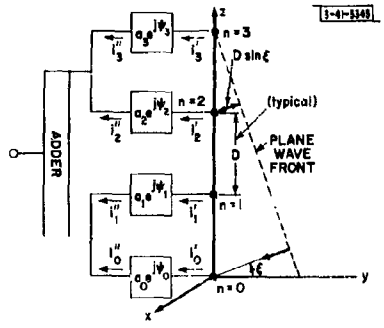

Fig. 4. Basic linear array configuration.

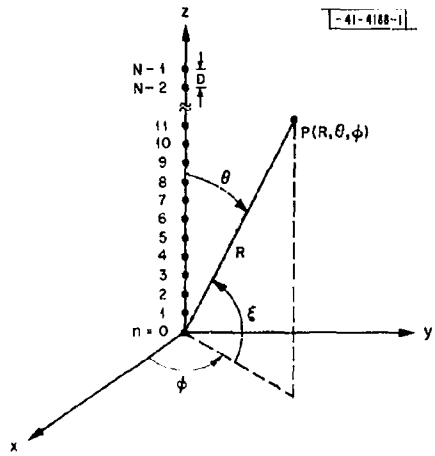

Fig. 5. N-element linear array geometry.

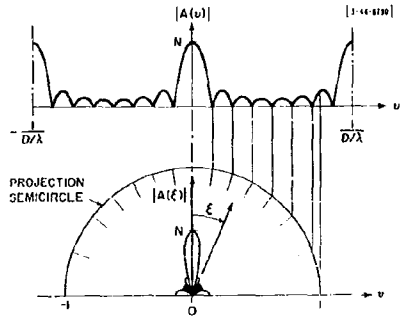

Fig. 6. Array function $A(\upsilon)$ and array factor $A(\xi)$ magnitudes for 8-element uniformly illuminated array $D/\lambda = 0.8$.

It is frequently more convenient to deal with the related function

$$A(\upsilon) = \sum_{n=0}^{N-1} i_n \exp[jnkD\upsilon] \tag{5}$$

which we shall denote an "array function" in contrast to the array factor $A(\xi)$. It is obvious that $A(\upsilon)$ and $A(\xi)$ are related by a one-to-one mapping in the region $|\upsilon| \leq 1$, by the identification $\upsilon = \sin\xi$. It is also apparent that $A(\upsilon)$ is a periodic function of υ of period $2\pi/kD = 1/(D/\lambda)$, and that Eq. (5) is of the form of a Fourier series representation, a fact of practical utility and an aid in visualization.

For example, if we take $i_n = 1$, all n, it is easily shown that,† for an N-element array,

$$A(\upsilon) = \frac{\sin \pi \frac{ND}{\lambda} \upsilon}{\sin \pi \frac{D}{\lambda} \upsilon} \exp\left[j\pi(N-1) \frac{D}{\lambda} \upsilon\right] \quad . \tag{6}$$

This special case is termed "uniform" illumination. A plot of the amplitude of $A(\upsilon)$ for an 8-element array is shown in Fig. 6, illustrating the general structure of the array function. There are several "major lobes" shown of amplitude N. The one at broadside ($\upsilon = 0$) is generally referred to as the "principal lobe" or main beam, and the others as "grating lobes" from the corresponding phenomena with optical gratings.

Figure 6 also illustrates a method for constructing the array factor from the array function. A semicircle of unit radius (corresponding to $\upsilon = \max|\sin\xi| = 1$) is centered under the array function and the array factor plotted by mapping onto the semicircle as indicated.‡ The region $|\upsilon| \leq 1$ that corresponds to real angles ξ is often referred to as the region of the array function "visible space."

2. Linear Array Patterns

A question that Eq. (5) raises is how to best choose the i_n's to synthesize a "desirable" far-field pattern.

The only explicit properties of the antenna that appear in the radar equation are the interrelated factors of effective aperture and gain. However, other system considerations, such as resolution requirements and coverage requirements, usually dictate further constraints on the pattern. Generally speaking, the system requirements tend to dictate the selection of beam "structure" from among two classes: (a) narrow, directive beams (so-called "pencil" beams) in which desirable compromises between high gain, low sidelobes and a narrow main beam are paramount, but in which the exact shape of the pattern is unspecified, or (b) beams of a specified shape in the main beam region with all other considerations secondary.

From Eq. (5) we appear to have many degrees of freedom at our disposal for synthesis. However, a closer examination indicates that some are of limited utility.

† See, for example, Kraus (Ref. 7, Ch. 4, Sec. 6).

‡ For investigation of spacing effects, it is often more useful to plot $A(D/\lambda\upsilon)$, in which case only the semicircle radius varies with D/λ. The resulting array functions are often called "universal array functions" (see Ref. 7, pp. 521-534).

First, we have the number of elements and their placement. The choice of the number of antenna elements will be seen to depend ultimately upon beamwidth and antenna gain considerations. There is no obvious reason why we should restrict the elements to equal spacing, as Eq. (5) indicates, and the use of unequal spacings has been investigated.[8,9] It can be shown that while such techniques can suppress grating lobes by rendering the array factor nonperiodic, they do so only at the expense of a markedly higher sidelobe level in the regions of the pattern removed from the main beam.[10] Such arrays also encounter practical difficulties when real antennas are used[11] (see also, Ref. 12, Part 3, Ch. I). Therefore, we shall confine our attention to arrays of equally spaced elements.

Second, we can vary the phase of the elements of the array. To assess the effects of phase tapering, we can expand any phase taper in a Taylor series about the array center as

$$\psi_n = \alpha_o + (n - n_o)\,\alpha_1 + (n - n_o)^2\,\alpha_2 + (n - n_o)^3\,\alpha_3 + \ldots$$

and write

$$A(v) = \sum_{n=o}^{N-1}{}' a_n \exp\{j[\alpha_o + (n - n_o)\,\alpha_1 + (n - n_o)^2\,\alpha_2 + (n - n_o)^3\,\alpha_3 \ldots + nkDv]\} \quad .$$

If we set

$$\begin{aligned} \alpha_o &= n_o\alpha_1 \\ \alpha_1 &= -kDv_o \\ \alpha_2 &= \alpha_3 = \ldots = 0 \quad , \end{aligned} \tag{7}$$

we have

$$A(v) = \sum_{n=o}^{N-1}{}' a_n \exp[jnkD(v - v_o)] \quad , \tag{8}$$

indicating that linear phase (constant phase differential) across the array "steers" the beam to a new pointing direction v_o given by α_1 of Eq. (7). Although we shall elaborate on beam steering and its effect on the array factor at length in Sec. II-A-3, for the array function it represents only a change of variable and will therefore not be explicitly considered in the remainder of this section.

The effects of the quadratic and cubic phase terms α_2 and α_3 have been investigated (Ref. 4, Sec. 6.7) and generally found deleterious for directive beams. Although this writer is not aware of explicit studies of higher-order phase variation, it does seem reasonable to conclude that it has little to offer for generating directive beams, although it is used as a technique for beam shaping.

Thus the number of variables we shall concentrate most of our attention on have been reduced to the number of elements N, their amplitudes a_n, and to a lesser extent, their phases. We shall see that the pattern can be shaped by using either a range of a_n's (amplitude tapering) or the binary choice $a_n = 0$ or 1 (density tapering). Before explicitly considering these choices (the so-called "synthesis" problem) further, let us digress to extend our base of attack.

Use of Line Source Techniques for Linear Arrays:– Note from Eq. (6) that the pattern of the uniformly illuminated array is, for large N and small v, of the form (ignoring the phase term)

$$A(v) \approx \frac{\sin(\pi L/\lambda)v}{(\pi L/\lambda)v} \quad , \quad L = ND \quad .$$

This behavior is the same as we should expect from a continuous line source of length L, illuminated by an equiphase, constant amplitude, linear current density, as derived from the relationship for continuous distributions

$$A_c(v) = \int i(z) \exp[jkzv]\, dz \quad . \tag{9}$$

If we can justify extending this one example into a general conclusion that the patterns of arrays (discrete radiators) and continuous sources are similar, many of the results of the extensive studies of continuous antennas can be applied to arrays with confidence. Thus the question of importance is the degree of similarity between a continuous antenna with illumination i(z) and an "equivalent array" with illumination $i_n = i(nD)$.

It is apparent that certain nonnegligible differences, particularly the possibility of grating lobes, exist between the array function and the corresponding line source function. However, we shall see in Sec. II-D-1 that the sidelobe structure in regions where the sidelobes are very low is mainly dictated by errors, not design, and we need not be particularly concerned with accurate predictions of the detailed sidelobe structure in this region. Consequently, the relevant region of importance for a similarity argument is that of the principal lobes and the high sidelobes near the principal lobes. The shape of the array function in grating lobe regions is identical to its shape in the main-lobe region. The locations of the grating lobes must, however, be determined from the discrete model.

Although it is difficult to formulate a useful, general argument regarding similarity, studies[13,14] show that generally good results are obtained using Eq. (9) to predict the shape of directive beams for arrays of 10 or more elements down to sidelobe levels of 20 db, and down to 40 db for a 16-element array. Since these numbers of elements are modest for long-range radar applications, it is concluded that Eq. (9) gives a satisfactory representation of the shape of the array factor for most applications.

Thus, for large arrays, we shall tacitly assume that either Eq. (5) or (9) is a valid representation of $A(v)$ in the region around any principal lobes, permitting the use of summation or integral representations for the array functions as convenient.

Array Pattern Directivity and Beamwidth:– The far-field pattern properties of most frequent concern to the array designer are the array gain, sidelobe levels, and beamwidth. Unfortunately, the concept of gain involves the impedance properties of real elements and must be deferred to Sec. II-C-2. The analogous parameter determined only by the array pattern is the directivity† $U(\xi)$, defined as the ratio of the power density per unit solid angle at the angle ξ to the average power radiated per unit solid angle over all space. We shall concern ourselves exclusively with directivity relative to the peak of the main lobe located at an angle ξ_o. From the

† The directivity is an upper bound on gain; the two are equal for matched, lossless antennas.

above definition, it follows that

$$U(\xi_o) = \frac{|A(\xi_o)|^2}{\frac{1}{4\pi}\int_{\substack{\text{all}\\ \text{space}}} |A(\xi)|^2 \, d\Omega} \quad , \tag{10}$$

where $d\Omega$ is the differential solid angle $d\Omega = \sin\Theta \, d\Theta \, d\varphi$, or in ξ notation, $d\Omega = \cos\xi \, d\xi \, d\varphi$. For isotropic radiators, there is no φ-dependence, and since $d\nu = \cos\xi \, d\xi$, we can write the directivity in terms of the array function as

$$U(\nu_o) = \frac{2\,|A(\nu_o)|^2}{\int_{-1}^{1} |A(\nu)|^2 \, d\nu} \quad . \tag{11}$$

Using Eq. (8), and integrating, gives

$$U(\nu_o) = \frac{\left(\sum_{n=o}^{N-1} a_n\right)^2}{\sum_{n=o}^{N-1}\sum_{n=o}^{N-1} a_m a_n \frac{\sin 2\pi(D/\lambda)(n-m)}{2\pi(D/\lambda)(n-m)}} \quad . \tag{12}$$

The denominator has the unhappy effect of clouding the picture. Only when $2D/\lambda$ is an integral number is the result easy:

$$U(\nu_o) = \frac{(\Sigma\, a_n)^2}{\Sigma\,(a_n)^2} \quad .$$

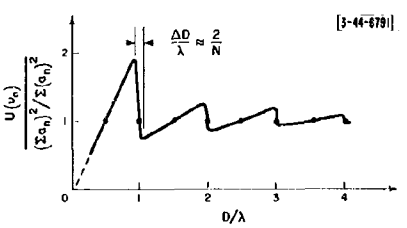

Fig. 7. Variation of directivity $U(\nu_o)$ of a linear array of isotropic elements with element spacing D/λ.

However, detailed consideration of the integral of Eq. (11) will indicate that the behavior of the denominator is such as to make the directivity vary with element spacing approximately† as indicated in Fig. 7, for beam shapes that concentrate most of the power in the main lobe. For spacings less than λ, for which only one principal lobe exists in visible space, we can write the simple result

$$U(\nu_o) \approx \frac{2D}{\lambda} \frac{(\Sigma\, a_n)^2}{\Sigma\,(a_n)^2} \quad . \tag{13}$$

†H. E. King (Ref. 15) examines in detail the curve in the interval $0 \leq D/\lambda \leq 1.2$ for uniformly illuminated arrays of various N.

By the Schwarz inequality,[16] we can write

$$\frac{(\Sigma a_n)^2}{\Sigma (a_n)^2} = \eta N \quad , \tag{14}$$

where $\eta \leqslant 1$. We shall call η the taper efficiency or illumination efficiency of the array, and note that for a given N and D/λ, η alone determines the directivity

$$U(v_o) \approx \frac{2\eta ND}{\lambda} \quad . \tag{15}$$

The maximum value of unity for η is achieved by the uniform illumination; its value for some other illuminations is discussed in the next topic.

The beamwidth of an array depends upon the array electrical length and the amplitude taper used. This dependence can be conveniently expressed by a constant K defined by the equation

$$\Theta = \frac{K}{L/\lambda} \quad , \tag{16}$$

where Θ denotes the beamwidth and L the array length. We shall be primarily concerned with the half-power beamwidth, which we shall denote Θ_o. The corresponding beamwidth coefficient will be denoted K_o. For example, for uniform illumination and large N, $K_o \approx 50.9°$; its value for some other tapers is also discussed below.

Directive Pattern Synthesis by Amplitude Tapering:– Let us now examine some particular techniques for achieving desirable directive beams from linear arrays by amplitude tapering. There are three principal classes of amplitude tapers which will be outlined and compared: (a) powers of cosine on a pedestal, (b) the "modified $\sin \pi u/\pi u$" of Taylor,† and (c) the Dolph tapers.

The "powers of cosine" are the earliest class of tapers, probably because they are functions that are amenable to fairly easy analysis and have useful properties. The continuous taper is of the form

$$a(z) = h + (1 - h) \cos^m \frac{\pi z}{ND} \quad , \quad |z| < \frac{ND}{2}$$

for an array centered on the z-axis. The parameter h is the normalized pedestal height (Figs. 8 and 9). The most frequently used families of this class are the cosine (m = 1) and cosine-squared (m = 2). The lowest first sidelobes achievable‡ with the cosine are 23 db, when h = 0, yielding an illumination efficiency of 0.81, and a half-power beamwidth coefficient of 69°.

The cosine-squared taper gives generally superior performance to the cosine. For small pedestals, the highest sidelobe of this taper may not be the first, but is one of those close to the main beam. After the highest lobe, the sidelobes decay monotonically.

† In addition, there is another family of line source (continuous) tapers associated with Taylor (Ref. 17) which represents approximations to the Dolph taper, and will not be discussed for that reason.

‡ Recall that the assumption of large N is basic to adapting continuous antenna tapers to arrays; the numbers given are accurate only for such a case.

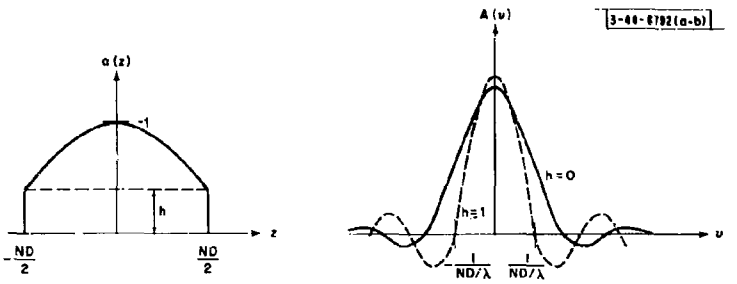

(a) Envelope of cosine-on-a-pedestal amplitude taper.

(b) Corresponding array function for h = 0 (no pedestal) and h = 1 (uniform taper).

Fig. 8. Cosine illumination and array function.

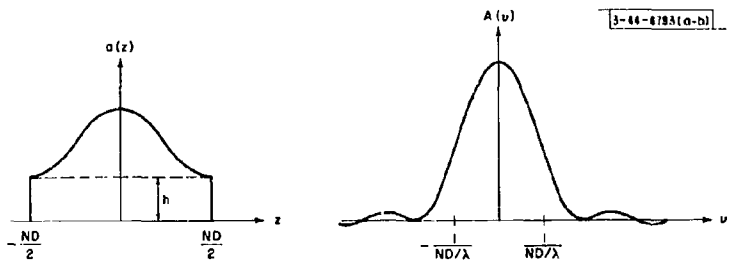

(a) Envelope of cosine-squared-on-a-pedestal amplitude taper.

(b) Corresponding array function for h = 0 (no pedestal).

Fig. 9. Cosine-squared illumination and array function.

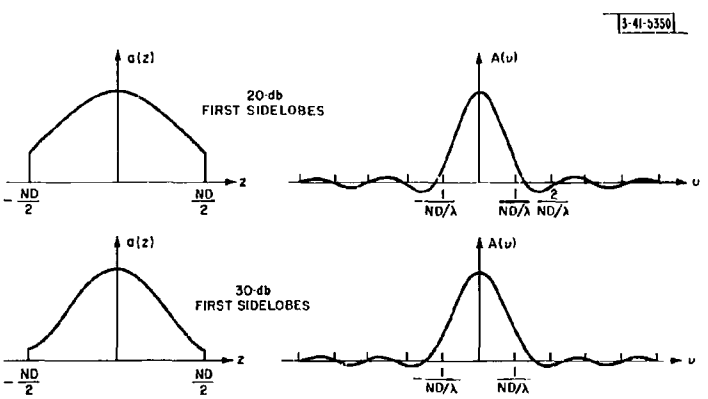

Fig. 10. Typical illumination and array functions for Taylor taper. (Reprinted, with permission, from Taylor, Ref. 18).

The modified $\sin \pi u / \pi u$ taper of Taylor[18] produces monotonically decreasing sidelobes. The amplitude envelope is of the form (for an array centered on the z-axis)

$$a(z) = J_0\left[j\pi B\sqrt{1 - (\frac{2z}{ND})^2}\right] \quad , \quad |z| \leq \frac{ND}{2} \quad , \tag{17}$$

where $j = \sqrt{-1}$, $J_0(x)$ is the zero-order Bessel function of the first kind, and B is the parameter fixing the ratio R of the main-beam amplitude to the amplitude of the first sidelobe by

$$R = 4.60333 \ \frac{\sinh \pi B}{\pi B} \quad . \tag{18}$$

Figure 10 shows typical amplitude tapers and array functions.

The taper of Dolph[7,19] is "optimum" in the sense that it yields the narrowest beamwidth for a given sidelobe ratio, and vice versa. It is not necessarily optimum in any other sense (e.g., efficiency vs highest sidelobe level), as will become evident below. This taper is derived specifically for arrays and makes use of the properties of Tchebycheff polynomials to generate the a_n's and is consequently often referred to by the joint name Dolph-Tchebycheff. The computation of desired illuminations, which must be carried out independently for each array size and sidelobe level, is extremely tedious. Fortunately, both tables[20] and asymptotic descriptions[21,22] exist.

A striking property of this taper is that it yields an array function with equal amplitude sidelobes, as shown in Fig. 11. This fact, and its effect on the amplitude taper, leads to some secondary considerations regarding use of this taper. Since the sidelobes do not decay, the percentage of power in the main lobe varies with N for a given sidelobe level. Hansen[23] has shown that for this reason, in order to maintain high efficiency, large Dolph-tapered arrays must use low sidelobe tapers.

The amplitude taper producing the array function of Fig. 11(a) is shown in Fig. 11(b). The "peaked" edge drives are typical of a large array and high sidelobe design (a 30-db sidelobe taper would have edge drives approximately the same as neighboring elements). Such "peaked" distributions are prone to error effects that arise in edge elements of arrays using real radiators (Sec. II-C-1).

The properties of several tapers, including Dolph tapers for both 10- and 40-element arrays, are compared in Fig. 12. The pedestal heights of the cosine-squared tapers are indicated by the values of h given.

Directive Pattern Synthesis by Density Tapering:– For some array applications, it is desirable to operate all driven elements of the array at the same amplitude. This is particularly true of transmitting arrays in which a separate transmitter is used with each antenna of the array, since it is generally inefficient to operate identical transmitters at different output levels and uneconomical to use more distinct types of transmitters than absolutely necessary.

A technique useful in such cases is "density tapering,"† in which the beam of an array is shaped by the judicious deletion of the drive from certain elements of a regularly spaced array, with the undriven elements left in place and passively terminated in an impedance equal to the source impedance of the driven elements (terminating the undriven elements is necessary to

† The inventor of this technique is unknown to this writer, but the bulk of the early work was done at the Bendix Corporation (see Refs. 2 and 24).

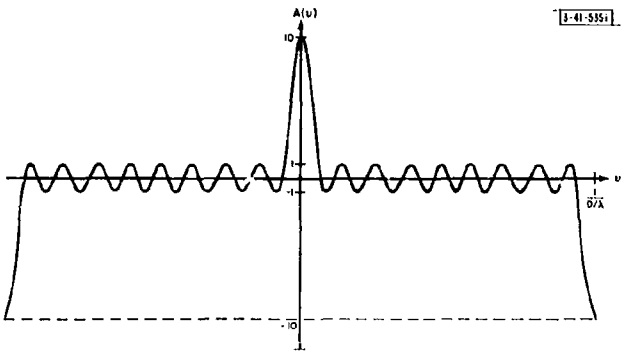

(a) Array function.

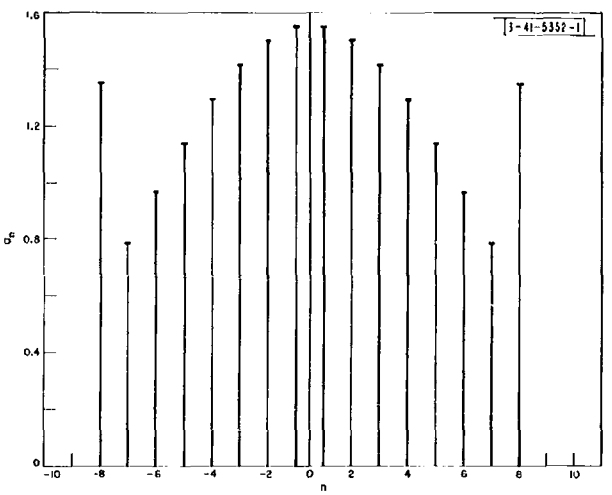

(b) Illumination coefficients.

Fig. 11. Illumination and array function for 20-db Dolph taper for 16-element array.

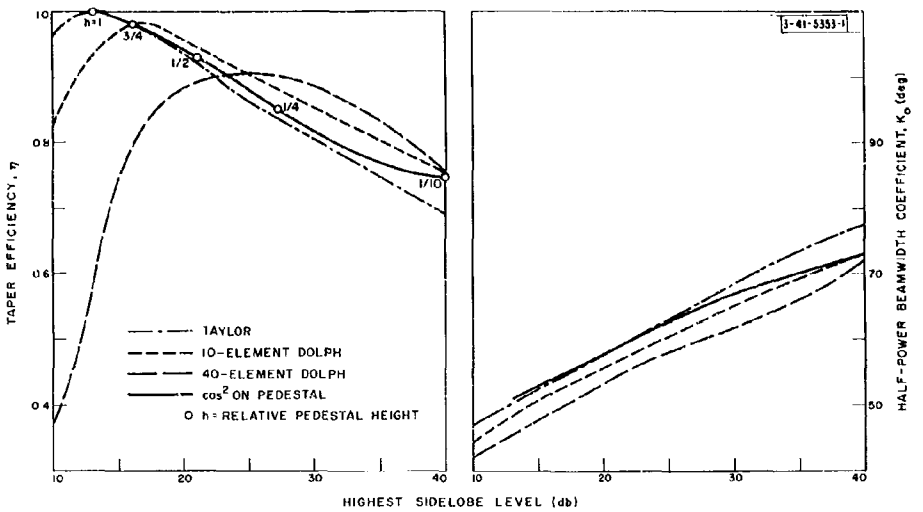

Fig. 12. Comparison of taper efficiency and beamwidth coefficient of linear array amplitude tapers vs highest sidelobe level.

regularize the environment that all driven antennas "see" to prevent pattern deterioration due to mutual coupling effects, as more fully explained in Sec. II-C-1).

The fact that varying the density of active (driven) elements will affect the array pattern should not be unexpected. It will be recalled that the far field of an antenna is related to the Fourier transform of the antenna current density. Further, we have seen that similar patterns are obtained from continuous sources and from arrays with "equivalent" amplitude tapers [Eq. (9) and following], at least over a period of the array function, for arrays of large numbers of elements. The concept of "density tapering" can therefore be viewed as an extension of the change-over from a continuous to a discrete antenna in which we not only discretely localize the currents in space, but also discretely choose the element currents from the binary possibilities of zero or, for example, unity.

Density tapering, however, does not produce exactly the same results as amplitude tapering. To see why, a convenient approach is to presume that some amplitude taper represented by a set of N_T nonzero taper coefficients will produce a satisfactory array function. We now wish to approximate† the same array function with an array of N_T total elements using a density taper.

We proceed to choose the density-tapered amplitude coefficients to be zero or one such that over any interval of several elements of the array, the total current in that interval is the same in the density-tapered array as it is in the amplitude-tapered array. Since the total current in any interval of the density-tapered array is constrained to be an integral number of units, we cannot exactly "match" the two array current densities. In fact, if no precise criterion for a "good fit" can be stated, a large number of density tapers can be generated as an

† It would be scientifically satisfying to define approximate precisely by some "best fit" criterion such as least mean square, etc. Unfortunately a criterion which is both physically meaningful and mathematically tractable eludes this writer. A criterion which is not at the outset very tractable (uniform sidelobe amplitude) is investigated later.

approximation to a single amplitude taper. As the number of samples becomes large, we should expect that if we pick a particular element -- e.g., the n^{th} -- and note the fraction of density tapers that have element n driven, this fraction will tend to vary with n in the same manner as the taper coefficient associated with the amplitude and tapered array. That is, a plot of the average density of all the density-tapered samples (the "ensemble average") assumes the same shape as the amplitude taper. However, any one sample varies in a more-or-less random manner from this average.

If we now examine the array functions generated by all these approximations, we find that, at any particular angle υ, the ensemble average of all density-tapered array functions tends toward the array function associated with the amplitude-tapered array. However, particularly in the low sidelobe region of the pattern, any one of the density-tapered arrays may have an array function value at a particular angle that is considerably different from the average. In fact, it is found from a probabilistic analysis (Ref. 10, Part 3, Ch. III, Sec. G) that the normalized† array function amplitude $|A(\upsilon)|$ is distributed in a modified Rayleigh distribution‡ (Sec. II-D-1) characterized by the parameter σ_R

$$\sigma_R^2 = \frac{1}{2\eta N_T}\left(\frac{\eta N_T}{N_a} - 1\right) \quad , \tag{19}$$

where N_T is the total number of antenna elements, η is the taper efficiency of the amplitude-tapered array whose performance it is desired to duplicate, and N_a is the number of active elements in the density-tapered array. Note that $2\eta N_T$ is of the order of the amplitude-tapered array directivity; hence, for large arrays, $\sigma_R << 1$.

The significance of σ_R is that in regions where the magnitude of the normalized array function of the amplitude-tapered array $A_a(\upsilon)$ satisfies

$$|A_a(\upsilon)|^2 >> \sigma_R^2 \quad , \tag{20}$$

the density-tapered array pattern and the equivalent amplitude-tapered array pattern will be essentially identical. [Note that the above inequality is satisfied in the main-lobe region of $A(\upsilon)$ and perhaps in the near-in sidelobe region.] However, in most regions [the qualification "most" is explained following Eq. (25)] where the amplitude-tapered array function is much less than the σ_R of Eq. (19),§ the quantization effects dominate the pattern and the ensemble average sidelobe level magnitude can be shown to be

$$\overline{|A(\upsilon)|^2} = 10\log_{10} 2\sigma_R^2 \quad , \tag{21}$$

and thus is primarily dependent only upon the number of elements in the array. This dependence can be better appreciated by quantitatively examining the values of the ratio $N_a/\eta N_T$ appearing in Eq. (19) which are to be expected in practical cases.

First, just as Fig. 12 indicates that achievement of a specified highest sidelobe level in an amplitude taper places an upper bound on the illumination efficiency η, the achievement of the

---

† Such that $|A(0)| = 1$.

‡ The justification for the distribution, as explained in Ref. 10, is that originally put forth by Ruze (Ref. 25).

§ Recall that, in the far-out regions of the array function, $|A_a(\upsilon)|^2$ is of the order of $1/N_T^2$.

same result in a density-tapered array places an upper bound on how "full" the array can be (the ratio of N_a/N_T). Put another way, the desired close-in sidelobe structure defines the "shape" of the plot of the active element density. Bearing in mind that low sidelobe patterns result from tapers that have maximum illumination at the array center and less at the array edges, we can do no more than have <u>all</u> elements in the center of the array active in a density taper.† The shape of the density then determines the maximum ratio of active to total elements, which we shall denote $N_{a_{max}}/N_T$. This maximum is of fundamental importance, since it is the condition giving (as will be affirmed quantitatively below) the maximum gain and lowest "far-out" sidelobe level for a particular density shape. To quantitatively determine likely values of $N_{a_{max}}/N_T$, note that Fig. 12 indicates that, for linear arrays, the cosine squared on a pedestal yields performance roughly equivalent to the best of the tapers examined, over sidelobe levels of interest. We shall therefore examine the variation of $N_{a_{max}}/N_T$ to be expected for a cosine-squared <u>density</u> taper as a function of highest sidelobe level (close-in, in the density-tapered case, since we may lose control farther out in the pattern – a possibility dwelled upon below).

The appropriate density of active elements can be represented by a function $d(z)$ related to the amplitude taper function a(z) by

$$d(z) = P\,\frac{a(z)}{a(0)} \quad , \tag{22}$$

where the a(0) normalizes the amplitude taper function, and P is the density of active elements at the array center. We can interpret $d(nD)$ as the probability that the n^{th} element is active. Consequently, the ratio of active to total elements is given by

$$\frac{N_a}{N_T} = \frac{\int_{-N_TD/2}^{N_TD/2} d(z)\,dz}{\int_{-N_TD/2}^{N_TD/2} dz} \tag{23a}$$

or, equivalently,

$$\frac{N_a}{N_T} = \frac{P\int_{-N_TD/2}^{N_TD/2} a(z)\,dz}{\int_{-N_TD/2}^{N_TD/2} a(0)\,dz} \quad . \tag{23b}$$

A plot of the resulting values of $N_{a_{max}}/N_T$ as well as the factor $N_{a_{max}}/\eta N_T$ of Eq. (19), for this taper, is shown in Fig. 13 as a function of highest close-in sidelobe level. The values for this taper would appear to be representative of the ratios to be expected with other efficient linear array tapers as well.

In order to determine the quantitative effects of density tapering on far-out sidelobe levels, we note that the quantity in parentheses of Eq. (19) appears from the data of Fig. 13 to be numerically about 0.3 for low sidelobe tapers using the maximum number of active elements. Thus

† We may, of course, "scale" the density so that the center density is representable by some fraction $P < 1$ and achieve a savings in the ratio of active to total elements for economic reasons. By such a technique, we can, for example, realize the beamwidth associated with a "full" array (dependent only upon array size) with only a fraction of the number of active elements in a full array, but at a sacrifice in directivity and far-out sidelobe levels [see Eqs. (21) and (25)].

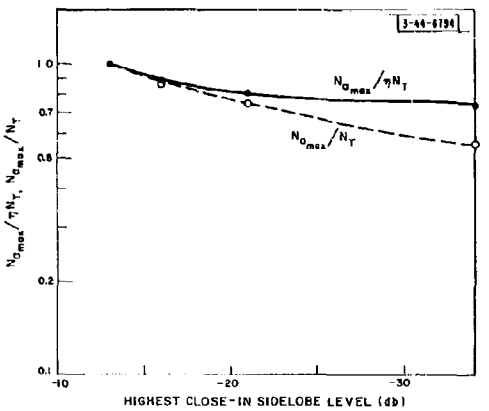

Fig. 13. Maximum value of $N_a/\eta N_T$ and N_a/N_T for a specified highest sidelobe ratio for a cosine-squared-on-a-pedestal linear array taper.

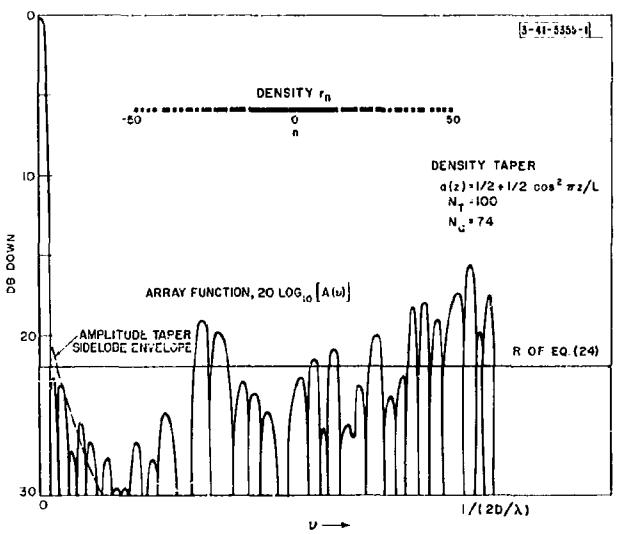

Fig. 14. Linear array with cosine-squared density taper.

Eq. (19) indicates that the average far-out sidelobe level of a density-tapered array can only be suppressed by a factor of the order of $1/N$. Recalling that even a uniform amplitude taper produces a far-out sidelobe level of the order of $1/N^2$, it is apparent that one must surrender control of far-out sidelobes when using even modest density tapering. Probably the most that can be asked from a systems viewpoint is a fairly uniform level of the far-out sidelobes. Equation (19) and Fig. 13 indicate that if we achieve such uniformity, assuming the sidelobes to be of such a shape that their peaks are 3 db above their average power level (so that the peaks are numerically equal to $4\sigma_R^2$), the sidelobe peaks will be down from the main lobe by the ratio

$$R_{db} \approx 10 \log_{10} \frac{0.6}{\eta N_T} \tag{24}$$

for dense ($P = 1$) tapers. If the density-tapering technique is used to "thin out" the array ($P \ll 1$), we have $N_a \ll \eta N_T$, and Eq. (19) indicates that, for this case,

$$R_{db} \approx 10 \log_{10} \frac{2}{N_a} \quad , \tag{25}$$

making obvious the dependence of the sidelobe level on the number of active elements used.

An apparent characteristic of density tapering which the referenced statistical analysis does not predict is the tendency of the density-tapered antenna to reproduce the close-in sidelobe structure of the amplitude-tapered antenna, even when these sidelobes may be considerably below the value of R of Eq (24) or (25). For such cases, by a conservation of power argument, we should expect that the use of an amplitude taper which produces sidelobes below this value close to the main lobe would result in sidelobes above the value of Eq. (24) or (25) farther out in the pattern. An example illustrating this possibility is shown in Fig. 14 which indicates the array function of an array of $N_T = 100$, using a cosine-squared ($h = 1/2$) density taper which, as an amplitude taper, would produce the sidelobe envelope indicated by the dashed lines. The density taper is seen to follow the amplitude taper pattern well near the main lobe, but "pops up" badly farther out. By contrast, Fig. 15 shows the result of an attempt at a 20-db sidelobe density taper, using Taylor's[17] approximation to the Dolph taper, which normally produces several equal amplitude sidelobe levels before the sidelobes begin to decay. The tendency toward a more uniform sidelobe level is apparent.

The statistical approach[10] can also be used to show that the directivity of a density-tapered array U_d is related to the directivity of an equally spaced, equivalently amplitude-tapered array U by

$$\frac{U_d}{U} = \frac{N_a}{\eta N_T} \quad . \tag{26}$$

Note from this result and Eq. (15) that for arrays which are either amplitude tapered only ($N_a = N_T$) or density tapered only ($\eta = 1$, if we confine η to an amplitude taper efficiency), we can write the directivity as

$$U(v_o) = 2\eta N_a \frac{D}{\lambda} \quad . \tag{27}$$

From Eqs. (19) and (26), it is apparent that the density-tapered array directivity will be less than that of an array using the equivalent amplitude taper for equal values of N_T. From Fig. 13,

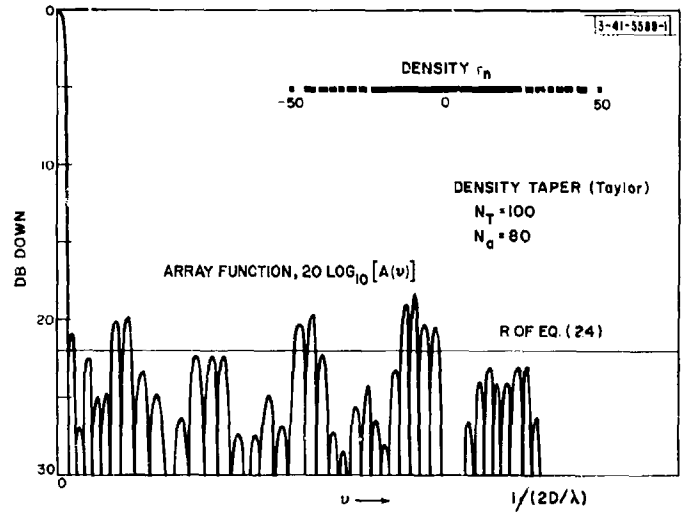

Fig. 15. Linear array with 20-db Taylor density taper.

for P = 1 and low sidelobe tapers, the difference is seen to be about 1 db. However, while density tapering leads to decreased directivity for arrays of equal N_T, it is apparent from Eq. (27) that this tapering produces greater directivity for arrays of equal N_a, and in some cases the cost of an array may be more nearly dependent upon N_a rather than N_T.

In summary, density tapering is a useful technique for beam shaping in arrays in which amplitude tapering is inconvenient. It can also be used to generate narrow beams with fewer active elements than an amplitude-tapered array, at a sacrifice in directivity and far-out sidelobe levels.

Unfortunately, although we have put forward its virtues and vices at some length, little has been said about the mechanics of synthesis of density tapers. With the present state of knowledge, any density taper eventually degenerates into a "cut and try" process. However, a technique which has been found useful for getting started is to match the integrated densities of the density-tapered array and the amplitude-tapered array

$$\left.\begin{aligned} g(z) &= \int_o^{z_o} P\,\frac{a(z)}{a(o)}\,dz \\ g(n) &= D\sum_{n=o}^{n} d_n \end{aligned}\right\} \quad z_o = nD$$

as functions of z_o, where $d_n = d(nD)$ is the density function desired as given by Eq. (22).

Synthesis of Patterns of Prescribed Shape:– Many techniques exist for generating shaped beams [c.g., cosecant-squared power pattern for surveillance radars (Ref. 4, Ch. 13)], and even a brief description of each would be quite lengthy in total. Therefore, we shall enumerate only the various approaches and refer the interested reader to the literature.

Since the array illumination and array function are a Fourier transform pair, this fact can be used to find an illumination to approximate a desired array function.[26] Woodward[27] gives a synthesis technique which resembles the results of the temporal sampling theorem of network theory (reconstruction of functions by orthogonal, weighted sets of $\sin x/x$ functions) and is a useful analytical tool, as well as a synthesis method (use will be made of his result in Sec. III-B-2). The principle of stationary phase can also be used to synthesize,[28,29] using both element amplitude and phase as parameters. Ksienski[30] has described a method for producing "flat-topped" beams, and has outlined another technique which is basically the same as the "scanning function" technique described by Ruze (Ref. 25, Secs. III-D and III-E).

Comparisons of the relative merits of the various synthesis techniques can be found in the references, usually in terms of their ability to generate one or more of the common beam shapes (e.g., cosecant squared or rectangular). Although none of the references explicitly makes use of density tapering, the previously established correspondence between amplitude and density can be utilized for beam shaping in conjunction with many of the above techniques.

Synthesis of Monopulse Patterns:– The more common methods of obtaining the so-called "sum" and "difference" patterns for monopulse† (simultaneous lobing) angular determination are:

(1) Adding and subtracting the output of the two halves of an array, as indicated in Fig. 16.

(2) Adding and subtracting two adjacent beams from an array capable of forming simultaneous beams (see Figs. 70, 72, and 73 in Sec. III-B-2).

For (1), if the amplitude taper chosen for the sum beam is the set a_n, the difference pattern illumination d_n will be related to the a_n's by

$$d_n = \begin{cases} -a_n & , \quad n < 0 \\ a_n & , \quad n > 0 \end{cases}$$

for an array centered on the coordinate system, thus producing an equivalent difference taper as shown in Fig. 17.

In (2), if we choose a set of amplitudes

$$i_n = a_n \exp[\pm jnkD \frac{\Delta\nu}{2}]$$

for the two individual beams, so that they point at $\nu_o = \mp \frac{\Delta\nu}{2}$, the sum pattern is

$$A_s(\nu) = \frac{1}{2} \left\{ \sum a_n \exp[jnkD(\nu - \frac{\Delta\nu}{2})] + \sum a_n \exp[jnkD(\nu + \frac{\Delta\nu}{2})] \right\}$$

which gives

$$A_s(\nu) = \sum [a_n \cos(nkD \frac{\Delta\nu}{2})] \exp[jnkD\nu] \quad ,$$

corresponding to a sum amplitude taper of the form

$$s_n = a_n \cos nkD \frac{\Delta\nu}{2} \quad , \tag{28}$$

† For a more thorough treatment of the subject, see Ref. 31.

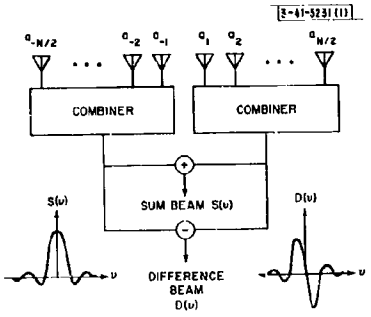

Fig. 16. Technique for generating a set of monopulse beams.

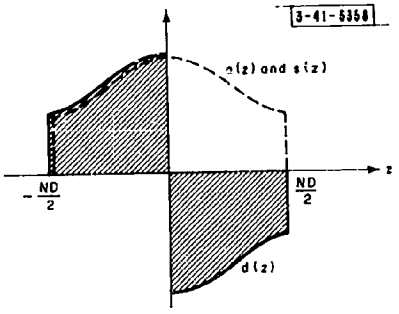

Fig. 17. Sum and difference tapers for type (1) monopulse for cosine-squared-on-a-pedestal basic illumination.

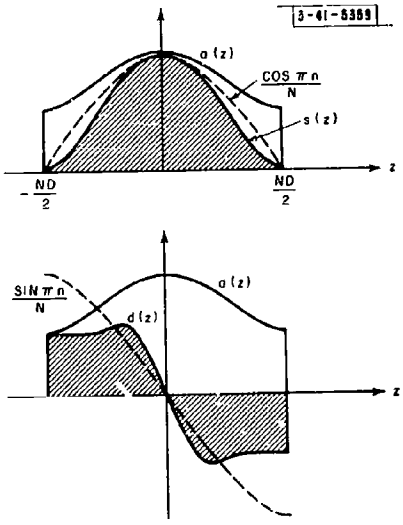

Fig. 18. Sum and difference tapers for type (2) monopulse for cosine-squared-on-a-pedestal basic illumination.

with the sum beam pointed halfway between the original beams. Commonly, $\Delta\upsilon$ is approximately a beamwidth which, for highly directive beams, is approximately $\Delta\upsilon \approx 2\pi/kND$. Thus the apparent sum beam amplitude taper is the original taper multiplied by a factor $\cos\beta(\pi n/N)$, where $\beta \approx 1$, indicating that the sum beam amplitude is altered somewhat as indicated in Fig. 18. In a similar manner, the difference beam amplitude taper can be shown to be of the form

$$d_n = a_n \sin\beta \frac{\pi n}{N} \quad , \tag{29}$$

as indicated in the figure.

Sum and difference patterns for (1) and (2) taken on a 16-element array with a basic uniform illumination are shown in Fig. 19. These examples are indicative of a fundamental difficulty with monopulse patterns derived by either method (1) or (2): low sidelobe sum patterns are accompanied by high sidelobe difference patterns. Further, the difference patterns which yield the most sensitive angular information tend to have high sidelobes. To see why, let us examine a fundamental measure of the sensitivity† of difference patterns: the normalized slope S, at $\upsilon = 0$. This quantity is related to the amplitude distribution of the difference pattern by

$$S^2 = \frac{|\Sigma n d_n|^2}{\Sigma d_n^2} \quad . \tag{30}$$

The value of S is most sensitive to the amplitude of the end elements; for large S, the a_n's, from which the d_n's are derived, should be large near the array ends. In fact, application of the Schwarz inequality to Eq. (30) yields the optimum difference taper (in the sense of maximum slope) as

$$d_n|_{\max S} = n \quad . \tag{31}$$

By contrast, the results of the previous section indicate that the edge a_n's should be small but finite (i.e., a pedestal used) for good sidelobe performance. The two requirements are incompatible in both systems of (1) and (2). However, more complex techniques can be used (Secs. III-B-2 and III-B-3) to permit the use of independent amplitude tapers on a sum and a difference beam, thus allowing each pattern to be optimized independently.‡ As might be expected, these systems are generally somewhat more complex and costly than those which produce the two simple monopulse types described.

3. Beam-Steering Effects on Array Factors and Array Design

It was pointed out in Eq. (8) that by the use of a linear phase taper, the beam of the array could be steered. That is, if a set of drive currents i_n produces an array function of the desired shape having some reference value (e.g., a maximum) in the direction $\upsilon = 0$, then a set $i_n \exp[-jnkD\upsilon_0]$ produces the same shape of array function with its reference point at $\upsilon = \upsilon_0$. While this effect on the array function amounts merely to a shift in reference point, the effect on the array factor is more complex. For example, consideration of Fig. 20 indicates that steering the beam off broadside can result in (a) beam broadening, (b) beam asymmetry, and

† The angular measurement accuracy is proportional to S (Sec. II-D-3).

‡ The independent optimization of difference patterns has been studied by Price and Hynemen (Ref. 32).

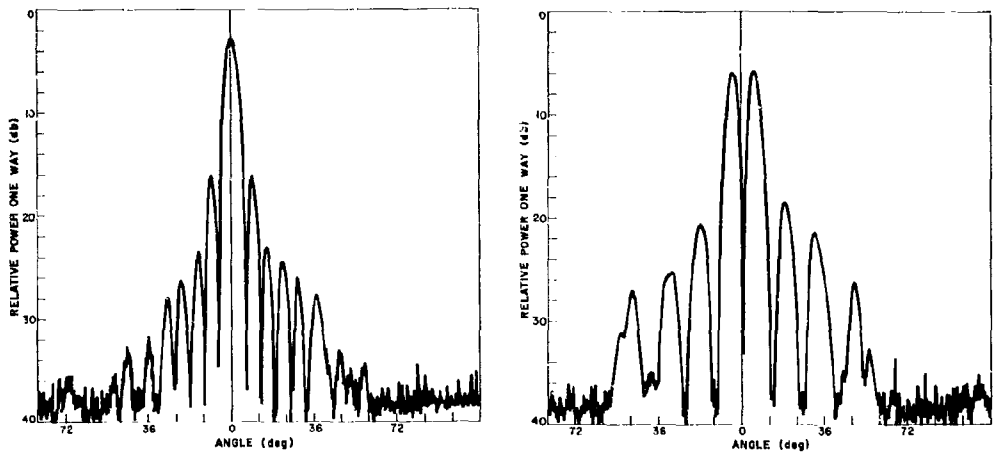

(a) Sum pattern. (b) Difference pattern.

Type (1) monopulse.

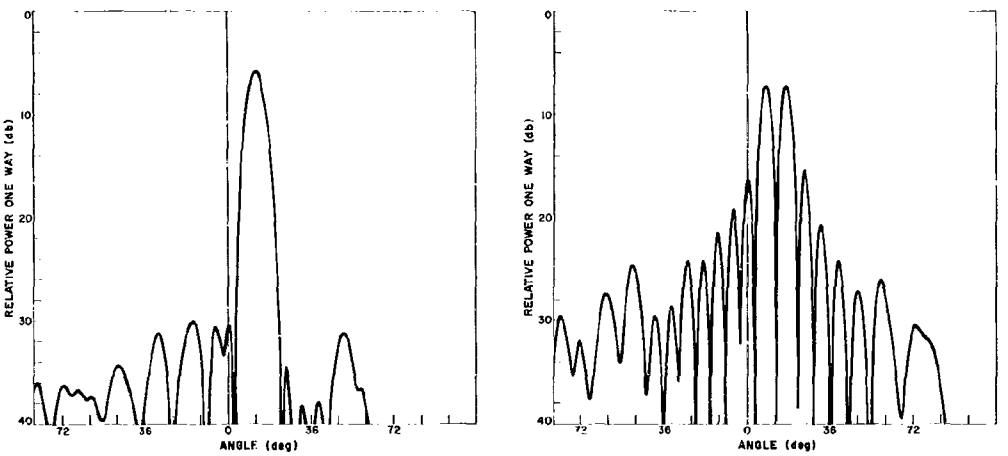

(a) Sum pattern. (b) Difference pattern.

Type (2) monopulse.

Fig. 19. Typical sum and difference patterns for two types of monopulse.

(c) the appearance of grating lobes in the visible space of the array factor. There are also effects less evident, such as variation in beam pointing with frequency and consequent bandwidth limitations. In this section, we shall examine these effects and some resultant implications on array design.

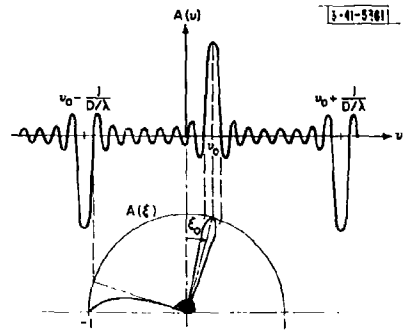

Fig. 20. Beam-steering effects on array factor $A(\xi)$ and array function $A(\upsilon)$.

We shall begin by examining the element spacing allowable to avoid grating lobes for a desired angle of scan. The effects of scanning on the shape of the beam will then be examined, with attention to beam broadening and asymmetry. Next, some useful rules for beam pointing angle as a function of phase shift will be developed and applied to the determination of the number of beamwidths that exist in a given angular segment of space. Finally, the frequency limitations of some typical array feeds will be examined.

Attention will be concentrated on highly directive array functions; consequently, the use of phase tapering for other than steering purposes will not be explicitly considered. However, most of the results may be extended to shaped beams.

Element Spacing to Avoid Grating Lobes:– Equation (8) stated that

$$A(\upsilon) = \sum_n a_n \exp[jnkD(\upsilon - \upsilon_o)] \quad , \tag{32}$$

where the pointing "direction" υ_o is related to the differential phase α by Eq. (7)

$$\alpha = -kD\upsilon_o \quad .$$

Using $\upsilon = \sin\xi$, we can construct the correspondence between α and ξ given in Fig. 21 for various D/λ. The curves for wider spacings are discontinued at scan angles for which a grating lobe comes into visible space. This occurs whenever the argument of Eq. (32) is a multiple of 2π; consequently, at υ_i given by

$$\upsilon_i - \upsilon_o = \frac{i}{D/\lambda} \quad , \tag{33}$$

a grating lobe will just appear in visible space if $|\upsilon_i| = 1$. Thus the element spacing criterion stated in terms of the desired maximum scan angle ξ_{max} is

$$D/\lambda < \frac{1}{1 + \sin|\xi_{max}|} \quad . \tag{34}$$

Equations (15) and (16) indicated that D/λ should be made as large as possible without grating lobes to achieve maximum directivity and minimum beamwidth. If an equality sign were used

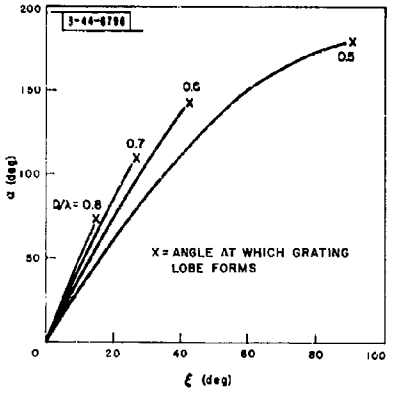

Fig. 21. Differential phase vs pointing angle ξ_o.

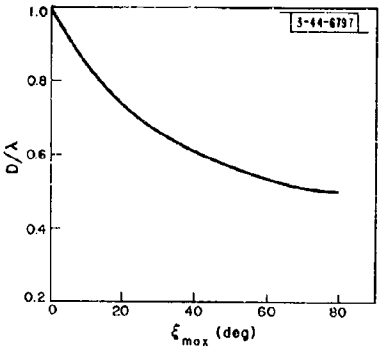

Fig. 22. Maximum allowable element spacing D/λ vs maximum scan angle ξ_{max}.

in statement (34), we might actually incur, rather than avoid, the grating lobe. For narrow beams, however, the error committed by applying (34) is frequently small enough [particularly when the effects on real radiators are included (Sec. II-C)] to justify using it rather than the more cumbersome exact formula which accounts for the finite width of the grating lobe. Figure 22 presents a plot of statement (34).

Beam Broadening as a Function of Scan Angle:– In the array function notation of Eq. (32), it is apparent that the width of the main lobe of the array function for a given amplitude taper is a function of the difference $\Delta\nu = \nu - \nu_o$. Therefore, the incremental phase shift required to move a beam through an angle measured in numbers of beamwidths is independent of ν_o and depends only upon the a_n's chosen. Consequently, if we take derivatives of both sides of $\nu = \sin\xi$, relating ν to the angle ξ in visible space, we see that

$$d\xi = \frac{d\nu}{\cos\xi}$$

or, for narrow beams, if ξ is not near $\pi/2$,

$$\Delta\xi \approx \frac{\Delta\nu}{\cos\xi_o} \quad .$$

If $\Delta\nu$ represents the change in the argument of Eq. (32) which produces a change in amplitude of $A(\nu)$, corresponding to the amplitude change which defines a beamwidth of the array factor $A(\xi)$ ($1/\sqrt{2}$ if the beamwidth of interest is the half-power beamwidth), it is seen that the corresponding beamwidth of the array factor is inversely proportional to the cosine of ξ_o. Consequently, the beamwidth as a function of scan angle Θ_{ξ_o} can be written in terms of the beamwidth Θ_o at broadside as

$$\Theta_{\xi_o} \approx \frac{\Theta_o}{\cos\xi_o} \quad , \tag{35}$$

if Θ_o is small, indicating that the beamwidth broadens as the secant of the scan angle. This relationship fails near the endfire condition ($|\xi_o| \approx \pi/2$), but a more precise and cumbersome expression can be derived[33] for that case.

Beam Asymmetry as a Function of Scan Angle:– The array factor also becomes "lopsided" as the beam is scanned off broadside. By Eq. (35), we can write the angle from the beam center to the outer beam-edge angle (the 3-db point) as approximately

$$\Delta\Theta_{+} \approx \frac{\Theta_o/2}{\cos(\xi_o + \Theta_o/2)} \quad ,$$

and similarly for the angle between the beam center and the inner beam edge. For $\Theta_o/2 \ll 1$, by small angle approximations, it can be shown in a straightforward manner that the asymmetry ratio is approximately equal to

$$\frac{\Delta\Theta_{+}}{\Delta\Theta_{-}} \approx 1 + \Theta_o \tan\xi_o \quad , \quad \Theta_o \text{ in radians} \quad . \tag{36}$$

Thus it can be seen that an asymmetry greater than 10 percent between the halves of the beam is incurred only for broadside beamwidths of the order of 6° or more for scan angles as great as 45°.

This beam asymmetry can have a nonnegligible effect upon the interpolation accuracy of an otherwise accurate monopulse system, however, since it causes an asymmetry of the slope of the difference pattern on the two sides of the difference pattern null.

Phase Increment Vs Scan Angle:– Since a given change in ν_o moves the main lobe of the array function a specified fraction of the main-lobe width, independently of the value of ν_o, the differential phase shift required to move the beam one beamwidth is constant. In particular, it can be seen from Eq. (37) that a change in α of $2\pi/N$ produces a change in ν_o of

$$\Delta\nu_o = \frac{1}{ND/\lambda} \quad .$$

Near $\xi = 0$, this change in ν_o is approximately the same as the change in the angle ξ in radians. Further, if the broadside beamwidth of the pattern is

$$\Theta = \frac{K}{ND/\lambda} \quad ,$$

the differential phase shift required to move one beamwidth is

$$\Delta\alpha = \frac{2\pi K}{N} \quad . \tag{37}$$

Thus, if the half-power beamwidths are the beamwidths of interest, the factor K can be determined from Fig. 12 for directive beam tapers. Roughly, $K_o \approx 1$ radian for directive beams, and a useful rule of thumb is that a total phase difference of 2π radians across the array moves the beam one beamwidth.

In addition to the usefulness of Eq. (37) for determining phase shift vs pointing angle, it is also useful in easily resolving the question of how many beamwidths are contained within a certain included angle in space. The phase shift required to point the beam at the extreme scan angle ξ_{max} is

$$\alpha = kD \sin\xi_{max} \quad ,$$

and using the above relation for the differential phase per beamwidth, we can write the number of beamwidths b between broadside and the angle ξ_{max} as

$$b = \frac{\sin|\xi_{max}|}{\Theta_o} \quad . \tag{38}$$

where Θ_o is the broadside beamwidth.

Transient Response of Arrays:– Up to this point, the behavior of array patterns has been discussed in terms of their response to continuous-wave (CW) signals. For such signals, it has been shown that the use of phase shifters is sufficient to form and scan a beam. However, if we visualize a plane wave as representing a transient (a step function) incident upon a linear array, as in Fig. 4, the output from all antennas will not coincide in time. The output of the combining network will not reproduce the transient faithfully if the "boxes" in the feed network are only phase shifters and the difference in arrival time at opposite ends of the array is greater than a period of the carrier frequency (which, as pointed out above, corresponds to an angle greater than a beamwidth from broadside). However, if we were to insert a delay in the boxes behind each element of the antenna so that the earlier-arriving signals were appropriately delayed, the antenna would have perfect time response to a signal arriving in the direction for which the delays were chosen, regardless of its transient behavior. Such an array is commonly referred to as a "delayed array."

The delays in such an array must operate at the received frequency and not, for example, at an intermediate frequency, since, for a modulated CW signal, we must both delay the modulation and phase shift the carrier in order that the signals from the element add properly. It is only at the received signal frequency that the required delay and required phase shift correspond. At other frequencies, the correspondence between delay and phase shift is lost and both operations cannot be simultaneously affected correctly by a single device.†

Even the delayed array gives perfect reproduction of the signal (within component bandwidth limitations) only when the signal arrives exactly from the direction for which the delays are properly chosen. For other angles, a "build-up phenomenon" similar in nature to that associated with arrays using only phase shifters occurs. This phenomenon for a delayed array is a function of the difference between the signal arrival angle and the "pointing" angle of the array (rather than the difference between broadside and the arrival angle, as will be seen when phase shifters are used) and is of minor significance in delayed arrays.

In order to see how a nondelayed array affects an incoming signal, a particular case of a "constant-phased" array (one using phase shifters whose phase shift is independent of frequency) will be examined. Such a device is of more than academic interest, since many phased arrays closely approximate this behavior. Such an array has a differential phase shift given by

$$\alpha = -k_o D \sin\xi_o \quad , \quad k_o = \frac{\omega_o}{c} \quad ,$$

such that the array is phased to point the beam in a direction ξ_o when the frequency is ω_o. The array response to a signal of an arbitrary frequency ω, arriving from a direction ξ, can then be written as

$$A(\omega,\xi) = \sum_n a_n \exp\left[j \frac{nD}{c} (\omega \sin\xi - \omega_o \sin\xi_o)\right] \quad . \tag{39}$$

† In some cases, a phase-shifted carrier and separately delayed video modulation may be used successfully.

It is seen that a shift in the received center frequency from ω_o causes the beam pointing to be in error. If the received signal is at a frequency ω_1, the beam pointing angle ξ_1 will be given by

$$\sin \xi_1 = \frac{\omega_o}{\omega_1} \sin \xi_o \quad .$$

For a small difference in frequency, differentiating this expression indicates that the change in pointing angle is

$$d\xi = -\tan \xi_o \frac{d\omega}{\omega_o} \quad .$$

The impulse response of the antenna is the Fourier transform on ω of Eq. (39), which is found to be a series of impulses spaced $D/c \sin \xi$ apart in time with an envelope of the form

$$h(t) = a\left(\frac{tc}{\sin \xi}\right) \exp\left[j \frac{\sin \xi_o}{\sin \xi} \omega_o t\right] \tag{40}$$

for a centered array of length $L = ND$, where $a(z)$ is a continuous function such that the a_n of Eq. (39) can be considered samples of $a(z)$; that is, $a_n = a(nD)$.

This impulse response is of the form $\rho(t) \exp[j\Theta(t)]$, with a magnitude $\rho(t)$ which is a time reproduction of the shape of the amplitude taper across the antenna, and has a duration equal to the time required for the wave to propagate the projected length of the array, which, for a pointing angle of b beamwidths from broadside, is equal to b/f_o. Since the real part of the expression is implied, the "phase term" is a cosine term that has the argument of the exponential, "modulating" the amplitude. For a signal arriving at the pointing angle ξ_o, the exponential is unity and the impulse response has the same shape as the amplitude taper, as indicated by Figs. 23 and 24

If the received signal s(t) has a step-function envelope

$$s(t) = \begin{cases} \exp[j\omega_o t] & , \quad t > 0 \quad , \\ 0 & , \quad t < 0 \quad , \end{cases}$$

the envelope of output of the antenna, which we shall denote O(t), is just the integral of h(t) up to the time of interest. Figure 25(a-d) shows O(t) corresponding to a target at angles corresponding to (a) the pointing angle, (b) the 3-db point, (c) the peak of the second sidelobe, and (d) the third null of the array factor for a step function s(t). For small β, the finite rise time of O(t) is primarily due to the amplitude part of the impulse response. For large β, the exponential part of h(t) dominates the behavior of the antenna and instead of a monotonic rise of O(t) to its final value, there is an oscillatory rise. It is also apparent that a time-invariant antenna pattern is, strictly speaking, only a CW phenomenon.

The effects of this so-called "build-up" phenomenon, which is really a bandwidth limitation, are to decrease radar sensitivity (received signal-to-noise ratio), resolution, and range measurement accuracy. The magnitude of these effects depends upon the bandwidth of the signal relative to the propagation time across the array. Sklar† has examined these effects for a radar transmitting and receiving through identical, uniformly illuminated, constant-phased arrays, for a rectangular pulse from the transmitter of T seconds (the "build-up" effect is thus twice as

† The remainder of this section is based largely upon the work of Sklar in Ref. 10 (Part 3, Ch. II).

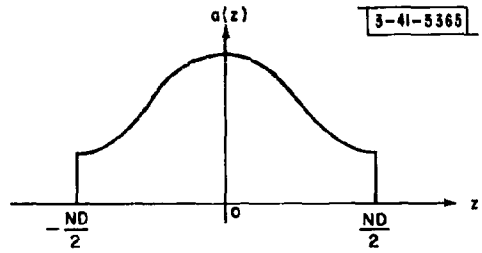

Fig. 23. Typical amplitude taper.

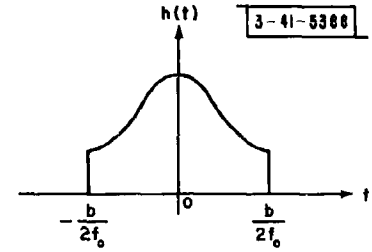

Fig. 24. Resulting impulse response envelope for target at ξ_o which is b beamwidths from broadside.

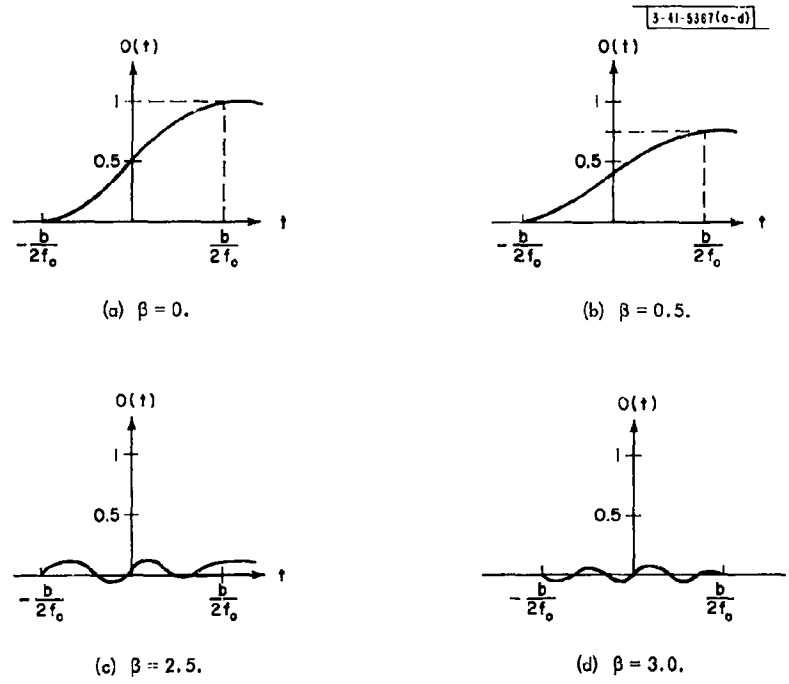

(a) $\beta = 0.$

(b) $\beta = 0.5.$

(c) $\beta = 2.5.$

(d) $\beta = 3.0.$

Fig. 25. Envelope of response of antenna of Fig. 23 to step function signal arriving β beamwidths from the pointing direction, which is b beamwidths from broadside.

pronounced as for one-way operation through an array). It is assumed that the target is at the center of both beams. The results are given in terms of the parameter T/δ, where δ is the one-way transit time across the array

$$\delta = \frac{L}{c} \sin \xi_o = b/f_o \quad .$$

Figure 26 shows the decrease in signal-to-noise ratio (S/N) from a receiver (a) matched to the transmitted (undistorted) waveform, and (b) matched to the known distortion associated with the b beamwidth position. In Fig. 27, the lengthening of the base of the output waveform of a receiver matched to a square pulse is plotted against T/δ as a measure of the ultimate resolution capability of the radar (it was found that the ultimate resolution, by this measure, was better for the receiver matched to the undistorted pulse, but this judgment takes no account of the decreased S/N obtained). Figure 28 indicates the loss in range measurement accuracy associated with the bandwidth limiting of the array. In all cases, it is seen that things really deteriorate for T/δ of the order of two or less.

We have shown that $\delta \approx b/f_o$. Further, the bandwidth of a T-second rectangular pulse is approximately $W = 1/T$ cps. If we assume that Sklar's results can be generalized into bandwidth statements applicable to any waveform, we can write his T/δ parameter in the form

$$\frac{T}{\delta} = \frac{1}{b(W/f_o)} \quad .$$

Thus the bandwidth limitation of a constant-phased array dictates the maximum number of beamwidths we may scan from broadside as

$$b_{max} \approx \frac{50}{100\, W/f_o} \quad , \tag{41}$$

where $100\, W/f_o$ is recognizable as the percentage bandwidth of the signal.

Despite its emphasis in this section, the constant-phased array is not the worst offender with regard to bandwidth limitation and is used here only for illustrative purposes of the bandwidth limitation phenomenon. This effect is considerably more pronounced in some nonconstant-phased arrays and in so-called "frequency-scanned arrays." In Sec. III-B-1, we shall examine the magnitude of this effect on several different types of linear arrays, using the constant-phased array behavior as a reference point.

B. Two- and Three-Dimensional Arrays of Isotropic Radiators

An array that can form a beam having desired characteristics in two angular dimensions obviously must occupy two or more dimensions itself. In this section, we shall discuss such arrays, making frequent appeal to linear array results. Two-dimensional (planar) arrays will be discussed in some detail, and arrays on curved surfaces, such as cylinders and spheres, will be touched upon. The discussion will still be restricted to arrays with isotropic radiators, and consequently will center upon array functions and array factors.

For any surface, the n^{th} element can be located by a vector $\overline{\rho_n}$ from the origin to the element location at x_n, y_n, z_n, where

$$\overline{\rho_n} = x_n \bar{i} + y_n \bar{j} + z_n \bar{k} \quad ,$$

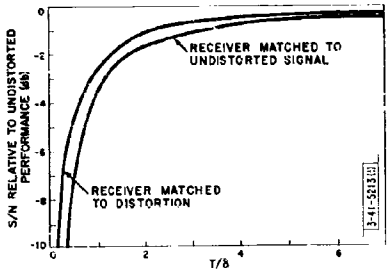

Fig. 26. Signal-to-noise ratio degradation vs T/δ.

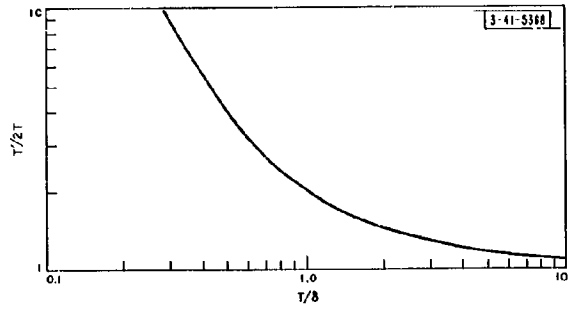

Fig. 27. Length T' of output of receiver matched to rectangular pulse length T vs T/δ.

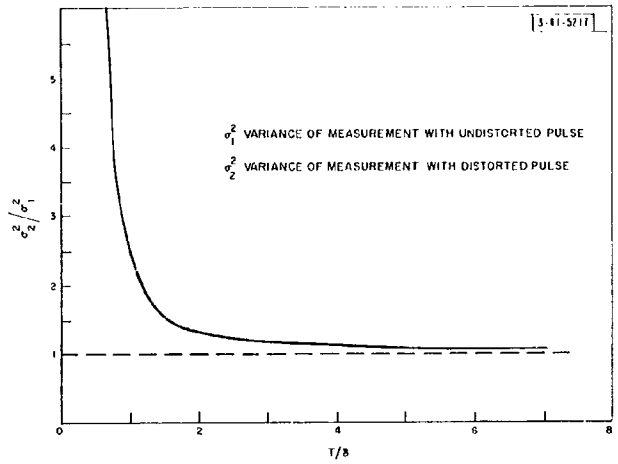

Fig. 28. Loss in range measurement accuracy vs T/δ.

with $\bar{i}$, $\bar{j}$, and $\bar{k}$ as the base unit vectors. A geometrical argument similar to that which led to Eq. (5) for linear array factors can be used to establish that, for a plane wave arriving from a direction specified by a unit vector $\hat{R}$, the array factor is

$$A(\varphi, \Theta) = \sum_n i_n \exp[jk\bar{\rho}_n \cdot \hat{R}] \quad , \tag{42a}$$

where, in spherical coordinates,

$$\hat{R} = (\sin\Theta \cos\varphi)\,\bar{i} + (\sin\Theta \sin\varphi)\,\bar{j} + (\cos\Theta)\,\bar{k} \quad . \tag{42b}$$

It is seen that the corresponding array function can be obtained by writing

$$\hat{R} = \tau\bar{i} + u\bar{j} + v\bar{k} \quad , \tag{42c}$$

where τ, u, and v are the respective direction cosines of R with the x-, y-, and z-axes.

1. Planar Array Factors and Array Functions

For a planar array of elements as shown in Fig. 29 in which the mn^{th} element is located at $x_m = mD_x$, $y_m = mD_y$, Eq. (42) can be rewritten as

$$A(\tau,\mu) = \sum_m \sum_n i_{mn} \exp[jk(mD_x\tau + nD_y\mu)] \quad . \tag{43}$$

For example, for a uniformly illuminated ($i_{mn} = 1$) rectangular array, with M rows and N columns, where both M and N are odd so that the center element is placed at x = y = 0 (the assumption of odd numbers and a centered array is strictly a mathematical convenience), we have

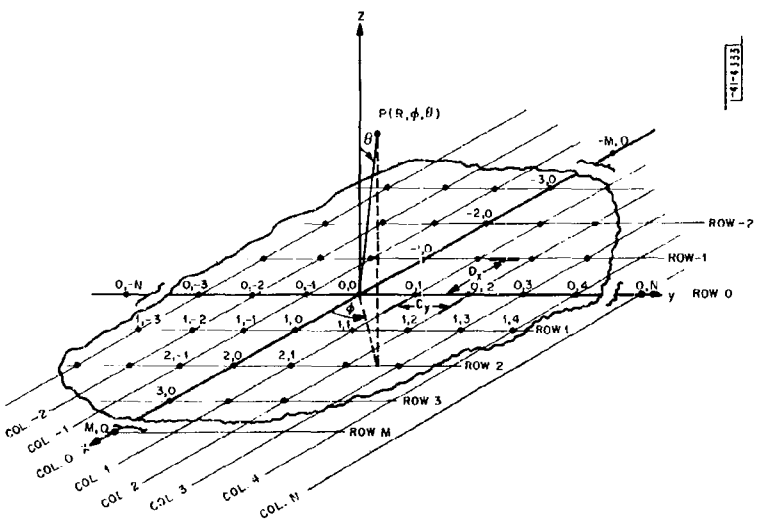

Fig. 29. Generalized planar array geometry.

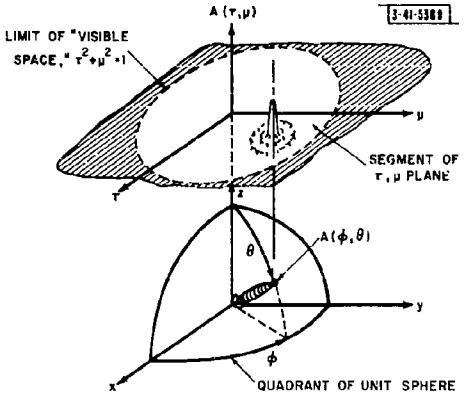

Fig. 30. Construction of planar array factor $A(\phi,\theta)$ by projection of array function $A(\tau,\mu)$ onto unit sphere.

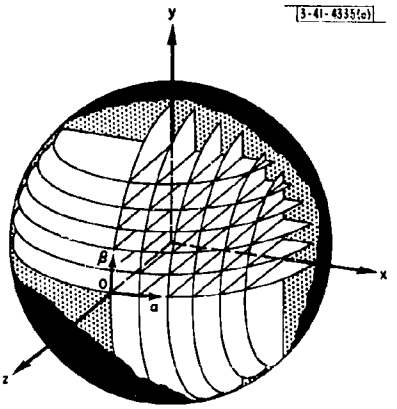

Fig. 31. Beam-steering contours for planar arrays lying in the x-y plane.

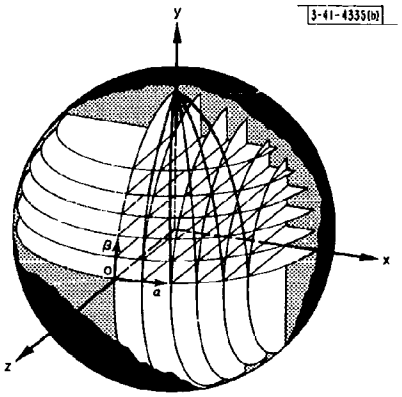

Fig. 32. Difference between lines of constant α and lines of constant azimuth (heavy lines).

$$A(\tau,\mu) = \sum_{m=-\frac{(M-1)}{2}}^{\frac{M-1}{2}} \exp[jkmD_x\tau] \sum_{n=-\frac{(N-1)}{2}}^{\frac{N-1}{2}} \exp[jknD_y\mu] \quad .$$

Each sum can be evaluated, producing a result analogous to Eq. (6) for a uniformly illuminated linear array:

$$A(\tau,\mu) = \left[\frac{\sin\left(\pi M \frac{D_x}{\lambda}\tau\right)}{\sin\left(\frac{\pi D_x}{\lambda}\tau\right)}\right]\left[\frac{\sin\left(\pi N \frac{D_y}{\lambda}\mu\right)}{\sin\left(\frac{\pi D_y}{\lambda}\mu\right)}\right] \quad . \tag{44}$$

Beam positioning with planar arrays is accomplished by linear phasing along both array coordinates. To point the beam at τ_o, μ_o, we choose the currents i'_{mn} to be related to the currents for a broadside beam i_{mn} by†

$$i'_{mn} = i_{mn} \exp[j(m\alpha + n\beta)] \quad ,$$

where α and β should be chosen so that

$$\alpha = -kD_x\tau_o$$

$$\beta = -kD_y\mu_o$$

so that

$$A(\tau,\mu) = \sum_m \sum_n i_{mn} \exp\{jk[mD_x(\tau-\tau_o) + nD_y(\mu-\mu_o)]\} \quad . \tag{45}$$

In this two-dimensional case, the array factor is found by projecting the array function onto the unit sphere, as indicated in Fig. 30. This construction makes evident the fact that all the effects of beam steering on the array factor (broadening, asymmetry, phase differentials, transient effects, etc.) are directly inferable from the linear array results by replacing the angle ξ of Sec. II-A-3 by 0 for planar arrays.‡

Note, however, that if we project lines of constant α and β onto the unit sphere, an "egg-crate" construction results, as indicated in Fig. 31. It is seen that the α and β phase shifts do not produce orthogonal beam movements. For example, if the array is oriented so that the y-coordinate is "up," α phase shift corresponds to pure azimuth pointing, but β phase shift is not pure elevation change, as indicated in Fig. 32.

It is obvious that planar array functions must possess grating lobes. In fact, they will have a two-dimensional array of such lobes in τ, μ space. Avoidance of these lobes in "visible space" hinges upon making proper choices of D_x and D_y. However, the additional degree of freedom gained in the planar array also permits "shaping" the grating lobe pattern with regard to the required scanning volume. Thus a potential savings in number of elements required for a specified array directivity and beamwidth may be realized, as will be seen.

---

† Note that with regularly spaced elements, this form of steering phase indicates that the phase of the mn^{th} element is the sum of a row phase $m\alpha$ and a column phase shift $n\beta$. This fact can be put to use in design of planar arrays in several ways, as explored in Sec. III-B.

‡ Such effects are also explored in Ref. 34 for planar arrays.

The grating lobes of the array function are given in terms of τ and μ by solutions of

$$k[mD_x(\tau - \tau_o) + nD_y(\mu - \mu_o)] = \ell 2\pi$$

for all m and n, for integer values of ℓ other than $\ell = 0$, which defines the main lobe. For a rectangular grid, this is equivalent to stating that grating lobes lie at the intersections in the τ, μ plane of the lines

$$\tau - \tau_o = \frac{i}{D_x/\lambda} \quad , \quad i = 0, \pm 1, \pm 2, \text{ etc.}$$

$$\mu - \mu_o = \frac{j}{D_y/\lambda} \quad , \quad j = 0, \pm 1, \pm 2, \text{ etc.}$$

The resultant grating lobe pattern is rectangular in τ, μ space, as shown in Fig. 33. This pattern must be mapped onto the surface of the unit sphere, as in Fig. 30, to give a true spatial distribution; therefore, only the portion of the pattern of Fig. 33 inside a unit circle centered at $\tau = 0$, $\mu = 0$ lies in visible space.

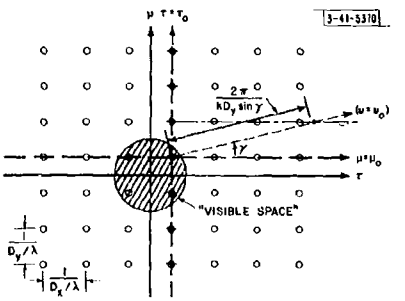

Fig. 33. Grating lobe pattern for rectangular grid ($D_x/\lambda = 5/6$, $D_y/\lambda = 1$).

The spatial distribution of grating lobes is rectangular, as was the original grid. If the grid were hexagonal, the grating lobe pattern would also be hexagonal (Ref. 10, pp. 152-154). This reproduction of the grid is characteristic, and it is the shaping of the grid to match a specified surveillance volume that can be used to minimize the number of elements required.[35,36] To demonstrate this fact as well as to derive a general spacing criterion, let us investigate the location of grating lobes along a cut through Fig. 33, making an angle γ with the $\tau - \tau_o$ axis. Note that, for $\gamma \leq 45°$, the nearest possible grating lobes will be those along the line $\mu - \mu_o = 1/(D_y/\lambda)$. Denoting "distance" measured along the new axis as $\nu - \nu_o$, the distance at which such a lobe can be intersected is

$$\nu - \nu_o = \frac{1}{(D_y/\lambda)\sin\gamma}$$

(note that this is the minimum distance if any lobes exist along the $\nu = \nu_o$ axis, for the angle in question).

It is seen from Fig. 34 that the quantity $(D_y/\lambda)\sin\gamma$ is the projected element spacing on an axis making an angle γ with the x-axis.† Comparison of the above equation with Eq. (33) immediately establishes the general result that there will be no grating lobes in visible space when

†Note that the particular γ chosen for illustration in Fig. 33 does not actually yield a grating lobe along the line $\mu = \mu_o + 1/(D_y/\gamma)$, since the particular angle chosen does not correspond to an angle which yields equal projected spacings along the line of Fig. 34.

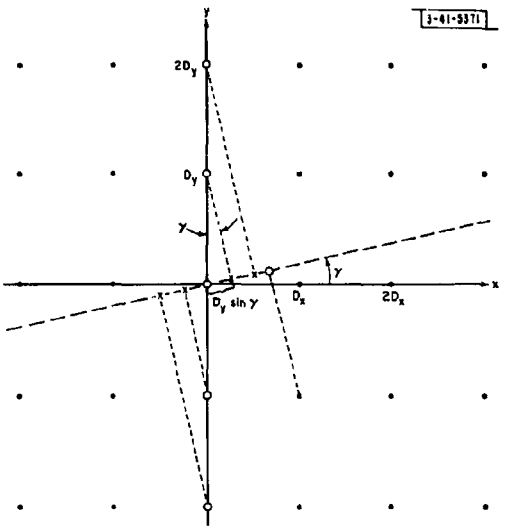

Fig. 34. Projected element spacings.

scanning off broadside to an angle Θ_{max} if the element spacing, projected on the scanning axis, satisfies

$$\frac{D}{\lambda} < \frac{1}{1 + \sin|\Theta_{max}|} \quad ,$$

which is precisely the criterion for linear arrays [Eq. (34)] as plotted in Fig. 22.

2. Planar Array Taper Considerations

The predominant factors affecting the choice of the i_{mn}'s for planar arrays are the same as those for linear arrays: taper efficiency (directivity), sidelobe levels, and beamwidth considerations, and perhaps beam shaping as well.

The properties of several amplitude tapers for directive beams will be discussed and compared in this section, and it will be pointed out that linear array synthesis techniques can often be conveniently used by reducing the planar array to a number of "equivalent" linear arrays.

Since we shall be most interested in highly directive beams, let us first investigate the explicit relationship for the directivity of a planar array in terms of the illumination function. The directivity of a planar array is defined exactly as in Eq. (10) with appropriate notation changes to include both spatial angles:

$$U(\varphi_o, \Theta_o) = \frac{|A(\varphi_o, \Theta_o)|^2}{\frac{1}{4\pi}\int_{\substack{\text{all} \\ \text{space}}} |A(\varphi, \Theta)|^2 \, d\Omega} \quad . \tag{46}$$

It was established in Sec. II-A-2 that the array factor of a large array closely approximates that of a continuous antenna near the main lobe. Thus, if the array function is such that almost all the power in a period of the pattern is in the main beam and first few sidelobes and no visible grating lobes exist, the directivity expression for a continuous aperture [Ref. 4, Eq. (19), p. 177 and Eq. (55), p. 188] may be used:

$$U(\varphi_o, \theta_o) \approx \frac{4\pi}{\lambda^2} \cos\theta_o \frac{\left|\iint i(x,y)\, dx\, dy\right|^2}{\iint |i(x,y)|^2\, dx\, dy} \quad , \tag{47}$$

where the integrals are understood to extend over the antenna. By the Schwarz inequality,[16] it can be shown that

$$\frac{\left|\iint i(x,y)\, dx\, dy\right|^2}{\iint |i(x,y)|^2\, dx\, dy} = \eta A \quad , \quad 0 \leq \eta \leq 1 \quad , \tag{48}$$

where A is the physical area of the antenna and η is, as for linear arrays, the taper efficiency or illumination efficiency. It is unity for i(x,y) constant over the entire aperture and is tabulated for other common tapers.†

The directivity can be expressed in terms of the actual taper coefficients by noting that, for large numbers,

$$\iint i(x,y)\, dx\, dy \approx \sum\sum i_{mn} D_x D_y$$

for $i_{mn} = i(mD_x, nD_y)$. By a similar equivalence in the denominator of (48), it follows that

$$\frac{\left|\iint i(x,y)\, dx\, dy\right|^2}{\iint |i(x,y)|^2\, dx\, dy} \approx \frac{\left|\Sigma\Sigma\, i_{mn} D_x D_y\right|^2}{\Sigma\Sigma\, |i_{mn}|^2 D_x D_y}$$

$$\approx \eta N D_x D_y \quad , \tag{49}$$

where N is the total number of elements in the array. Thus, for a large array, since $ND_xD_y = A$, we can write

$$U(\varphi_o, \theta_o) \approx 4\pi \frac{A}{\lambda^2} \eta \cos\theta_o \tag{50}$$

or, alternatively,

$$U(\varphi_o, \theta_o) \approx 4\pi \eta N \frac{D_x D_y}{\lambda^2} \cos\theta_o \quad , \tag{51}$$

if no grating lobes exist. In the event that grating lobes exist at angles θ_ℓ, the denominator of Eq. (46) will be altered and

$$U(\varphi_o, \theta_o) \approx 4\pi \frac{A}{\lambda^2} \eta \frac{1}{\sum_{\ell=0}^{L} \frac{1}{\cos\theta_\ell}} \quad , \quad \theta_\ell \neq \frac{\pi}{2} \quad , \tag{52}$$

indicating that, very crudely, the directivity is reduced by the factor of 1 + L for L grating lobes in visible space. From Eq. (51) it is seen that for a fixed number of elements, the directivity is maximized by using the widest element grid spacing commensurate with the requirement that grating lobes be avoided in visible space.

---

†See, for example, Fig. 36(a).

Our results from linear arrays would lead us to expect that planar arrays have broadside beamwidths in the x-z and y-z planes related to the array dimensions by

$$\Theta_x \approx \frac{K_x}{MD_x/\lambda} \quad , \quad \Theta_y \approx \frac{K_y}{ND_y/\lambda} \quad . \tag{53}$$

The value of each K depends upon the array taper in the plane in question (see the discussion of "equivalent linear arrays" below).†

The shape of the array grid is dictated by the shape of the scanning volume required,‡ whereas the shape of the array outline is often dictated by the shape of the beams one wishes to generate.

If markedly different patterns are desired in two orthogonal planes (azimuth and elevation), it is often advantageous to use rectangular arrays with sides parallel to the specified planes and separable illumination; that is, $i_{mn} = i_m i_n$, such that

$$\begin{aligned} A(\tau,\mu) &= \sum_m \sum_n i_m i_n \exp\{jk\,[mD_x(\tau - \tau_o) + nD_y(\mu - \mu_o)]\} \\ &= \sum_m i_m \exp[jkmD_x(\tau - \tau_o)] \sum_n i_n \exp[jknD_y(\mu - \mu_o)] \\ &= A_1(\tau)\, A_2(\mu) \quad , \end{aligned} \tag{54}$$

where A_1 and A_2 are synthesized by linear array techniques.

When more symmetrical patterns are desired, the use of separable illumination has a disadvantage which may or may not be serious. Along the $\mu = \mu_o$ axis, for example, the sidelobe levels are those of $A_1(\tau)$ only, since A_2 is a maximum. Away from both the $\tau = \tau_o$ and $\mu = \mu_o$ axes, the sidelobes are lower as a result of the product of $A_1 A_2$, both less than their maximum. For example, the array function for a uniformly illuminated rectangular aperture was given by Eq. (44). The function yields first sidelobes of about 13.2 db below the main beam along the two axes. Off the axes, the sidelobes are lower. In particular, along the diagonals ($\tau - \tau_o = \mu - \mu_o$), the first sidelobes are twice as low in decibels, −26.4 db.

Consequently, for a given highest sidelobe level, the taper efficiency ($\eta = \eta_1 \eta_2$) is lower for separable illumination than can be realized by nonseparable means, although the average sidelobe level should be comparable to tapers of like values of η.

If a circularly symmetric pattern is desired,§ an array shape approximating a circle may be desirable, for which specific amplitude tapers have been developed. We shall therefore discuss first the circular array case, for which tapers have been designed. In addition, since certain phasing techniques are more easily adapted to rectangular arrays, the necessity for a procedure for nonseparable illumination synthesis exists. Therefore, we shall also outline a technique for more general synthesis.

---

† For circularly symmetrical tapers, values of K are independent of the plane in question and are tabulated in Fig. 36(b).

‡ Ignoring for now the practical hardware compromises which may favor certain grid shapes or array shapes. These considerations are discussed in Sec. III-B.

§ Note, however, that the array symmetry will dictate only the symmetry of the beam shape and near-in sidelobe structure. The element grid will still govern the grating lobe location.

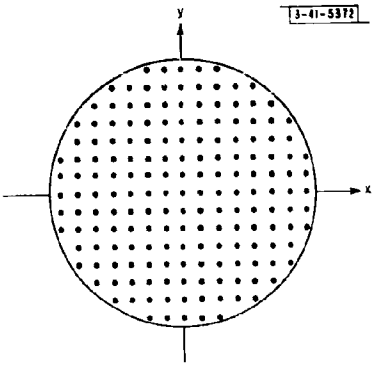

Fig. 35. Circular array with square grid.

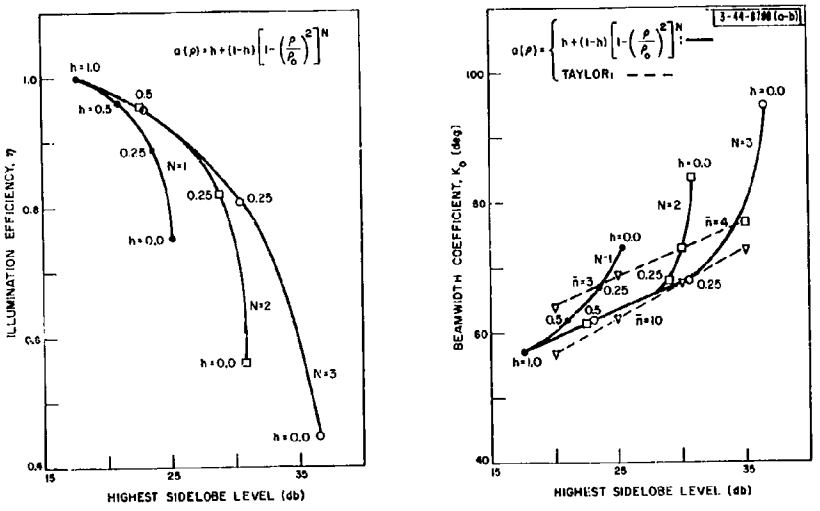

(a) Illumination efficiency.

(b) Half-power beamwidth coefficient.

Fig. 36. Properties of some tapers for circular arrays.

By the continuous antenna model, the array factor of a large, evenly illuminated, circular-shaped array, as shown in Fig. 35, will have a near-in structure of the form

$$A(\Theta) \approx \frac{J_1(k\rho_o \sin\Theta)}{k\rho_o \sin\Theta} \quad , \tag{55}$$

where $J_n(x)$ is the Bessel function of the first kind of order n. This function has a half-power beamwidth coefficient of $K_o = 58.5$, defined by

$$\Theta_o = \frac{K_o}{2\rho_o/\lambda} \quad , \tag{56}$$

where ρ_o is the radius of the aperture. The first sidelobes are approximately -17.6 db.

If lower close-in sidelobes are desired with a circular array, additional techniques from the theory of continuous apertures can be used. The properties of two important classes of circularly symmetric amplitude tapers for obtaining narrow beams from circular antennas are summarized in Fig. 36(a-b), with respect to illumination efficiency η and half-power beamwidth coefficient K_o.

The family of tapers of the form†

$$a(\rho) = \begin{cases} h + (1-h)\left[1 - \left(\frac{\rho}{\rho_o}\right)^2\right]^N & , \quad 0 \leq \rho < \rho_o \\ 0 & , \quad \rho > \rho_o \end{cases} \tag{57}$$

has been investigated, where h is a parameter denoting the normalized "pedestal" height in the same manner as for linear array "cosine tapers." In fact, the radial variation of these amplitude tapers is similar to that of the cosine taper (for N = 1), and cosine-squared taper (for N = 2) shown in Figs. 8 and 9. Figure 36 shows that the performance of this class is quite good if a sufficiently large N is used.

The taper derived by Taylor[38] and tabulated by Hansen[39] is an approximation to an "optimum" in the Dolph sense of minimum beamwidth for a given highest sidelobe level; as an approximation, it is occasionally inferior to the previous class in terms of beamwidth, as seen in Fig. 36. (To the best of this writer's knowledge, no aperture efficiency data exist for the Taylor taper; therefore, Fig. 36 presents only highest sidelobe level vs beamwidth data.) The parameter $\bar{n}$ given in Fig. 36 is numerically one greater than the number of sidelobes that are chosen to be of approximately equal amplitude, before the sidelobes begin to decay, as indicated in Fig. 37 (this decay is immediate for the other tapers). Larger values of $\bar{n}$ tend to sharpen the beam but would be expected to decrease the gain. Representative small and large values of $\bar{n}$ are included. The corresponding amplitude taper for a large array is shown in Fig. 38. Note that large values of $\bar{n}$

---

† The corresponding far field is of the form

$$A(u) = h\Lambda_1(u) + \frac{1-h}{N+1}\Lambda_{N+1}(u) \quad , \quad u = k\rho_o \sin\theta \quad , \tag{58}$$

where the Λ-functions are tabulated functions (Ref. 37) related to the Bessel functions. The sidelobes are monotonically decreasing, except for certain combinations of large N and small h, for which the highest sidelobe may not be the first, but will be close-in.

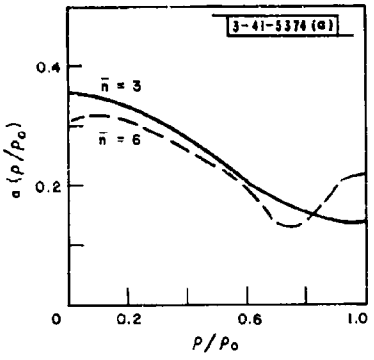

(a) Amplitude taper for 25-db sidelobes.

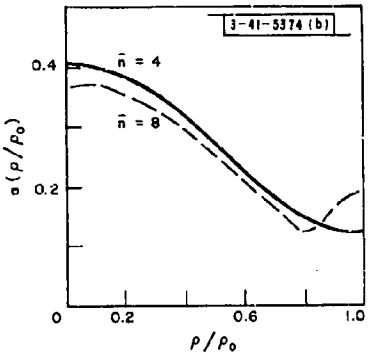

(b) Amplitude taper for 30-db sidelobes.

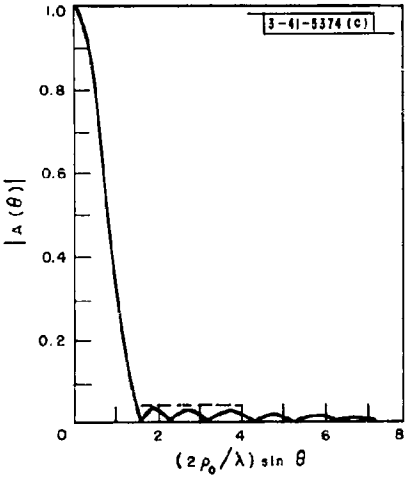

(c) Relative array factor for 30-db sidelobes, $\bar{n} = 4$.

Fig. 37. Characteristics of Taylor taper for circular antennas. (Reprinted, with permission of the IRE, from Hansen, Ref. 39.)

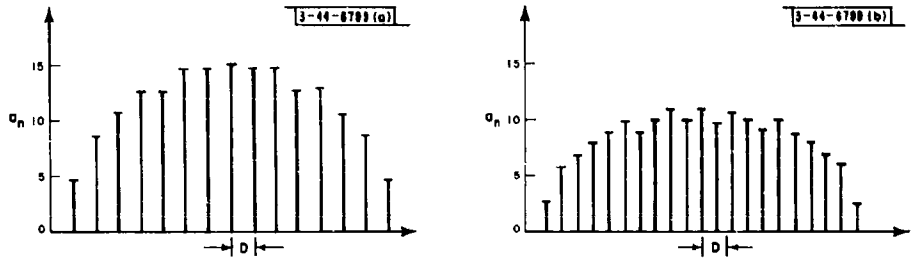

(a) Principal plane cut.

(b) Cut at 45° to principal plane.

Fig. 38. Two equivalent linear arrays contained in the uniform circular array of Fig. 35.

(many equiamplitude sidelobes) require amplitude tapers peaked at the array edges. Such distributions are sensitive to edge effects when real elements are used.

For more general analysis and synthesis of planar array patterns, a useful technique is that of reducing the planar array to "equivalent" linear arrays. Although this technique does not represent a panacea as far as the actual amount of work required to analyze or synthesize a planar array taper is concerned, it puts the problem into a simple linear array context, facilitating the formal mathematics and clarifying the cause-and-effect relationships.

It can be seen that the array function of Eq. (45) along the axis $\mu = \mu_o$ is given by

$$A(\tau,\mu_o) = \sum_m \left[\sum_n i_{mn}\right] \exp[jkmD_x(\tau - \tau_o)] \quad . \tag{59}$$

This is of the form of an array function for a linear array of elements along the x-axis of Fig. 29:

$$A(\tau) = \sum_m i'_m \exp[jkmD_x(\tau - \tau_o)] \quad , \tag{60}$$

where the currents of this equivalent linear array are given by

$$i'_m = \sum_n i_{mn} \quad .$$

That is, the drive to the m^{th} element of the equivalent linear array is the sum of all the drives of the m^{th} row of the planar array (the linear array "elements" are the rows of the planar array).

Similarly, we can choose an equivalent linear array to generate the $\tau = \tau_o$ pattern. For the simple case of separable amplitude taper ($i_{mn} = i_m i_n$) discussed previously, these two pattern "cuts" suffice to define the entire planar array function. For more complicated situations, additional cuts are usually necessary. Cuts parallel to, but not coincident with, the $\tau = \tau_o$ and $\mu = \mu_o$ axes can be made, but the resulting expressions are complex and afford little insight. It is usually preferable to take additional cuts by (at least conceptually) rotating the array in the coordinate system about an axis through its center and take all cuts along the $\mu = \mu_o$ axis as the array is rotated. Two such cuts on an evenly illuminated circular array are shown in Fig. 38.

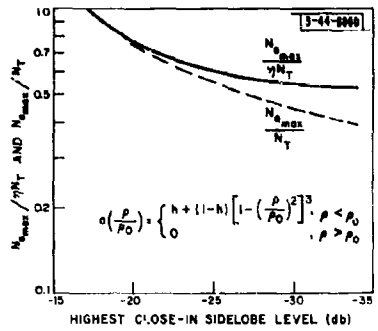

Fig. 39. Maximum value of $N_a/\eta N_T$ and N_a/N_T for specified highest sidelobe ratio for typical circular array taper.

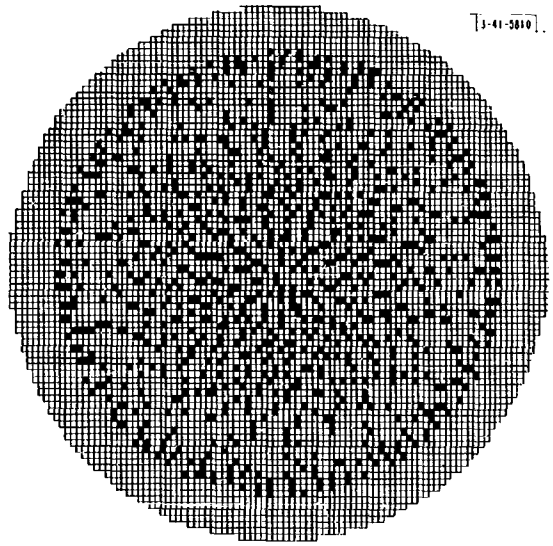

Fig. 40. Density-tapered circular planar array. (Reprinted, with permission of the IRE, from R. E. Willey, Ref. 24.)

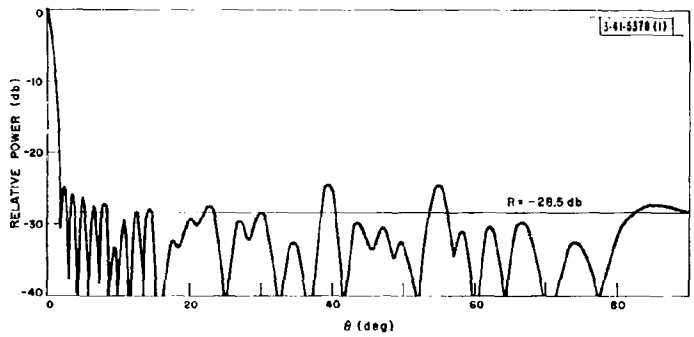

Fig. 41. Pattern cut on density-tapered array. (Reprinted, with permission of the IRE, from R. E. Willey, Ref. 24.)

While the element spacing can become quite complex, it will be recalled that the envelope of the illumination is of primary importance and taking cuts in this manner makes the envelope shape evident. If the desired general taper shape is known, a great deal of preliminary "juggling" can be carried out on the taper before any patterns are computed.

The formulas derived for density tapering of linear arrays can be directly generalized to include the planar array. However, for specified first sidelobe levels, the quantity $N_{a_{max}}/\eta N_T$ (which, it will be recalled, determines the lowest far-out rms sidelobe level and the maximum directivity attainable in a density-tapered array) is numerically different. For example, for a circular array with the highest order (N = 3) taper whose efficiency is tabulated in Fig. 36(a), the curves of Fig. 39 can be generated (compared with Fig. 13 of Sec. II-A-2 for linear arrays). By an argument similar to that put forth for linear arrays, and the data of Fig. 39, it follows that for low sidelobe tapers (≈−30 db) on planar arrays with maximally dense tapers (P = 1), the sidelobes should be down about

$$R = 10 \log_{10} \frac{1.7}{\eta N_T} \quad , \tag{61}$$

if all sidelobe peaks are of equal height. If the array is thinned (P << 1), Eq. (25) applies directly to the planar array case

$$R_{db} = 10 \log_{10} \frac{2}{N_a} \quad . \tag{25}$$

Figure 40 shows a density taper with $N_T \approx 4000$ and $N_a = 900$, and Fig. 41 shows a typical pattern cut, and the R = 28.5 level predicted by Eq. (61). The design was based on Taylor's circular antenna taper discussed above for −25-db first sidelobes and $\bar{n} = 10$.

The directivity of a planar density-tapered array is related to that of the equivalent amplitude taper by Eq. (26):

$$\frac{U_d}{U} = \frac{N_a}{\eta N_T} \quad . \tag{26}$$

Thus Eq. (51) can be used for the directivity of either density- or amplitude-tapered arrays by interpreting η as the amplitude taper efficiency ($\eta = 1$ for density taper) and replacing N by N_a, the number of active elements ($N_a = N_T$ for an amplitude-tapered array).

The minimum directivity degradation factor for circular density-tapered planar arrays is easily determined from Fig. 39. It is seen that for arrays with a maximum center density (P = 1), for low sidelobe tapers and for equal N_T, the density-tapered array has about 2 to 3 db less directivity than a similar amplitude-tapered array. However, as P becomes small, the ratio of the directivities approaches P.

The actual technique used for designing density tapers involves much "cut and try." Willey[24] uses an "annular ring" approach in which the array is divided into rings of one element spacing in width, and an attempt is made to distribute the elements evenly over the ring with a density corresponding to the integral over that ring of the amplitude taper being used as a model.

3. Array Factors for Arrays on Curved Surfaces

It has been pointed out that there are a number of pattern effects which accompany the scanning of the beams of a linear or planar array. These effects become so pronounced at wide angles

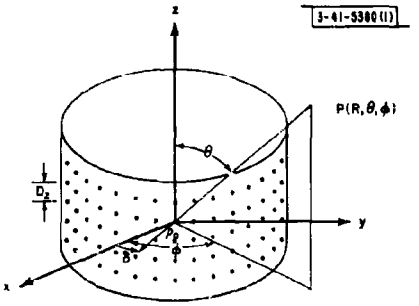

Fig. 42. Array of isotropic sources on a cylindrical surface.

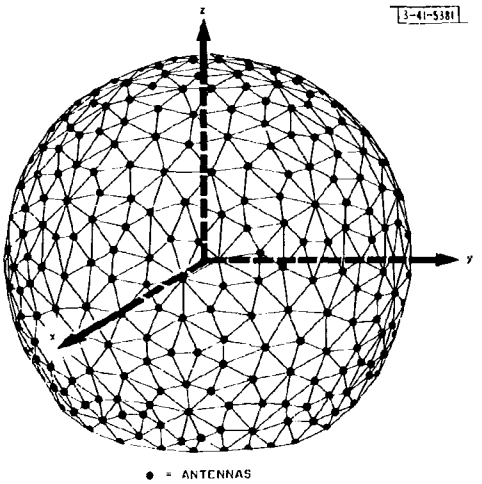

Fig. 43. Array of isotropic sources on a spherical surface.

of scan that the usable "field of view" of such arrays is limited. It seems logical, then, to examine arrays on surfaces of revolution such as cylinders and spheres, as indicated in Figs. 42 and 43.

There are a number of obvious advantages to such arrays and some disadvantages. Constancy of beam shape with scan angle along the curved surface is an obvious advantage. Furthermore, no grating lobes will be obtained from such arrays, since the appropriate form of Eq. (42) is not periodic. Finally, there are certain phasing techniques which are naturally adaptable to arrays on such surfaces.†

These advantages have led to widespread use of cylindrical arrays, particularly in communications applications where scanning in only one plane is required (φ-plane of Fig. 42).

Despite the lack of real grating lobes, it is found necessary to use a spacing along the array arc of appreciably less than a wavelength‡ with most published synthesis work based on using $\lambda/2$ or less.[40-42]

† For example, the Luneburg lens (Sec. III-B, also Ref. 43), the Wullenwebber array (Ref. 44) and the radial waveguide scanner (Ref. 45).
‡ Unpublished work of R. Tang, Hughes Aircraft Co., Fullerton, California.

The spherical surface possesses some intrinsic difficulties for array design. For large numbers of elements, it is impossible to space all elements by equal distances, and one incurs the difficulties of unequally spaced arrays, as pointed out in Secs. II-A-2 and II-C-1. In addition, there are polarization difficulties that arise with real elements, in that it is impossible to preserve the spherical symmetry; one cannot arrange the radiators so that all appear to be polarized in the same direction from all angles. Thus, if in-phase radiation is to be obtained over wide angles, one must vary both the phase of the elements and their polarization as a function of scan angle.

An important consideration to the systems designer is the number of array elements required for a given radar task, and the question of what array surface minimizes the total number of elements is certainly germane. However, a discussion of this point will be deferred to Sec. II-C-1, since the properties of real antenna elements influence the conclusion.

In addition to synthesis techniques tailored to arrays on curved surfaces,[40-42] one can make use of the amplitude and density tapers appropriate for planar arrays and linear arrays for large curved arrays, at least qualitatively, by choosing the element drives such that a geometrical optics projection of the array illumination onto a fictitious flat aperture between the observer and the array has desirable properties.† However, it will be seen that the transition from isotropic elements to real elements can alter any conclusions about curved arrays much more so than for flat arrays.

C. Arrays of Real Radiators

The extension and modification of the results of the previous discussions for application to arrays of nonisotropic radiators will be pursued in this section. We shall hereafter restrict ourselves only to the assumption that all elements are nominally identical.

There are many types of radiators usable in array antennas, even for wide-angle scanning arrays in which the element spacing requirement somewhat restricts the number of usable types to those of small ($\approx\lambda/2$) cross section. Among element types considered for such arrays are dipoles, slots, helices, spirals, open-end waveguides (horns), log-periodics,[47] conical log-spirals[48] and polyrods.[49] These radiators, when examined singly (an isolated antenna in free space), offer a range of polarization, pattern, and impedance characteristics which have been the subject of investigation elsewhere in the literature and will not be explored here. This restriction is due not only to a space limitation, but also to the fact that the properties of an antenna when isolated are not the sole, or often even the dominant, determinant of the performance of the array. An important additional parameter is the "mutual coupling" between antenna elements.

For example, the modification that must be made of our isotropic radiator theory to account for the effect of real radiators on array patterns will be shown to involve the patterns obtained when the elements of a large array are excited, one at a time, while all others are passively terminated in the impedance from which they are usually driven. If the antennas did not couple to each other through their fields, these "element patterns" would all be identical to the pattern of an isolated antenna of the same type. However, the radiators do couple, and for close spacings the coupling is sufficiently strong so that the radiation from the surrounding elements, due to parasitically induced currents, causes the pattern of an element in the environment of an array

† Some computed patterns for cylindrical arrays based on this technique can be found in Ref. 46.

of terminated elements to differ markedly from the pattern of an isolated element in amplitude, phase, and perhaps polarization as well.

In addition to affecting the array pattern performance through its effect on the element factors, the coupling between antennas represents a source of concern to transmitter and receiver engineers. On transmission, the coupling of energy from one antenna into a second sets up a wave in the field of antenna number two traveling toward the generator of that antenna. Since the output of generator one is coherent with the output of generator two, differing only in relative phase (depending upon the direction in which the array beam is pointed), a standing-wave pattern is set up in the feed of the antenna. This coupling between transmitting antennas, therefore, can be conveniently modeled by considering the antenna as possessing an apparent driving impedance that would cause the same standing-wave pattern. This impedance varies with the phasing of the array (beam pointing direction). The transmitter engineer has to contend with this load variation and its possible attendant problems, such as transmitter detuning (pulling) and breakdown problems due to the standing wave. In a receiving array, the current excited on each antenna by the incident wave sets up a scattered field which couples to other antennas. The effect of this coupling is such that the receiver input impedance that extracts the maximum power from the incident wave is the same as the optimum generator impedance for the same array as a transmitting array. Thus the receiver engineer must be concerned with coupling for receiver input impedance consideration.

In the following pages, we shall attempt to examine the magnitude of the foregoing effects and their implications on array performance. First, we shall examine the effects of real radiators on the patterns of arrays and arrive at a relatively simple representation for the patterns which is applicable to the most important types of arrays for radar use. An expression for the gain of such arrays of real radiators will then be formulated. The expression for the pattern shape and the gain of the array will include mutual coupling effects implicitly through an "element factor" and a related "element gain function" (the latter is later demonstrated to involve the element impedance variation with scan). We shall then present analytic results for the element pattern, gain function, and impedance variations for an important (and analyzable) type of array element: dipoles above a ground plane. Finally, we shall estimate the extent to which the dipole results are applicable to other types of radiators, and indicate a possible fundamental limit on the extent to which the choice of radiator type can reduce the coupling problems, particularly that of the apparent element impedance variation with scan angle.

1. Effects of Real Radiators on Array Patterns

For a large class of arrays, it is possible, both in theory and practice, to drive one single element of an array while all others are terminated in their normal drive impedance. Such is the case whenever we can consider the element drives to be independent generators,† as shown in Fig. 44, such that all voltage generators but one can be shorted without affecting the circuit impedance of any antenna. We can determine the pattern of each element in the array when that element is driven with a voltage such that one ampere of current flows into the antenna terminals

† Some additional effects of mutual coupling on arrays which cannot be considered to be independently driven are examined in Sec. III-B-1.

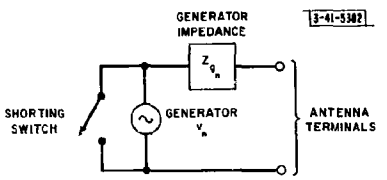

Fig. 44. Equivalent circuit for n^{th} element drive of independently driven elements.

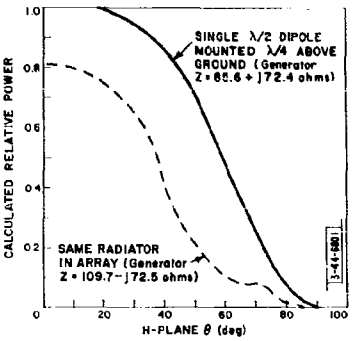

Fig. 45. Comparison of magnitude of single dipole pattern and pattern of dipole in large array of similar radiators on a 0.6-λ square grid.

at some zero phase reference and call this vector quantity $\vec{f}_n(\varphi, \Theta)$ for the n^{th} element. Then, by superposition, for an arbitrary array surface, we have from Eq. (42) that the array vector far field is

$$\vec{F}(\varphi, \Theta) = \sum_n' i_n \vec{f}_n(\varphi, \Theta) \exp[jk\overline{\rho_n} \cdot \hat{R}] \quad , \tag{62}$$

where,† more explicitly stated,

$\vec{f}_n(\varphi, \Theta)$ is the vector pattern obtained when only the n^{th} element is driven, with one ampere of current, with all other elements terminated in their usual generator impedance and any ground planes and reflectors in place, and

i_n is the current in amperes that would be flowing in the n^{th} feed line if all other elements were passively terminated in their usual generator impedance (i.e., the current in the n^{th} feed due solely to the n^{th} element generator, not including that coupled into the n^{th} element from any other generators).

The utility of these definitions (Sec. II-C-3 considers a different, compatible set) arises from the fact that, both computationally and experimentally, one driven element in a passively terminated array is easier to cope with than all elements simultaneously driven, and many important effects of mutual coupling can be ascertained from the element patterns.

Since $\vec{f}_n(\varphi, \Theta)$ is actually the pattern of the entire array when the excitation of the array is that due to mutual coupling among the elements when only the n^{th} element is driven, it is a function not only of the particular radiator configuration, but also of the location of the driven radiator relative to the other elements of the array and the element generator impedances.

For example, Fig. 45 illustrates a typical computed difference between a power pattern ($|\vec{f}_n|^2$) of a single dipole above ground and the element pattern of that same dipole completely surrounded by a field of similar dipoles. The dipoles are spaced on a $D_x = D_y = 0.6\lambda$ grid, and are mounted

† The quantities $\vec{F}(\phi, \theta)$ and $\vec{f}(\phi, \theta)$ may be thought of as representing either the E- or H-fields, as long as the two are compatible.

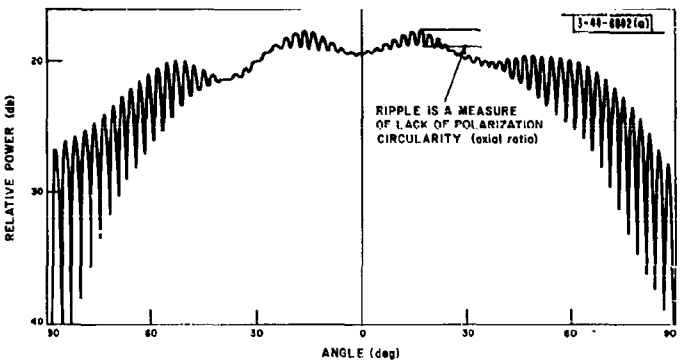

(a) Pattern of single element in large ground plane.

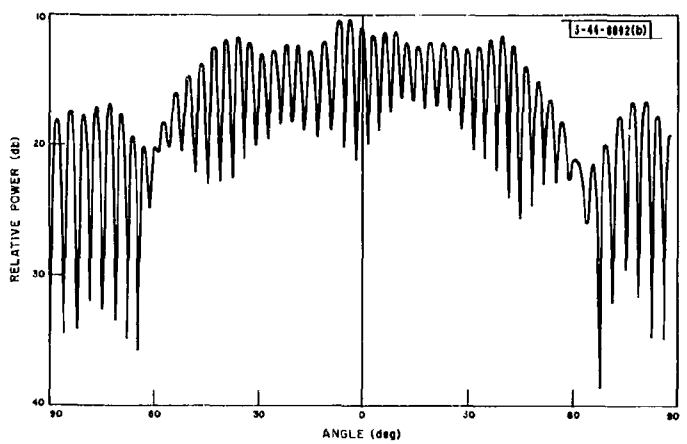

(b) Gain function of center element of 7-element array.

Fig. 46. Depolarization of element when placed in array. (Both figures reprinted, with permission, from L. I. Parad and R. W. Kreutel, Ref. 50.)

a quarter-wavelength above a large, perfectly conducting ground plane. The generator impedances indicated are those that maximize $|f(0,0)|^2$ in the two cases. The difference between the isolated behavior and the "in the array" behavior is evident.

For radiators which can support more than one polarization mode, the polarization of an element may also be different in and out of an array. Circularly polarized radiators, such as helices, spirals, etc., have been shown[50] to be capable of coupling in such a manner that if one excites the terminal of such a radiator which produces left-hand circularly polarized radiation in an isolated radiator, the "first-time-around" coupling to adjacent radiators appears at the terminal which would radiate right-hand circular polarization. If this terminal is not properly terminated (as might be the case if the radiators were designed for only a single polarization, such that no physical termination is provided for the opposite sense), the parasitically induced radiation caused by the coupling to the driven radiator will be largely opposite sense. Thus the mutual coupling can cause undesirable deviations from circular polarization. Furthermore, the deviation varies with angle. An example of this effect is indicated by Fig. 46, showing the pattern of an open-waveguide, circularly polarized radiator when isolated, and when it is the center element of a 7-element array.[50] The patterns were taken by spinning a receiving dipole rapidly so that the "fine-grain" ripple measures the departure of the pattern from pure circular polarization. The depolarization and its variation are evident.

Finally, coupling may alter the phase of the radiator pattern at a given point in space, but the consequences of this alteration are usually negligible in large arrays.

Unfortunately, expressions for the $\vec{f}_n(\varphi, 0)$ for any radiator type are quite complicated if they are obtainable at all. Nevertheless, all the element patterns as defined in Eq. (62) could be individually measured or perhaps numerically calculated. This is not usually necessary, fortunately, if the array is regularly spaced. One can formulate an argument (Ref. 14, pp. 187-193) that for the usual radar case of elements polarized parallel to a ground plane, the effects of mutual coupling (e.g., induced current between two elements) varies with separation D, at least as fast as $1/D^2$ for large D. With this asymptotic behavior, the effect of mutual coupling is quite localized in cases of practical interest. Thus the variation of element patterns and element impedance in a large, regularly spaced array can be satisfactorily measured or calculated on a much smaller array. For example, measurements on dipole arrays usually indicate that elements more than two positions from the array edge have practically identical element patterns, as typified by Fig. 47, which shows the H-plane power patterns of some of the first eight elements of an array of 16 equally spaced (0.58λ) parallel dipoles (the second eight patterns tend to be mirror images). It is seen that only the outer element patterns differ noticeably, and the other three elements shown are, for practical purposes, identical. The degree to which the similarity of element patterns depends upon the elements being equally spaced can be seen by reference to Fig. 48, which shows some of the patterns of the first eight elements of an unequally spaced array (Ref. 11 and Ref. 12, Part 3, Ch. I, Sec. C).

It is seen from Eq. (62) and Figs. 47 and 48 that the element patterns weight the currents in a manner which varies with angle; that is, if we fix the angles φ_1 and θ_1, the scalar representation of the far field of the array at those angles will be the same as that of an array of isotropic (nondirectional) radiators, having exciting currents i'_n:

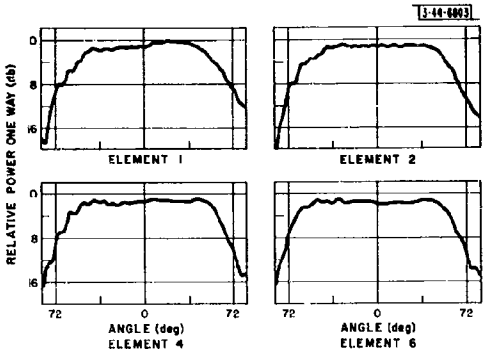

Fig. 47. H-plane element patterns of dipoles $\lambda/4$ above ground in equally spaced parallel linear array.

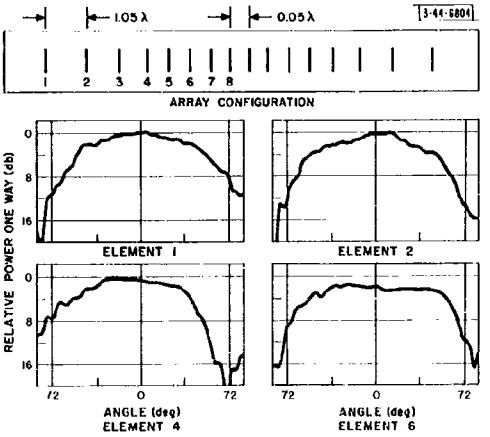

Fig. 48. H-plane element patterns of dipoles $\lambda/4$ above ground in unequally spaced parallel linear array.

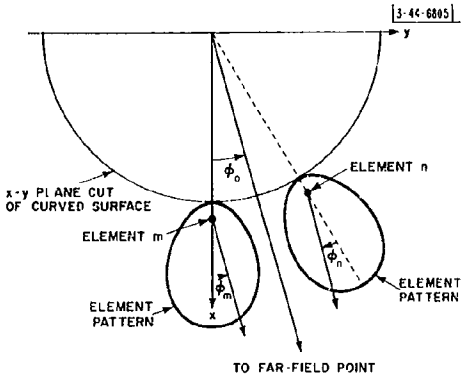

Fig. 49. Element pattern geometry for curved arrays.

$$F(\varphi_1, \Theta_1) = \sum_m \sum_n i'_n \exp[jk(x_n \sin\Theta_1 \cos\varphi_1 + y_n \sin\Theta_1 \sin\varphi_1)] \quad , \tag{63}$$

where the apparent drives i'_n are given by the product of the actual current and the scalar element pattern at the angles in question:

$$i'_n = i_n f_n(\varphi_1, \Theta_1) \quad .$$

Let us assume that we were dealing with an array on a flat surface, so that the broadside angle relative to each array element is the broadside angle of the array (as contrasted to, for example, a cylindrical array for which the element broadsides differ, as indicated in Fig. 49). Then reference to Fig. 48 indicates that for an equally spaced array, if the i_n were adjusted so that all i'_n were unity at broadside (zero degrees), over a region of perhaps ±45° scan angle the apparent drives would differ by a more-or-less random variation of only about half a decibel with the outer elements ± 1 db from the average (recalling that the remaining 8-element patterns are nearly mirror images). Consequently, it is seen that for large arrays of identical, equally spaced radiators, all the element patterns are nearly identical; therefore, for a flat array, we can approximately factor the element pattern and define a typical element factor as

$$\vec{f}(\varphi, \Theta) = \vec{f}_{mn}(\varphi, \Theta) \quad , \quad \text{for nearly all m, n, } \varphi, \Theta$$

and write the array pattern as

$$\vec{F}(\varphi, \Theta) \approx \vec{f}(\varphi, \Theta) \sum_m \sum_n i_{mn} \exp[jk(mD_x \sin\Theta \cos\varphi + nD_y \sin\Theta \sin\varphi)] \quad , \tag{64}$$

where the summation is recognized as the array factor of the previous sections. This approximation is called "pattern multiplication," inasmuch as the array pattern is approximately the product of the element factor and array factor. For this case, we see that the effect of $\vec{f}(\varphi, \Theta)$ is just to scale the entire array factor with angle. The array factor governs the pattern "fine structure" with the element factor playing the role of an "envelope," if the element factor is reasonably smooth.

For arrays on curved surfaces, we cannot factor Eq. (62). However, if the elements are regularly spaced, the $\vec{f}_n(\varphi, \Theta)$ will be nominally identical relative to their own element broadside; and the $\vec{f}_n(\varphi, 0)$ will produce a smooth taper on the array which varies with angle, as indicated by Fig. 49, and can usually be satisfactorily accounted for in pattern computation.

In some cases, we should expect trouble if Eq. (64) is used without care even for flat arrays. Therefore, let us delineate some of the troubles that might be expected, since we shall use this equation extensively.

First, we have seen by an example (Fig. 47) that the outer elements represent the worst deviation from the typical element factor. The squint of the outer elements can cause pattern deterioration, raising sidelobe levels and causing pointing error. The extent of these errors depends upon the relative contribution of the outer elements; hence, upon the size of the array and the i_{mn}'s used. For both planar and linear arrays, the two outer elements (rows and columns for planar arrays) differ notably from the remainder. Thus, for arrays small enough that the "outer" elements are a substantial fraction of the total, it may be desirable to add "dummy" elements at the array edges to regularize the outer element patterns. Second, for similar reasons, and in a similar manner, ending the ground plane close to the outer elements can contribute

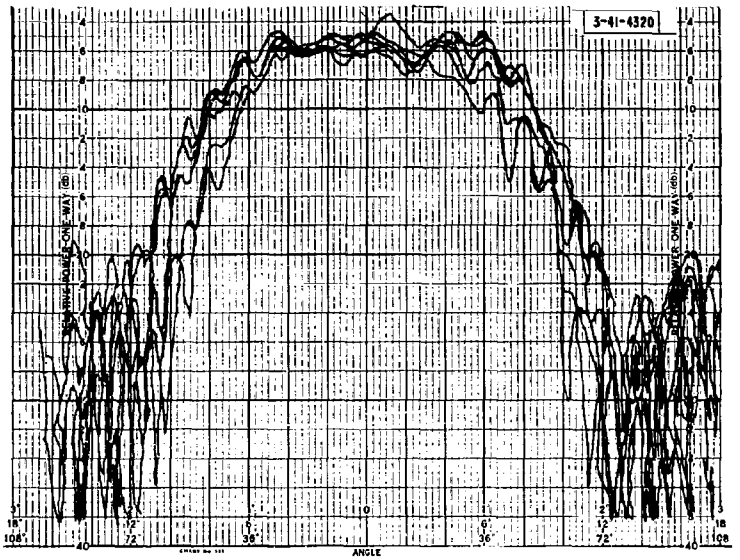

Fig. 50. Superimposed element pattern of even-numbered elements of log-periodic array, looking into reflector.

to irregularities in the edge element patterns, as can edge effects of reflectors when arrays are used as reflector feeds. Third, if some care is not exercised in the design and construction of "identical" elements, they may not have repeatable patterns even near the center of the array, as illustrated by the superimposed patterns of even-numbered elements of a 16-element linear array shown in Fig. 50. Even in this case, however, Eq. (64) can be useful if an average element pattern is used and the deviations of the element patterns are treated as random errors (Sec. II-D). Finally, element factors must be reasonably smooth, with any ripple slowly varying compared with the array beamwidth. If this criterion is not met, the weighting of the element factor of Eq. (64) can produce objectionable pattern distortion with scan angle (Ref. 14, pp. 24-38).

It is apparent that ideal element patterns are identical and smooth. As usual, the ideal is not quite achieved in practice, but is well approximated with careful engineering.

2. Gain of Arrays as a Function of Scan Angle

We are now in a position to investigate the gain of the array as a function of the beam pointing (scan) angle, since gain is related to the properties of real radiators through both the element factor of the radiators and their impedance properties.

A definition of gain, consistent with the common usage of the term in the radar equation, is obtained by defining the gain as the ratio of the power density per unit solid angle at the beam pointing angle to the total power available to the antenna per unit solid angle (the total power divided by the factor 4π). By this definition, the degradation in system performance due to any impedance mismatch in the antenna structure is assigned as a decrease in array gain, including mismatches due to mutual coupling effects. It will be recalled that directivity is defined with respect to the total power radiated; hence, only for arrays which are lossless and exactly impedance matched will gain and directivity be equal.

Proceeding with the above gain definition, if it is assumed that the n^{th} antenna of a linear or planar array is connected (as shown in Fig. 44) to a voltage generator having an open-circuit voltage v_n and an impedance whose real part is R_g for all n, we can then proceed to show that (Ref. 10, Part 3, Ch. I) if edge effects are neglected (the array is assumed to be very large), the gain of the array at scan angle φ_o, Θ_o is given by†

$$G(\varphi_o, \Theta_o) = g(\varphi_o, \Theta_o) \frac{\left|\sum_n v_n\right|^2}{\sum_n |v_n|^2} \quad , \tag{65}$$

where $g(\varphi_o, \Theta_o)$ represents the gain of an individual, typical element measured in its array environment at the angle of scan φ_o, Θ_o and is termed the element "gain function." It is, except for a scale factor, the square (power pattern) of the magnitude of the element factor $\vec{f}(\varphi_o, \Theta_o)$ of Eq. (64). The ratio of the summations is of the same form as the analogous quantity in the directivity expression; therefore, we can write the gain of an array by using either a density or amplitude taper as

$$G(\varphi_o, \Theta_o) = g(\varphi_o, \Theta_o)\, \eta N_a \quad , \tag{66}$$

where η and N_a are as defined for the directivity equations (27) and (51). Thus the gain of an array is specified by the number of active elements, the amplitude taper efficiency, and the gain function of a typical element. The effects of scan on the gain of an array are completely described by the gain function of a typical element in the array environment.

This element gain function is an important tool for array design, since it can be accurately determined from an array of elements only large enough so that the pattern behavior of the center element is unaffected to whatever degree desired by the addition or deletion of outer elements. For experimental work, we can inexpensively construct such an assembly and study the effects of antenna element types, spacing, terminations, and so forth, by noting these effects on an antenna pattern recorder. In fact, for types of antenna elements for which no satisfactory analytic description of mutual coupling exists, this is the most convenient approach to a description of the effects of mutual coupling on array gain. It will also be shown that mutual coupling effects on element impedance can often be inferred to some extent by use of the gain function.

A qualitative indication of the shape of gain function can be inferred from the array factor directivity discussion of Sec. II-B-2. For a large planar array, which is tapered so that almost all the radiated power is in the region close to the main beam, if the element pattern is smooth over such a region (an assumption which can always be improved by making the array larger), the element pattern should have little effect on the array directivity. Therefore, Eq. (51) expresses the directivity of arrays of <u>real</u>, as well as isotropic, radiators when no grating lobes

---

† The restriction to a flat array is required in order to factor out the gain function. A corresponding relationship for arrays on curved surfaces is

$$G(\phi_o, \theta_o) = \frac{\left|\sum \sqrt{g(\phi_n, \phi_o, \theta_n, \theta_o)}\, v_n\right|^2}{\sum |v_n|^2} \quad , \tag{66a}$$

where the n^{th} element gain function now depends on the difference between the beam pointing angle ϕ_o, θ_o and the n^{th} "element pointing angle" ϕ_n, θ_n.

are visible. Furthermore, since the directivity bounds the gain, comparison of Eqs. (51) and (66) indicates that

$$g(\varphi, \theta) \leq 4\pi \frac{D_x D_y}{\lambda^2} \cos\theta \quad , \tag{67}$$

where equality can apply only for a lossless structure at an angle for which the array is matched, including mutual impedance effects. Finally, we can even remove the restriction that Eq. (67) applies only to planar arrays if any curvature is negligible over the region of appreciable mutual coupling (according to the results cited in the previous and following sections, an interval of perhaps three elements in all directions).

3. Mutual Coupling in Arrays of Dipoles Above a Ground Plane

In order to give the reader some quantitative appreciation for the attributes of the gain function achievable in practice, the extent to which the shape of the gain function can be "tailored," and the type of element impedance variations which may be encountered in a scanned array, we shall examine an array of one type of radiator in some detail. The only types of radiators for which the mutual coupling has been analytically described are resonant types of simple geometry (idealized dipoles and slots). Therefore, in this section, attention will be focused on the important practical case of equally spaced arrays of thin, half-wavelength dipoles above a large ground plane. Some analysis of slot arrays and arrays of dipoles without ground planes can be found elsewhere.[51]

The primary reasons that the theoretical analysis of mutual coupling has been restricted to such a limited sample of possible radiators arise from the fact that quantitative analysis of the coupling between two closely spaced antennas represents a very complex problem. The complexity is due to several factors. First, in addition to radiation field coupling, induction and static field coupling may predominate close to the antenna.† Second, a traveling wave on one of a pair of conductors tends to couple energy directionally to the other[52] (in effect, is a directional coupler); hence, it appears that antenna elements of the traveling-wave variety (helices, spirals, log-periodics) may experience directional coupling effects between close neighbors (Ref. 49, Figs. 9 and 13; Ref. 53; Ref. 14, pp. 183-186).

All these factors can be accounted for by an equivalent circuit of the form shown in Fig. 51 (for independently driven elements), but the effects of the resulting coupling have not been extensively analyzed in terms of such a circuit.

However, for geometrically simple standing-wave antennas, such as dipoles and slots, a simplification of this equivalent circuit to that of Fig. 52 can be made, and the mutual coupling between antennas can be completely described in terms of measurements made at the antenna terminals. A conventional description is that of the mutual impedance Z_{mn}, defined as the ratio of the mutually coupled open-circuit voltage v'_m, existing at the m^{th} antenna terminals due to a current‡ I_n flowing in the n^{th} antenna terminals:

---

† An example of the latter is the case of two collinear dipoles having very little separation between the ends of the dipoles. The result is heavy coupling due to capacity effects, in addition to radiational coupling.

‡ Note that this I_n is the total current flowing in the n^{th} element terminals, whereas the i_n's previously used are partial currents (the current in the n^{th} antenna due only to the n^{th} element generator).

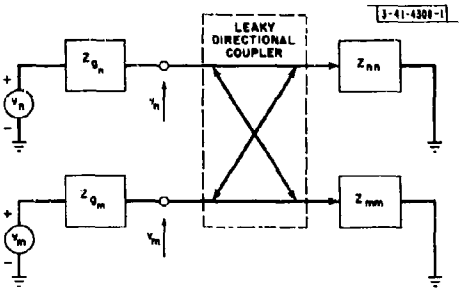

Fig. 51. General equivalent circuit for independently driven, mutually coupled antenna elements.

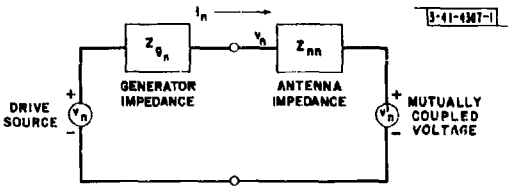

Fig. 52. Simplified equivalent circuit for standing-wave elements.

$$Z_{mn} = -\frac{V'_m}{I_n}$$

and, by reciprocity, $Z_{nm} = Z_{mn}$. The negative sign accounts for a positive mutually coupled voltage exciting a current flow in a direction opposite to that of the generator driving the element, as can be seen from Fig. 52.

This concept allows the analysis of the effects of mutual coupling in standing-wave elements to be pursued on a circuit-analysis basis, and the effects of mutual coupling on dipole arrays can be completely described by a set of simultaneous equations. For the circuit configuration of Fig. 52 (assuming that the coupling between feed structures, which carry traveling waves, is negligible), the currents actually flowing on the elements of the array are related to the drive voltages by the matrix equation

$$[V] = [Z][I] \quad , \tag{68}$$

where [V] and [I] are column matrices of the drive voltages and total element currents and the Z-matrix is composed of diagonal elements $Z_{nn} = Z_{g_n} + Z_{a_n}$, where Z_{g_n} is the n^{th} generator impedance and Z_{a_n} is the n^{th} antenna self-impedance, and off-diagonal elements which are the mutual impedances.

The validity of this approach rests upon the assumption that one can define the plane of the antenna termination such that open-circuiting the antenna at that point entirely negates that element's effect on the array. For example, for thin dipoles and thin slots, an open circuit at the junction of the feed line and the radiator proper forces the current to be zero everywhere on the element, which is equivalent to its physical removal.

Calculated mutual impedance values† for infinitely thin, half-wavelength dipoles mounted a quarter-wavelength above an infinite ground plane are plotted in Fig. 53, in terms of center-to-center spacing. For comparison, the self-impedance (Z_a) of the dipole a quarter-wavelength above ground is approximately 85.7 + j72.5 ohms. It is seen that for close spacings, particularly in the collinear case, the mutual impedance is nearly comparable to the self-impedance but decays rapidly for greater spacings.

† Data from Carter's equations, as given by Ref. 7, Ch. 10.

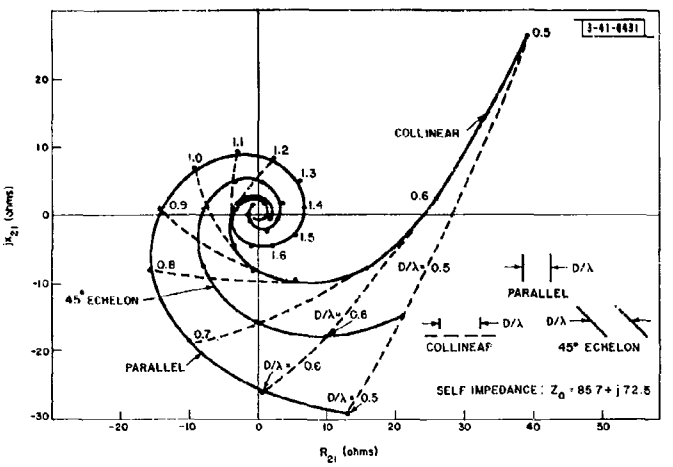

Fig. 53. Mutual impedance vs center-to-center spacing D/λ for infinitely thin λ/2 dipoles, λ/4 above ground plane.

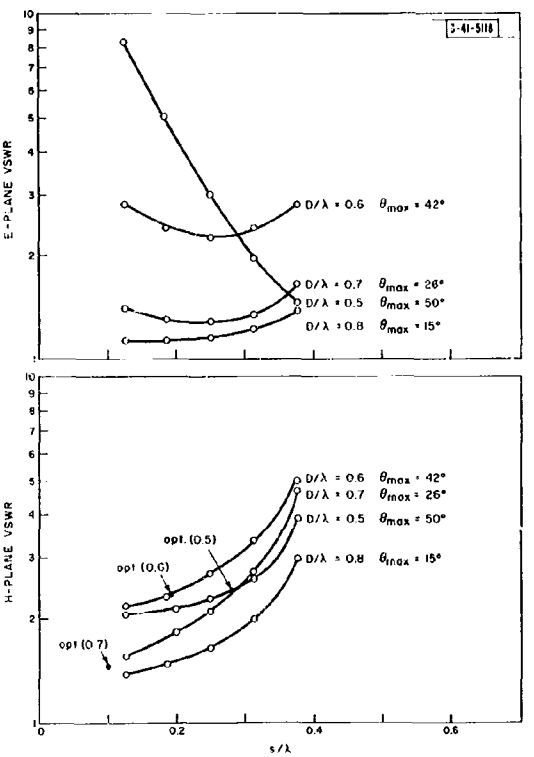

Fig. 54. Maximum VSWR encountered in scanning planar array of dipoles to θ_{max} (match at $\theta = 0$).

The set of equations (68) can be formally solved for the I_n's by matrix inversion

$$I] = [Y]\, v] \quad . \tag{69}$$

For a large array, this is a gruesome task, even for one specific configuration. Fortunately, a useful approximate solution can be obtained by physical reasoning, and some insight gained in the process.

If the array is very large so that edge effects, amplitude taper, and any curvature of the array surface are negligible over an interval of several elements in each direction, the currents in the elements not near the array edges will bear a known relation to each other, and a constant relation to their drive voltages independent of n (they will all have the same apparent impedance). In a linearly phased planar array, if an element near the center is chosen as the origin of coordinates, the relationship between the currents for a pointing angle φ_o, θ_o must be of the form

$$I_{mn}(\theta_o, \varphi_o) \approx I_{oo} \exp[-jk(mD_x \sin\theta_o \cos\varphi_o + nD_y \sin\theta_o \sin\varphi_o)] \quad .$$

In this case, a typical equation of (68) can be manipulated to give the apparent driving point impedance of a typical antenna when it is phased to "look" in the direction φ_o, θ_o, denoted $Z_D(\theta_o, \varphi_o)$, as (Ref. 54; also Ref. 10, Part 3, Ch. I)

$$Z_D(\varphi_o, \theta_o) = Z_a + \sum_{\substack{m\ n \\ m,n\neq 0}}\sum' Z_{oo,mn} \exp[-jk(mD_x \sin\theta_o \cos\varphi_o + nD_y \sin\theta_o \sin\varphi_o)] \quad , \tag{70}$$

where the notation $m, n \neq 0$ implies that the term $m = 0$, $n = 0$ is omitted, and the unsubscripted terms are understood to apply to the element under consideration, which is taken for reference as the element centered on the coordinate system ($m = 0$, $n = 0$).

This driving impedance is the sum of the self-impedance of the antenna Z_a and the "phased" mutual impedances, represented by the summation. Studies[54] of $Z_D(\varphi_o, \theta_o)$ show that for given element spacings and maximum scan angles, there is a height for the dipoles above the ground which minimizes the maximum VSWR when the array is scanned; for example, Fig. 54 shows the maximum VSWR encountered in a planar array with a square element grid ($D_x = D_y$) in scanning to the grating lobe angle θ_{max} in both principal planes or, for $D/\lambda = 0.5$, to an arbitrary value of 50°. Figures 55 through 57 show Smith chart plots of the impedance vs scan for three different spacings for nearly optimum heights s. The impedances are normalized to the indicated value of $Z_D(0,0)$. Also shown, as an indication of the change in element impedance due to mutual coupling, is the normal impedance of an isolated dipole mounted the same distance s above ground, normalized to $Z_D(0,0)$. It is apparent that attempts to achieve scan angles with dipole planar arrays greater than 90° to 100° central angle will meet with severe VSWR problems, and that even modest scan angles produce VSWR's that may be of concern to transmitter and receiver designers concerned with maintaining the high gain and phase stability required for good antenna patterns (see Sec. II-D).

The maximum scan angles indicated in Figs. 55 through 57 for each spacing represent the scan angles at which the main lobe and a grating lobe are symmetrically disposed about broadside, indicating that one has scanned through a complete period of the array factor. Beyond this angle, the impedance variation retraces backward along the indicated path.

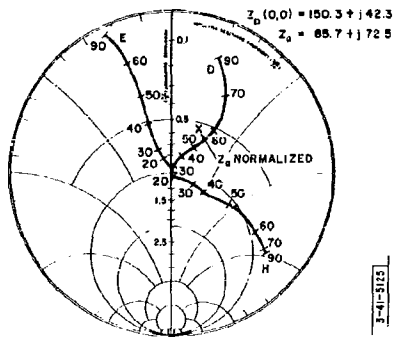

Fig. 55. Variation in normalized driving impedance with scan angle for element spacing $D = 0.5\lambda$ and element height above ground plane $s = 0.25\lambda$.

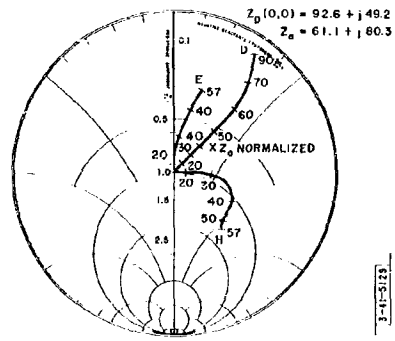

Fig. 56. Variation in normalized driving impedance with scan angle for element spacing $D = 0.6\lambda$ and element height above ground plane $s = 0.187\lambda$.

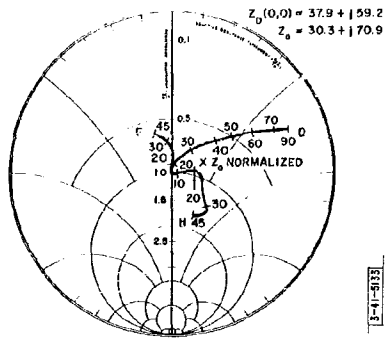

Fig. 57. Variation in normalized driving impedance with scan angle for element spacing $D = 0.7\lambda$ and element height above ground plane $s = 0.125\lambda$.

The element gain function $g(\varphi_o, \theta_o)$ can be formulated in mutual impedance terms for dipoles in terms of the gain function of a single, isolated, matched element† $g_{max}(\varphi_o, \theta_o)$ as

$$\frac{g(\varphi_o, \theta_o)}{g_{max}(\varphi_o, \theta_o)} = \frac{4R_g R_a}{|Z_g + Z_D(\varphi_o, \theta_o)|^2} \quad . \tag{71}$$

To maximize the gain function at an angle φ_1, θ_1, the generator impedance should be chosen so that

$$Z_g = Z_D^*(\varphi_1, \theta_1) \quad ,$$

where the asterisk denotes the complex conjugate. For such an impedance, the element gain function and the reflection coefficients $\Gamma(\varphi_o, \theta_o)$ seen by the generator (for zero line length between the antenna and the generator) are easily shown to be related to the scan angle by

$$\frac{g(\varphi_o, \theta_o)}{g_{max}(\varphi_o, \theta_o)} = \frac{R_a}{R_D(\varphi_1, \theta_1)} |1 - \Gamma(\varphi_o, \theta_o)|^2 \quad . \tag{72}$$

It is apparent from this relationship that "tailoring" the element parameters so that the gain function of an isolated element and that of the element in the array are as similar as possible will lead to minimum impedance variation. This is one method of explaining the variation of the maximum VSWR with dipole height above ground and the success of some workers in using "fences" or "baffles" as part of an element.[55]

By the use of well-known formulas for $g_{max}(\varphi, 0)$ [see Ref. 7, Eq. 11-87, p. 305], and a relationship for $R_D(\varphi, 0)$,[56] one can show that if the elements are matched for maximum gain with the array phased for broadside radiation, the broadside gain of the array will be the well-known result predicted by Wheeler[57] and implied by directivity considerations (as outlined in Sec. II-C-2)

$$G(0, 0) = \frac{4\pi A \eta}{\lambda^2} \quad . \tag{73}$$

Equations (67) and (72) represent a useful practical connection between element impedance properties and array geometry for elements which do not exactly fit the theoretical model. For example, one can measure the value of R_a and $g_{max}(\varphi_o, \theta_o)$ associated with an element. Consequently, one can determine the optimum generator resistance $R_D(0, 0)$ for a given spacing for minimizing the gain of the array at broadside by noting that, from the cited equations,

$$R_D(0, 0) = g_{max}(0, 0) \frac{R_a}{4\pi D_x D_y / \lambda^2} \quad .$$

Actual calculations of the element gain functions[10,53] indicate that the gain function shape depends primarily upon the element spacing (the area allotted each element), as Eq. (67) indicates. It is little affected by dipole-to-ground plane spacings, if the optimum driving impedance is used for each spacing.

Figures 58 through 60 show computed gain functions of dipoles on square grids, approximately‡ optimally matched at broadside. It is seen that the effect of the mutual impedance is to

† If the elements of the array are mounted on a ground plane, the term "isolated element" implies a single element similarly mounted.

‡ The computational program used in the gain function calculations (Refs. 12 and 54) was slightly inaccurate in determining the impedance for best broadside match, resulting in a slightly less than optimum choice. This factor also accounts for the "ripples" in the gain functions, as especially noticeable in Fig. 58.

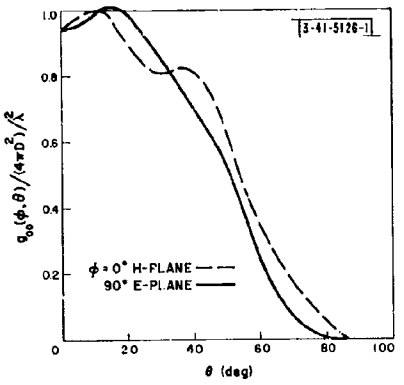

Fig. 58. Normalized gain function for element spacing D = 0.5 λ and element height above ground plane s = 0.25 λ.

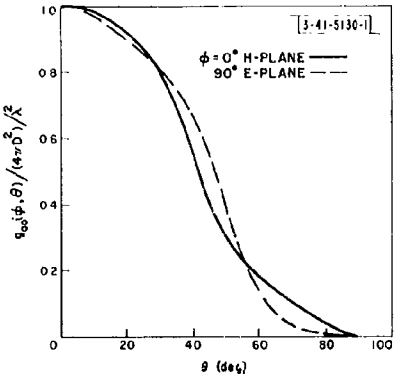

Fig. 59. Normalized gain function for element spacing D = 0.6 λ and element height above ground plane s = 0.187 λ.

"impart the knowledge" of the antenna spacing to the gain variation of the element, and hence to the gain of the array. The element gain increases with increasing spacing around broadside but drops for angles that correspond to grating lobe formation for flat arrays.

4. Some Comments on the Dependence of Coupling Effects on the Type of Radiators Used

Perhaps the most likely objection to dipoles as radiators, as indicated in the previous section, is the substantial variation in impedance that must be coped with when scanning in two dimensions.† Thus the logical question arises as to what type of radiators, if any, can be used to achieve more constant element impedance.

Unfortunately, the present state of knowledge is lacking for confirmed answers. Mathematical analysis of the coupling between more complex elements than dipoles and slots does not exist. Furthermore, the experimental data that exist for more complex radiating elements are generally contradictory or inconclusive. However, we are not at a total loss for further theoretical indications concerning the impedance variation of arbitrary elements in large arrays. Although we cannot describe the configuration of the "best" element from an impedance variation standpoint, we may be able to bound its behavior.

A recent theoretical analysis (Ref. 12, Part 3, Ch. 1, Sec. B. 5) predicts that the minimum VSWR obtainable as a function of scan angle from any linearly polarized, lossless‡ element in a regularly spaced planar array is only slightly (less than 10 percent) superior to that attainable using thin dipoles on half-wavelength centers at their optimum height above ground (Fig. 55). The study predicts that no element can incur a VSWR in scanning to an angle θ in both principal planes that is less in <u>both</u> planes than that given by the curve of Fig. 61. Based upon a similar analysis, however, Hannan[58] has concluded that it may be theoretically possible to introduce additional coupling between element feed lines and arrive at an essentially constant impedance over wide ranges of scan angles.

Since both these conclusions presently lack experimental confirmation, the subject of mutual coupling remains in need of better understanding.

5. Some Considerations About Curved Arrays of Real Radiators

The element gain functions are also a factor in choosing element spacings for large arrays on curved surfaces since, if the radius of curvature of the surface is large, the element gain functions will be little affected by the curvature and will have the same general properties previously determined for elements in flat arrays.

If the dipole data are considered as typical of most elements, reference to Fig. 49 and the dipole gain functions of Figs. 58 through 60 indicates that as the element spacing gets appreciably greater than $\lambda/2$, the effects of the element factor "sharpening" that accompanies increased spacing are to: (a) reduce the contribution of elements off the pointing axis to the pattern main

---

†The dipole gain functions are quite smooth over the region for which the grid spacing permits scanning without grating lobe performance, which seems to be all one can ask in this respect (some element types have been observed to raise difficulties on this count as well; recall Fig. 50).

‡For elliptically polarized elements, the possibility of polarization variation with scan may render the analysis upon which the above conclusion is based invalid. Furthermore, even a small amount of loss in the element feed will reduce the VSWR at a small cost in gain; for example, a 2.5:1 VSWR is reduced by the insertion of a 1-db loss in a feed line to a VSWR of about 1.7:1 at a cost of 1 db in array gain.

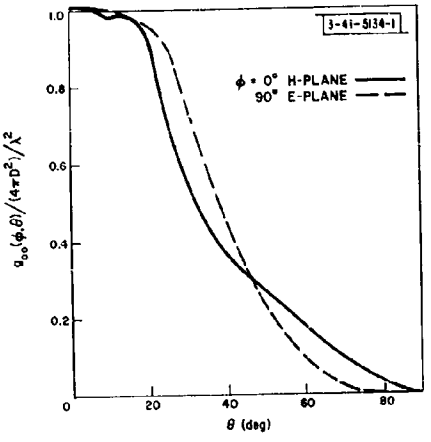

Fig. 60. Normalized gain function for element spacing D = 0.7 λ and element height above ground plane s = 0.125 λ.

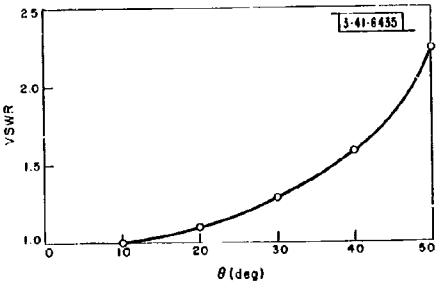

Fig. 61. Minimum VSWR obtainable with linearly polarized, lossless radiators when scanning to an angle θ_{max} in both principal planes of an array.

lobe, and (b) increase the radiation into the sidelobe region, unless one illuminates a smaller number of elements when wider spacings are used. Thus, whereas for planar arrays spacing limits the usable scan angle, for curved arrays it limits the subtended angle of the array which can contribute significantly to a beam in a particular direction. Consequently, spacings not much greater than $\lambda/2$ should be used for arrays on curved surfaces, with the exact spacing determined by calculation of array far fields in which element factors appropriate for the spacings are used.

Thus the restriction on element spacing is approximately the same for all geometries. Based upon this fact, we can also draw some conclusion about the dependence of the number of elements required for the frequently encountered task of hemispherical surveillance, as a function of the array surface chosen.

The element gain function of Fig. 58, Eq. (67), and the geometry of Fig. 49 indicate that for half-wavelength spacings, we could approximate the gain function of Eq. (66a) by

$$g(\varphi_n, \Theta_n, 0, 0) = \frac{4\pi a}{\lambda^2} \cos\Theta_n$$

for a pointing angle of $\Theta = 0$, where a represents the area allotted to a typical element. For a large spherical array, application of an integral approximation to Eq. (66a) for uniform illumination ($v_n = 1$) indicates that $G(0,0) \approx 8/9\pi R^2$. Thus, for hemispherical surveillance with a specified minimum gain, a comparison of this gain result with the surface area of a sphere $4\pi R^2$ indicates that very nearly the same number of elements are required for a spherical array as for four planar arrays.

D. Effects of Errors on the Patterns of Arrays

In the preceding sections, the effects of the inevitable errors in the mechanical and electrical alignment of arrays have been largely ignored. In this section, the effects of such errors will be surveyed and the modifications that must be made to some conclusions drawn earlier will be indicated.

Both mechanical and electrical errors arising in arrays can be loosely classified into one of two classes: (1) systematic errors (those to which some sort of a "pattern" can be ascribed), and (2) errors exhibiting no pattern, or patterns so complex as to defy reasonable description (so-called "random" or "pseudo-random" errors). A simple example of the first category is the case of a transmitting array utilizing separate transmitters behind each antenna. If blocks of transmitters are connected to a common power supply, the failure of one power supply would disable a complete block of transmitters, affecting the array performance in a manner susceptible to straightforward analysis. A typical example of a random error is represented by the inevitable errors of the placement of the antennas on the element grid. If done with reasonable care, there should be little systematic error in such placement, but there will inevitably be a random error in the mechanical location of each element about its desired location.

The analysis of systematic errors is usually straightforward, once the nature of the error is understood. Since particular types of array feeds are prone to certain types of systematic errors, a discussion of representative errors of this type will be included in Sec. III-B.

Random error effects, on the other hand, are amenable to a fairly general analysis by statistical methods, resulting in a statistical description of the antenna pattern. This description, while leaving something to be desired, is sufficient to be an enlightening and useful guide in array tolerance specification.

1. Effect of Random Errors on Pattern Sidelobe Level

If the far field of an array is written in the general form [analogous to Eq. (62) with $i_n = a_n \exp[j\psi_n]$

$$F(\varphi, \xi) = \sum_n f_n(\varphi, \xi)\, a_n \exp[j\psi_n] \exp[jknD \sin\xi]$$

(linear array notation is used for simplicity, but the results are applicable to planar configurations), numerous sources of error are seen to exist which can affect the array far field. In particular, the n^{th} element can contribute such errors as:

> The element pattern, at the particular angle of interest, can differ in amplitude and phase from the average element factor, thus weighting the element differently in phase and amplitude from the others.
>
> The amplitude of the drive to the element can be in error from its design value.
>
> The phase shift applied can be in error from its design value.
>
> The element physical placement can be in error, thus giving rise to both a phase error and an amplitude error due to displacement.

The effect of such errors on the patterns of arrays has been examined by many authors.[25,59] The usual assumption, made as often for mathematical convenience as for its physical reality, is that all the individual sources of error for any single element are independent of one another, and even like errors (errors in element phase) are independent from element to element.

For example, in the case of element amplitude, it is usually assumed that the actual amplitude of the n^{th} element a'_n is related to the desired amplitude by

$$a'_n = a_n(1 + \Delta_n) \quad , \tag{74}$$

where Δ_n is statistically independent of n and capable of representation by a single probability density function for all elements. The element phase is assumed to be of the form

$$\psi_n = -knD \sin\xi_o + \delta_n \quad , \tag{75}$$

where the δ_n are assumed independent of n and also representable by a single probability density function. Possible errors in element placement and element pattern deviation from the average are treated in a similar manner.[10]

It is usually assumed that the errors in all quantities are randomly distributed with mean zero (a nonzero mean is considered as a systematic error) and variance (mean-square error) σ^2. Since it is difficult by this assumed error distribution to account for catastrophic failures of elements, a multiplicative factor γ_n can be assigned to the amplitude of each element

$$a'_n = \gamma_n a_n(1 + \Delta_n) \quad , \tag{76}$$

where γ_n is assumed to be unity with a probability P and zero with probability $1 - P$, where $1 - P$ has the physical significance of representing the fraction of the number of elements expected to be completely inoperative on the average.

Under the above assumptions, it can be shown that the expected power density in the far field is of the form

$$p(\varphi, \Theta) = p_o(\varphi, \Theta) + \left|\frac{f(\varphi, \Theta)}{f(\varphi_o, \Theta_o)}\right|^2 \frac{\epsilon^2}{\eta NP} \quad , \tag{77}$$

where p_o is the normalized (peak value unity) "no-error" power distribution of the far field, and the second term represents an error term which is independent of direction except for the weighting by the element factor. The factor ϵ^2 is given by (assuming small phase error variance,† $\sigma_\varphi^2 \ll 1$)

$$\epsilon^2 \approx (1 - P) + \sigma_a^2 + P\sigma_\varphi^2 \quad , \tag{78}$$

where σ_a^2 and σ_φ^2 are the total variances in phase and amplitude due to all sources except catastrophic failure. The factors involving P account for the latter. Thus it is seen that, crudely, the magnitude of the error pattern is proportional to the total mean-square error and inversely proportional to the number of operating elements in the array NP multiplied by the taper efficiency.

From the argument of Ruze,[25] it can be shown that for an array of a large number of elements, the far-field amplitude $|F(\varphi, \theta)|$, which for notational simplicity we shall denote by the symbol ρ, is distributed in a modified Rayleigh distribution

$$p(\rho) = \frac{\rho}{\sigma_R^2} I_o\left[\frac{\rho\bar{\rho}}{\sigma_R^2}\right] \exp\left[-\frac{(\rho^2 + \bar{\rho}^2)}{2\sigma_R^2}\right] \quad , \tag{79}$$

where $\bar{\rho}$ is the normalized "no-error" far-field amplitude in the direction φ, θ of interest and the parameter σ_R^2 is half of the second term of Eq. (77)

$$\sigma_R^2(\varphi, \theta) = \frac{1}{2}\left|\frac{f(\varphi, \theta)}{f(\varphi_o, \theta_o)}\right|^2 \frac{\epsilon^2}{\eta NP} \quad , \tag{80}$$

where $I_o(x)$ is the modified Bessel function.

The form of the modified Rayleigh distribution for $\bar{\rho} = 0$ (a null of the no-error pattern) is the familiar Rayleigh distribution, whereas for $\bar{\rho} \gg \sigma_R$, the distribution tends to become Gaussian with the variance equal to σ_R^2. Thus, in areas of the antenna pattern where $\bar{\rho}$ is much greater than σ_R, the percentage error in the pattern is very likely to be insignificant. However, far out in the sidelobes of an antenna pattern with decreasing sidelobes, a point will be reached where σ_R becomes greater than $\bar{\rho}$. In this region, error effects will be most noticeable and will dominate the pattern. In this case, we can draw generally applicable curves giving the probability of holding the sidelobe level in the far-out regions of the pattern below the desired level with any assigned probability. Such curves are shown in Fig. 62. These curves give the probability that the pattern, in far-out regions where the designed sidelobes are essentially zero, will be below a specified level at a particular point. For example, if it is desired to hold a sidelobe level below 40 db at a desired point with a probability of 0.99 and the element factor neglected, ϵ must satisfy

$$\frac{\epsilon^2}{2\eta NP} < 10^{-5} \quad .$$

If we assume a 100-element array with uniform illumination, and only phase error, it is seen that an rms phase error of no more than 2.6° is permissible. The difficulty of maintaining a very low far-out sidelobe level is thus made apparent.

† See Ref. 10. The large error case is discussed therein.

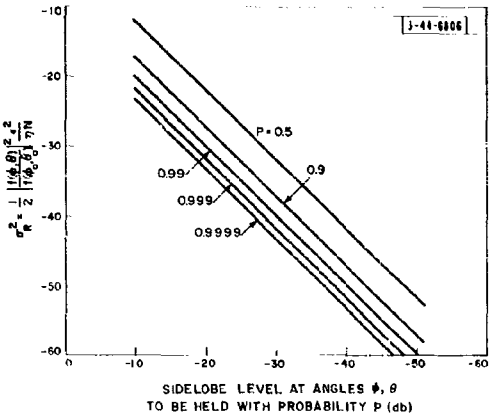

Fig. 62. Maximum σ_R^2 allowable in terms of desired sidelobe level for regions where the design sidelobe level $<<$ 10 log σ_R^2.

If it is desired to ascertain the probability of holding the pattern below a desired level over a range of angles, a modification of Fig. 62 is necessary. It can be established[10,60] that the error in an array pattern is nearly uncorrelated at intervals roughly corresponding to the distance between sidelobe peaks of a pattern. An N-element array tends to have approximately N sidelobes in visible space; hence, in order to insure holding all sidelobes below a desired level with a given probability, it is necessary to increase the probability of holding a single point below that level by approximately a factor of N. For example, if it is desired to hold all far-out sidelobes of a 100-element array below a given level with a probability of 0.99, the curve of Fig. 62 for a probability of 0.9999 should be used to set the allowable error. In this case, the previous example of a 100-element array can be reworked to indicate that to maintain a 40-db far-out sidelobe level with a 0.99 probability over all space (neglecting the area where the design sidelobes are above the permissible error sidelobe level), the phase error specification must be tightened to a maximum allowable rms phase error of 1.8°.

As an approximation, Fig. 62 indicates that σ_R^2 should be held about 10 db below the desired far-out sidelobe level. Recalling that for an element spacing of $\lambda/2$, the broadside no-error gain of a planar array is approximately $G \approx \pi\eta N$, if we denote the far-out sidelobe level by the symbol† $1/R$, we can state that, as a rule of thumb,

$$\epsilon^2 \lesssim \frac{1}{10\pi} \frac{G}{R} \quad .$$

Thus to hold a sidelobe ratio numerically equal to the no-error gain with high probability requires $\epsilon \lesssim 1/5.5$, corresponding to a maximum phase (only) rms error of about 10°.

It is apparent that the maintenance of low sidelobe levels in array patterns requires tight control of phase and amplitude of the elements and allows a little margin for catastrophic failure. It should be emphasized that the phase and amplitude error associated with the element factors and the antenna placement must also be included in the total error allowable. However, the specification can be less stringent for a larger array than for small arrays for a given permissible error sidelobe level. In fact, as the array becomes very large, the degradation in directivity may be a more stringent error limitation.

† Such that R is the ratio of main beam power to sidelobe power level.

2. Effect of Random Errors on Array Directivity and Gain

Based upon the far-field power density expression [Eq. (77)], it can be shown[10] that the directivity in the presence of errors U' is related to the "no-error" directivity U by

$$\frac{U'}{U} \approx \frac{1}{1 + \epsilon^2/P} \quad . \tag{81}$$

The loss in directivity is manifested in the raised sidelobe level. Since the directivity represents an upper bound on array gain, a similar gain degradation will occur.

3. Effect of Random Errors on the Beam Pointing Accuracy of Arrays

The effect of random errors on the beam pointing accuracy of arrays differs according to the manner in which one defines the pointing angle of the beam, particularly with regard to monopulse techniques. Somewhat different results are obtained for the effect of random errors on the pointing accuracy of a "sum" beam (one that has its maximum in the desired pointing direction)[10,60,61] and on the null direction of the "difference pattern" of a monopulse pair (Ref. 10, Part 3, Ch. III, Sec. H). The results for the latter also depend upon the technique used to estimate the null direction. In the following discussion, a monopulse system is assumed which estimates the angle from the beam null by

$$\Delta\Theta_{\text{diff}} \approx \text{Re}\left[\text{j}\,\frac{F_d(\Theta)}{F_s^*(\Theta)}\right] \quad ,$$

where $F_d(\Theta)$ and $F_s(\Theta)$ are the complex difference and sum patterns, respectively,† and the asterisk denotes the complex conjugate.

In defining the pointing error associated with random errors, it is useful to speak of the fractional pointing error in terms of some standard beamwidth. A useful standard beamwidth is

$$\Theta_s = \frac{1}{L/\lambda} \text{ radians} \quad , \quad L = ND \quad .$$

An analysis then indicates that the pointing error of the sum beam of a linear array, for small amplitude and phase error, will be normally distributed with zero mean and an rms error in fractional standard beamwidths given by‡

$$\left(\frac{\Delta\Theta}{\Theta_s}\right)_{\text{sum}} = \frac{N}{2\pi\sqrt{P}}\,\sigma_\varphi\,\frac{[\Sigma\,(ns_n)^2]^{1/2}}{\Sigma\,n^2 s_n} \quad , \tag{82a}$$

where s_n is the no-error sum beam amplitude taper, which is assumed to be an even function of n for an array centered on a coordinate system. The summations may be replaced by integrals with little error for large arrays, in which case the appropriate form is

† Note that in the absence of errors, $F_d(\theta)$ is purely imaginary and $F_s(\theta)$ purely real so that the bracketed term is real in the error-free case.

‡ Leichter's result differs from that of Eq. (82) in notation and by a factor of $\sqrt{2}$. The latter difference arises from Leichter's continuous model, as more fully explained in Ref. 10.

$$\left(\frac{\Delta\Theta}{\Theta_s}\right)_{sum} = \frac{L\sqrt{D}}{2\pi\sqrt{P}}\,\sigma_\varphi\,\frac{\left[\int_{-L/2}^{L/2}[zs(z)]^2\,dz\right]^{1/2}}{\int_{-L/2}^{L/2} z^2 s(z)\,dz}\quad, \tag{82b}$$

where $s(z)$ is related to s_n by $s_n = s(nD)$.

For the difference beam null error, the Gaussian distribution holds, with the rms error in null pointing for the estimation technique described above given by

$$\left(\frac{\Delta\Theta}{\Theta}\right)_{diff} = \frac{N}{2\pi\sqrt{P}}\,\sigma_\varphi\,\frac{[\Sigma\, d_n^2]^{1/2}}{\Sigma\, nd_n} \tag{83a}$$

$$\approx \frac{L\sqrt{D}}{2\pi\sqrt{P}}\,\sigma_\varphi\,\frac{\left[\int_{-L/2}^{L/2}[d(z)]^2\,dz\right]^{1/2}}{\int_{-L/2}^{L/2} zd(z)\,dz}\quad, \tag{83b}$$

where d_n and $d(z)$ represent the no-error amplitude taper associated with the difference pattern of the antenna, an odd function relative to the array center.

The form of the above results appears to indicate that the pointing error increases with N for a fixed σ_φ. However, closer inspection of the summations (or integrals) will indicate that the dependence is actually

$$\frac{\Delta\Theta}{\Theta} \propto \frac{1}{\sqrt{NP}}\quad.$$

By way of a specific example, evaluation of the appropriate integrals for the case of a large array, with a basic uniform taper, yields the following rms pointing errors for the two types of monopulse discussed in Sec. II-A-2 and the "optimum" difference taper of Eq. (31).

Monopulse Type	Rms Sum Beam Error	Rms Difference Beam Error
Sum and difference of two halves of array (uniform sum taper, step difference taper)	$0.55\,\frac{\sigma_\varphi}{\sqrt{NP}}$	$0.64\,\frac{\sigma_\varphi}{\sqrt{NP}}$
Sum and difference of two adjacent beams (cosine sum taper, sine difference taper)	$0.67\,\frac{\sigma_\varphi}{\sqrt{NP}}$	$0.56\,\frac{\sigma_\varphi}{\sqrt{NP}}$
"Optimum" difference $d_n = n$		$0.55\,\frac{\sigma_\varphi}{\sqrt{NP}}$

As with the case for array directivity, the insertion of the values of ϵ required for good sidelobe pattern considerations indicates that if the requirements on error for the latter case are met, the expected pointing error due to random errors will usually be small.

4. Some Conclusions on the Effects of Random Errors on Array Patterns

It has been shown that, in most cases, the most severe constraint on allowable small random errors is that of achieving low sidelobes in the far-out regions of antenna patterns. However, it should be emphasized that only random errors have been treated here. An examination of some typical cases of systematic error (Sec. III-B-1) shows that the effects of systematic errors are

often more pronounced than those of random errors [e.g., a "rough" element pattern may cause considerably greater pointing error than random phase errors (Ref. 14, pp. 24-38)]. Thus one should avoid the temptation to become overwhelmingly preoccupied with good control of random errors to the exclusion of potentially harmful effects of systematic errors.

III. ARRAY SYSTEM CONSIDERATIONS AND TECHNIQUES

In the following sections, the physical realization of array radar systems will be examined and system considerations peculiar to array-type radars will be pointed out by use of the radar equation. The techniques for feeding the array antennas to realize the array tapers and phasing previously discussed will be examined and qualitative comparisons drawn between various techniques with regard to performance and complexity. Emphasis will be on electronic scanning techniques, but methods of achieving single, stationary beams will be evident. Some unusual requirements that array configurations place on components will be examined.

A. Array Radar System Considerations

In this section, the radar equation will be re-examined in a notation which emphasizes the economic factors peculiar to arrays. In particular, the dependence of the number of elements required will be emphasized as a yardstick of array economics. Attention will then be focused upon the effect of different array configurations on the ability to achieve high powers and/or low losses.

1. Radar Equation Formulation for Arrays

The radar equation appropriate for a surveillance radar is expressible in the form

$$\frac{P_{AV}A}{T} = \left(\frac{4\pi k}{K_1 \mathcal{L}}\right)\left(\frac{\Omega_s}{T_s}\right)\left(\frac{S/N}{\sigma}\right) LR^4 \quad , \tag{84}$$

where

P_{AV} = average power,

A = effective receiving antenna area,

T = effective system noise temperature,

Ω_s = solid angle to be surveyed,

T_s = time allowable to survey Ω_s,

S/N = signal-to-noise (power) ratio,

σ = target backscatter cross section,

L = system losses,

R = range,

k = Boltzmann's constant,

K_1 = ratio of transmitting antenna gain to beam solid angle (see below).

Useful measures of array economics are: (a) the performance parameters of the array on a "per-element" basis, and (b) the number of elements used. By straightforward manipulation,

Eq. (84) can be expressed in terms of these measures. In the following analysis, the subscript t will refer to the transmitting case and r to the receiving case, allowing the possibility of separate transmitting and receiving arrays.

The total average power of the array is given by

$$P_{AV} = \bar{p} N_{at} \eta_t \quad ,$$

where $\bar{p}$ is the average transmitted power of the most powerful element, and η_t is the efficiency of any amplitude taper used on transmission. The effective receiving array energy collecting as a function of "pointing" angle is

$$A(\varphi_o, \theta_o) = \eta_r N_{ar} D_x D_y \delta_e(\varphi_o, \theta_o) \quad ,$$

where $\delta_e(\varphi_o, \theta_o)$ is the ratio of the element aperture in the array at the angles φ_o, θ_o to the area allotted $D_x D_y$, which must be determined by the methods of Sec. II-C, taking mutual coupling effects into account. As a useful bound, Eq. (67) indicates that

$$\delta_e(\varphi_o, \theta_o) \leqslant \cos \theta_o \quad .$$

Since the element spacing is determined in wavelengths, it is more useful to write

$$A(\varphi_o, \theta_o) = \eta_r N_{ar} \lambda^2 \left(\frac{D_x D_y}{\lambda^2}\right) \delta_e(\varphi_o, \theta_o) \quad .$$

Finally, the factor K_1 relates the gain to the principal cone beamwidths, Θ and Φ by

$$G = K_1 \frac{4\pi}{\Theta \Phi} \quad .$$

If we define a constant K_1' as the value of K_1 appropriate for an amplitude-tapered broadside array, then for an array which may be density tapered, pointing at an angle φ_o, θ_o from broadside,

$$K_1 = \frac{\eta_t N_{at}}{N_{Tt}} K_1' \delta_e(\varphi_o, \theta_o) \quad ,$$

where N_{Tt} is the total number of transmitting array antennas. The resulting radar equation can then be written

$$\frac{\bar{p} \eta_t^2 \frac{N_{at}^2}{N_{Tt}} \eta_r N_{ar} \lambda^2 \left(\frac{D_x D_y}{\lambda^2}\right) \delta_e^2(\varphi_o, \theta_o)}{T} = \left(\frac{4\pi k}{K_1'}\right) \left(\frac{\Omega_s}{T_s}\right) \left(\frac{S/N}{\sigma}\right) R^4 \quad . \tag{85}$$

From the above equations, it is seen that:

Tapering is more costly on transmission than on reception (since both the gain and total power are affected).

For equal N_r and N_t, the range varies as $N_a^{1/2}$ if N_a/N_T is fixed, but as $N_a^{3/4}$ if N_T is fixed.

If the maximum per-element average power varies as $\lambda^n (n \geqslant 0)$ and the target cross section varies as $\lambda^m (m \geqslant 0)$, then to maintain range performance for N_a/N_T fixed, N_a must vary with frequency f as

$$f^{n},q = 1 + \frac{m+n}{2} \quad ,$$

indicating that the variation of number of elements required varies at least as the first power of frequency. At VHF and below, the variation of sky temperature with frequency may alter this result considerably, but above VHF, the price of utilizing a higher frequency than absolutely necessary is evident.

The performance parameters of significance are seen to be the per-element power and the system temperature.

2. Effect of Array Configuration on System Performance.

In discussing achievable element power and system temperature, two classes of array configurations can be delineated. They are conveniently designated by the terms active-element arrays and passive-element arrays. The term active element is applied to an array which utilizes an active transmitter and/or receiver with each element. Passive element will be used to designate an array in which transmitters or receivers are placed only after beams have been formed. Thus, in the former category, there will be as many transmitters and/or receivers as there are active elements, while in the latter, there may be only one transmitter and/or receiver or as many receivers as the number of beams desired to be simultaneously formed.

Active-element systems are potentially capable of higher radiated power than "single-feed" radars, since the power from many elements is effectively "combined in space," circumventing the breakdown limitation of more conventional radars using single-feed lines or small numbers of feed lines. Passive-element arrays generally offer little increase in power capacity over conventional radars, and may incur additional losses of a few decibels over those of some conventional radars, due mostly to long RF lines and/or phase shifter losses. They do, however, represent an economic method for realizing much of the flexibility of operation characteristics of arrays without the attendant cost associated with active-element arrays.

In the case of an active-element system (Ref. 10, pp. 79-81), if all element receivers have the same effective noise temperature, a straightforward analysis will show that the effective temperature to be used in the radar equation is that of a single typical receiver. This is true regardless of any amplitude tapering accomplished by varying the element receiver gain, so long as the minimum gain used is sufficient to fix the channel noise figure independent of postamplifier losses.

In passive-element systems,[62] if the combining system were lossless, a similar statement would hold. Generally speaking, under certain simplified assumptions usually well approximated in practice, the overall noise temperature of a passive element can be approximated by considering all RF losses equal to the input-to-antenna terminal loss of the feed as a transmitting device.

For active-element systems, it is sometimes preferable to use separate transmitting and receiving arrays, since such an approach can be a useful method of coping with the severe packaging problems in such arrays, particularly at higher frequencies. Separate arrays can also eliminate the need for many high-power duplexers, a factor that may lead to a cheaper radar over years of operation.

B. Array Beam-Forming and Beam-Steering Methods

In the following sections, methods of realizing the array illuminations discussed in Secs. II-A and II-B will be surveyed (i.e., methods of forming and steering the beams from arrays). For simplicity, linear array configurations will be used as illustrations. The extrapolation to planar arrays is straightforward, either by extrapolation of a single technique or by using "hybrid" systems with different techniques used, for example, in rows and in columns. In systems using separate transmitting and receiving arrays, it may also be advantageous to use different techniques in the two arrays.

The systems will be somewhat arbitrarily classified according to:

(1) Whether they (a) form a single beam which is then "steered" in space (beam-steering systems), or (b) form a family of stationary beams which "blanket" the angular regions of interest (multiple beam-forming, or, more briefly, "multibeam" systems).

(2) Whether the method is (a) adaptable to passive-element arrays, or (b) restricted to active-element array configurations.

These distinctions are often loose and subject to argumentation. For example, techniques that are low loss and adaptable to RF plumbing configurations will generally be classified as passive-element systems, even though they can also be profitably used as components of active-element systems by the insertion of transmitters and/or receivers between the elements and the beam-forming systems.

Another method of classification which will be referred to occasionally, distinguishes between phased arrays, frequency-scanned arrays and switched arrays. The term "phased arrays," while properly applied to any of the classes, is reserved for arrays in which element phasing is actually obtained through the use of phase shifters. "Frequency-scanned" arrays change phase by changing the frequency used. The term "switched arrays" covers what has been described above as multi-beam systems, since such systems are often operated by selecting one or several of the many beam outputs by the use of microwave switches, rather than providing as many receivers and/or transmitters as there are beams formed.

The various techniques to be examined will be approached either from the transmitting or receiving standpoint, as most appropriate for ease of explanation of the particular technique. The other case follows from reciprocity. In systems using nonreciprocal devices, such as amplifiers, transmitters or isolators, one can conceptually turn the nonreciprocal devices around and then apply reciprocity.

1. Passive-Element Beam-Steering Techniques

The first of the systems to be described is the class that forms a single beam, which can then be steered by varying the phase or time delay of the currents in the respective elements.

Serial RF Feed Systems:– Figure 63(a-b) illustrates two examples of serial feed systems, in which the elements are arranged serially along the main line (but not necessarily in series with the main line). They consist of a main transmission line from which energy is tapped (in the case of transmission) through loosely coupled junctions to feed the antennas. To steer the beam, phase shifters are added in either the "branch lines" between junctions, as shown in Fig. 63(a), or in the "main line," as shown in Fig. 63(b). The amplitude taper is established by properly designing the junctions. For example, if all junctions are identical, the amplitude taper envelope will be approximately exponential.

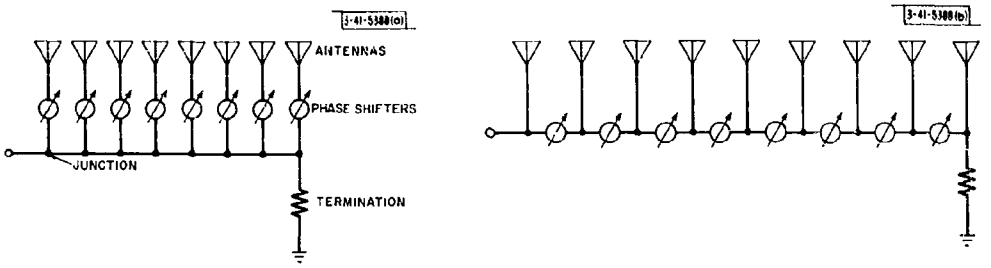

(a) Using branch-line phase shifters.

(b) Using main-line phase shifters.

Fig. 63. Basic serial RF array feeds.

Perhaps the greatest advantage of these two configurations over others to be discussed is their mechanical simplicity. The configurations are easily adapted to construction in waveguide, using cross-guide directional couplers or radiating slots as junctions. They are potentially capable of handling full waveguide power at the input (within the limitations of the phase shifters) and possess the loss associated with the corresponding length of waveguide plus that of the phase shifters. Perhaps the most severe limitation of this feed system is the dependence of pointing angle on frequency (see the discussion of frequency scanning below).

The choice between the configurations of Fig. 63(a) or 63(b) resolves mostly into a question of phase shifter capability. The configuration of Fig. 63(a) places lower power handling demands on the phase shifters, and also results in lower system loss for a given phase shifter loss. On the other hand, the configuration of Fig. 63(b) has an advantage in that all phase shifters will have identical phase shifts for a given pointing angle – a property which may result in simplified array control.

Some Practical Considerations in RF Feeds:– The junctions in RF feed systems may be either of two basic types: (a) three-port devices, such as the "tee" junctions shown in Fig. 64(a), which are characterized by the fact that they can be matched completely at only one of the three ports, and (b) four-port devices such as the "branch-line" directional couplers indicated in Fig. 64(b), with the fourth port terminated in a matched load. This type can be ideally matched at all ports.

If perfect impedance matches could be maintained throughout an array feed [in the case of three-port junctions, matched in the sense of looking into ports 2 of Fig. 64(a)], the three-port junction would usually be preferable on an economic basis. However, mutual impedance makes maintenance of good matches difficult when wide-angle scanning is required, producing systematic element mismatches with scan angle (neglecting end effects).†

Two distinct effects of these systematic mismatches in RF feed systems can be distinguished, although both will generally be present to some extent in any feed system of this type. The first effect arises from multiple reflections within the branch lines. If one considers the possibility of a mismatch at the input to the antennas (points A) of Fig. 64, the reflected waves will travel backward through the phase shifter (reciprocal phase shifters assumed), doubling their phase

† Random mismatches also occur, even in nonscanned arrays, due to component tolerances. Their effects can be included in the ϵ^2 quantity of Sec. II-D.

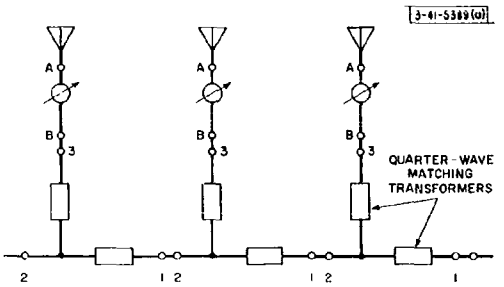

(a) Section of feed using tee junctions.

(b) Section of feed using directional couplers.

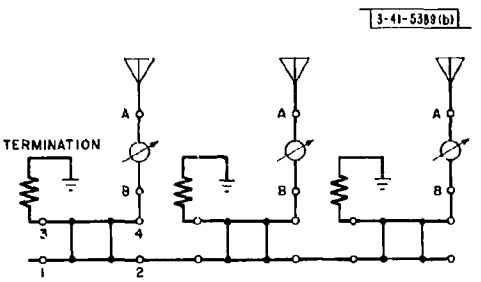

Fig. 64. Basic junction types for RF feeds.

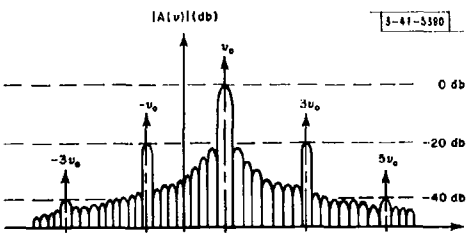

Fig. 65. Typical array functions showing spurious lobes for $|\Gamma_A| = 0.1$ for array using tee junctions, and $|\Gamma_A\Gamma_B| = 0.1$ for array using directional couplers.

shifts. If an appreciable portion of this reflected wave is then re-reflected from the points marked B in the figure, this wave passes through the phase shifters once more, and is recoupled into the antennas with three times the basic phase increment. Thus the array has an error in illumination corresponding to odd multiples of the basic phase increment arising from multiple reflection between points A and B. In the case of the three-port junction, since they are nominally matched only at the terminals marked 2 of Fig. 64, essentially all the waves reflected from A will be re-reflected from point B if the array is large (the coupling loose) and it can be shown[63] that the resultant illumination coefficients of the array, the a_n's, are related to the original coefficients $a_n \exp[-jnkD\upsilon_o]$ by

$$a_n' = a_n \sum_{q=o}^{\infty} (-1)^q (\Gamma_A)^q \exp[-jnkD(2q+1)\upsilon_o] \quad , \tag{86}$$

where Γ_A is the voltage reflection coefficient at points A. Thus, for a reflection coefficient at point A of magnitude 0.1 (a VSWR of 1.2; compare with Figs. 55, 56, and 57), the resultant far-field pattern would be approximately as shown in Fig. 65 for a phase shift setting corresponding to a three-beamwidth pointing angle from broadside.

For the four-port junctions of Fig. 64(b), however, points B would ideally appear matched and absorb the reflected wave from points A. Even if points B are systematically mismatches with a reflection coefficient Γ_B, the resulting illumination is of the form

$$a_n' = a_n \sum_{q=o}^{\infty} (-1)^q (\Gamma_A \Gamma_B)^q \exp[-jnkD(2q+1)\upsilon_o] \quad . \tag{87}$$

Thus the effect of antenna mismatch due to multiple reflection within the branch-line phase shifters is improved by a factor of Γ_B by the use of four-port couplers. Even with four-port devices, the results of Figs. 55 through 57 show that for very good sidelobe control, $\Gamma_B \ll 0.1$ (VSWR < 1.2:1) may be required, indicating the importance of accurate impedance matches in arrays.

The second effect of impedance mismatches is the cumulative effect in the main feed line of the small mismatches of the many junctions in a long array. If each of the junctions of Fig. 63 represents a slight mismatch, the resulting mismatch at the terminal of the main feed line can be quite large. The reflected energy, represented by the vector sum of the many small reflections, manifests itself in two ways. First, since it is a wave traveling the wrong way in the main line, it will radiate a spurious beam in the wrong direction. Second, it causes an input standing-wave ratio which varies with electrical distance between junctions in the main feed line.

If four-port junctions are used, it is apparent from Fig. 64 that the reverse traveling wave couples primarily into the terminated ports of the directional couplers, and the spurious beam is eliminated. However, the mismatch at the input to the array will be present in both cases.

In order to get a quantitative feeling for the main line mismatch problem, a particular example can be easily analyzed and some general conclusions drawn from this result. Consider the main line in Fig. 63(a) to be carrying an incident (traveling to the right) exponentially decreasing field (all couplers alike) of the scalar form†

† The actual decrease would be in the form of steps, but for a large array, little error is committed by using a more tractable "smoothed" representation.

$$E_i(z) = A \exp\left[-\left(\frac{a}{L} + jk\right) z\right] \quad ,$$

where the factor a determines the rate at which energy is coupled out of the feed lines and a factor of $\exp[j\omega t]$ is understood. It is assumed that at each junction ($z = n\ell$) there is a small reflection, which can be characterized by a reflection coefficient Γ_n. If all Γ_n's are small, we can neglect higher-order reflections, as well as the effect of the reflection on the transmitted wave. If all Γ's are also identical, the total reflected voltage at the terminal will be

$$E_r(0) = A\Gamma \sum_{n=0}^{N-1} \exp\left[-j2n\ell\left(k - j\,\frac{a}{L}\right)\right] \quad .$$

This summation is a geometric series, so noting that $L = N\ell$, we can write for large N,

$$|E_r(0)| \approx A|\Gamma|\, e^{-a} \left| \frac{\sin[kN\ell - ja]}{\sin\left[k\ell - j\,\frac{a}{N}\right]} \right| \quad . \tag{88}$$

The total reflection coefficient as seen at the input Γ_t has a magnitude

$$|\Gamma_t| = \left| \frac{E_r(0)}{E_i(0)} \right| \quad ,$$

which has the form shown in Fig. 66 for large N, resembling an array function but varying with the electrical spacing between junctions in the main line ℓ/λ_L, where λ_L is the wavelength in the line. For the case of Fig. 63(b), the effect of the phase shifters must be included, and the phase shift between taps is the quantity of significance, which is also indicated in Fig. 66.

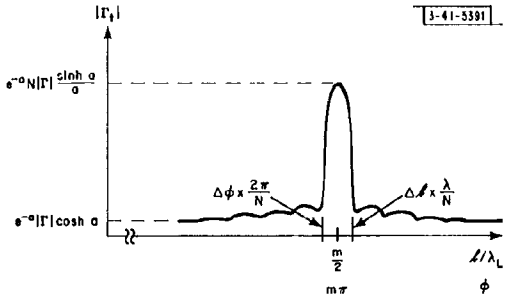

Fig. 66. Variation of terminal reflection coefficient with junction spacing (phase difference).

For typical values of a (≈ 2), the peak value of the reflection coefficient is approximately $(N/a)|\Gamma|$. Thus it is seen that $|\Gamma_t|$ may be of the order of $N|\Gamma|$, if the phase shift between taps is an integral multiple of 180° [which is the case for broadside radiation in the feed of Fig. 63(b), if the branch lines are of equal length]. The region of ℓ over which this high reflection coefficient exists is about $\Delta\ell = \lambda/N$, or a phase differential of 360°/N (a change in beam pointing angle of about one beamwidth). This phenomenon is appropriately termed resonance.

If broad bandwidth is desired of a serial array, $\alpha = m\pi$ is obviously to be avoided. On the other hand, for narrow-band arrays of the type of Fig. 63(a), it can be shown (Ref. 4, Sec. 9.17) that if $\ell/\lambda = m/2$, a "resonant" array can be built which yields a uniform amplitude taper for equal couplers. Thus a common procedure for building narrow-band resonant arrays consists of using an appropriate waveguide dimension so that taps can be one wavelength apart in the guide

(thus making the guide resonant), but closer in free-space wavelengths to realize the appropriate D/λ.

Frequency-Scanned Array Feeds:- As previously pointed out, the feed types of Fig. 63 are frequency sensitive with respect to pointing angle due to the difference in line length between the respective elements and the terminal. This fact can be utilized in realizing a frequency-scanned array, as shown in Fig. 67, by increasing still further the length of line between junctions, while holding the spacing between elements fixed. Relatively small changes in frequency can be made to produce appreciable change in element phase. The differential equation relating the change in pointing angle to the fractional change in frequency in terms of the length of line between junctions ℓ, the antenna spacings D, and the wavelengths λ_L in the line and λ_o in free space is

$$d\xi_o = \frac{\ell/\lambda_L}{D/\lambda_o} \frac{df}{f} \frac{1}{\cos \xi_o} \tag{89}$$

(λ_L may, in itself, be a function of frequency, as in waveguide). It is seen from this result that the effect of a given percentage change in frequency is multiplied by the ratio $(\ell/\lambda_L)/(D/\lambda_o)$, commonly referred to as the line "wrap-up" factor. From Eq. (89), if it is desired to scan ±30° with a ±5 percent frequency change, the wrap-up factor should be on the order of ten.

In order to accomplish wide-angle scanning with small change in frequency, large wrap-up factors must be used, and obviously the larger the wrap-up factor, the narrower the signal bandwidth that the array is capable of handling. A useful rule of thumb is that the usable array percentage signal bandwidth is on the order of the half-power beamwidth in degrees, divided by the wrap-up factor. For a 1° beam and a wrap-up factor of ten, the usable signal bandwidth is thus of the order of 0.1 percent [compare with Eq. (41) for a constant-phase feed].

The resonance phenomena previously described must also be coped with in this type of array by careful junction matching or the use of branch lines of different lengths.

In general, the frequency scan technique offers the advantage of simple RF construction, which is paid for in signal bandwidth restriction and the necessity for large component bandwidth. Although a planar frequency scanning array is possible in principle, if a large enough W is used to allow successive rows to be connected in series with a line length of ℓ, it is common for planar array applications to use frequency scan in only one direction, with a different technique used for the orthogonal scan direction (frequency-scanned linear arrays for the rows of an array, with the rows fed as if they were elements of a phased feed of the type described below).

RF Parallel Feed Systems:- Both the resonance phenomena and the frequency dependence associated with the serial feeds can be reduced by the use of parallel feeds at the cost of more complex mechanical structure, which usually is more costly to fabricate on a production basis than the serial feeds discussed.

A basic parallel feed system is that of Fig. 68(a), in which all antennas are connected to a common junction. This junction is essentially an N-way power divider designed to give the desired amplitude taper. It may consist of a simple junction with matching transformers in the antenna lines (analogous to three-port junctions in that no isolation is provided between antennas) or an N-way hybrid power divider[64] giving performance analogous to the directional coupler, with isolation between elements and attendant improved performance in the presence of errors. Note that Eq. (87) applies to parallel feeds, as well as to serial feeds, and thus indicates the requirements on impedance matches in any feed using four ports.

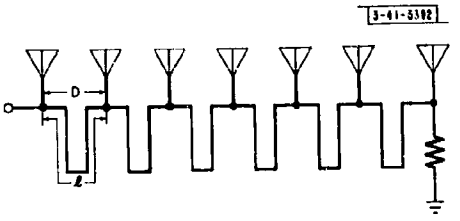

Fig. 67. Frequency scan feed.

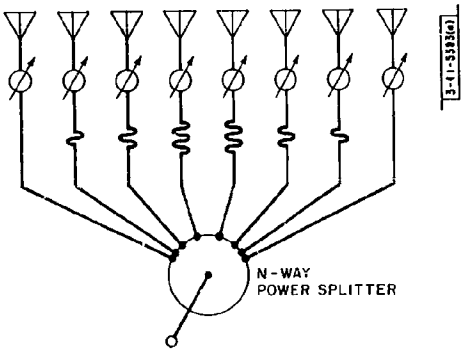

(a) Using N-way power divider.

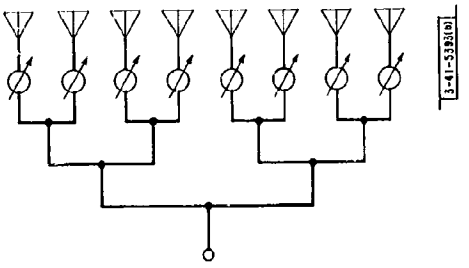

(b) Using corporate structure.

Fig. 68. Basic RF parallel feeds.

Another common technique for realizing parallel feeds is the "corporate" feed structure of Fig. 68(b). This structure also can make use of either three-port or four-port junctions.

The frequency dependence (change in beam pointing angle with frequency) of parallel feed configurations depends mainly on the frequency characteristics of the phase shifters and the junctions, if the line lengths from the antennas to the final junctions are all made equal. Thus, if variable delays were available and used in place of the phase shifters, the beam pointing angle would be essentially independent of frequency. When phase shifters are used, the feed closely approximates the "constant-phase" behavior discussed at length in Sec. II-A-3.

In addition to transmission line parallel feeds, use can be made of devices which are antennas in their own right (so-called "optical" techniques). For example, the "pillbox" antenna (Ref. 4, pp. 456-464) structure shown in Fig. 69(a) can be used to illuminate an array of "pickup" antennas to feed a linear array, as shown in Fig. 69(b). The array of pickups can be matched to the pillbox so that no reflections occur; hence, all the energy is collected by the pickups and the loss incurred is only the normal RF loss. By the use of a folded pillbox,[65] the feed can be made not to interfere with the pickup structure. If the back surface of the pillbox is made spherical, the array can be scanned over fairly wide angles mechanically, by motion of the feed structure.[65]

The cost of substituting the pillbox for a corporate feed is an exchange of some freedom in the choice of amplitude tapers and packaging configuration for a simpler mechanical structure.

The Use of Passive-Element Techniques in Active-Element Systems:– The previous configurations, which are basically low loss, high power RF techniques, are also useful as distribution and phasing techniques in active-element arrays. When they are used, little amplification is required in each element for high "per-element" power on transmit and low noise figure on reception. By contrast, most beam-forming techniques developed expressly for active-element arrays will be seen below to be quite power limited and quite lossy, thus necessitating the use of high-gain transmitters and receivers on each element.

2. Passive-Element Multiple-Beam-Forming Techniques

Another class of arrays is composed of passive-element feeds which can generate multiple beams from a single linear array. Each beam has a different pointing angle and all beams have essentially the full gain of a single-beam array of the same size and illumination for the same pointing direction, aside from a possible increase in RF plumbing losses over a single array. Since the desired beam is achieved by selecting one of several terminals of the array feed, the term "switched arrays" is often used to characterize such techniques.

The key to realizing such systems lies in a re-examination of the feeds of the previous sections. Such feeds form a beam on reception, for example, by either re-radiating (scattering) energy when three-port junctions are used or by absorbing energy in the termination of four-port devices. Thus, in the feed using directional couplers, when the signal arrives from an angle which corresponds to a pattern null, all the received energy is absorbed in the unused terminals of the couplers. For the same arrival angle, feeds using three-port devices re-radiate all the received energy. The question arises as to whether this energy cannot be used in some fashion to form more beams.

Serial Multiple-Beam-Forming Systems:– The first affirmative answer to this question was apparently supplied by Blass.[66] The technique is based on the serial feed of Fig. 63, using directional couplers, and is shown schematically in Fig. 70.

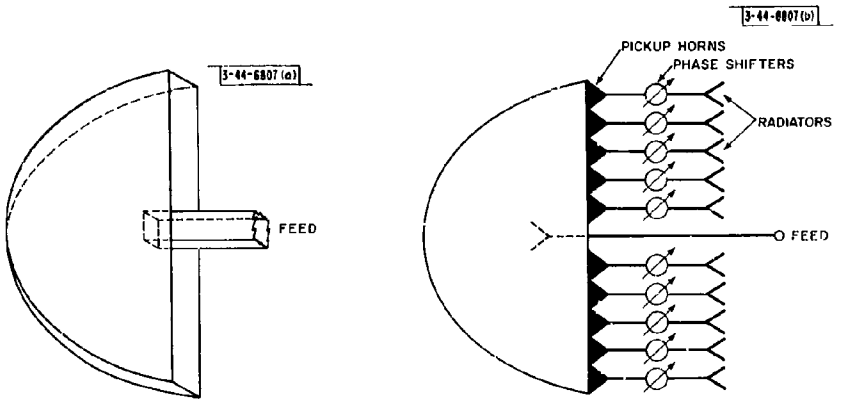

(a) Basic pillbox antenna.

(b) Pillbox used as array feed.

Fig. 69. Illustration of optical feeding techniques for arrays.

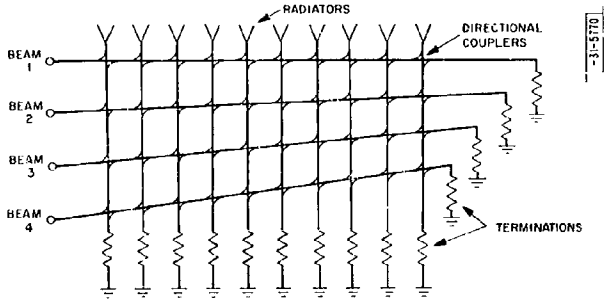

Fig. 70. Series-fed simultaneous beam-forming matrix.

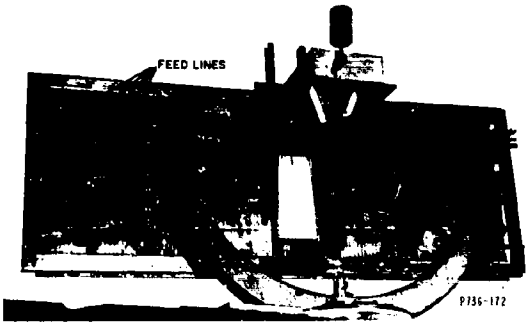

Fig. 71. Rear view of 120-element, 5-beam serial multibeam antenna. (Courtesy of Maxson Electronics Corporation.)

If a transmitter is connected to any of the beam terminals, each coupler leaks off a fraction of the incident energy in the feed line toward the antenna connected to that junction, in the same manner as the arrays of Fig. 63. In fact, if it were not for the additional feed lines in front of a given feed line (toward the antenna), there would ideally be no difference in operation between this configuration and those of Fig. 63. However, some of the energy coupled toward the antenna is subsequently coupled into the feed lines in front of the one in question. However, if the beams are spaced at least a beamwidth apart, for reasons that will be discussed later, it is found that this secondary coupling has little effect and the pattern generated by each feed line is not significantly degraded by the additional feeds. Furthermore, the power leaked into the other feed lines sums very nearly to zero, and little power is wasted in the terminations.

The phase shift between elements is governed by the "tilt" of the feed lines. This configuration is particularly adaptable to rectangular waveguides using cross-guide directional couplers. When waveguide is used, the array is capable of high power operation and has fairly low RF losses. A 120-element, 5-beam X-band array is shown in Fig. 71.

Brigham† has pointed out that Blass' matrix can be realized as a delayed array by using a modified configuration which can be represented conceptually as shown in Fig. 72. The lines to the antennas are areas of circles of radii nD_o. The broadside beam feed is placed at an angle of one radian from a line parallel to the antenna face.‡ Additional feeds are spaced in angle by multiples of some $\Delta\Theta$, so that the signal travels a different distance $nD\Delta\Theta$ to reach the n^{th} antenna. If the transmission lines have a constant velocity of propagation v, the beam pointing angle of the m^{th} beam ξ_m is given by the solution of

$$\sin\xi_m = \frac{c}{v}\, m\Delta\Theta \quad .$$

Parallel-Fed Multiple-Beam-Forming Systems:— An extrapolation of the corporate feed structure of Fig. 68(b) has been made independently by Butler[67] and by Shelton, et al.[68] The configuration is shown in Fig. 73, using directional couplers that have the 90° phase shift property (e.g., branch-line couplers) and fixed phase shifters as indicated.

† Private communication from E. Brigham, Sylvania Electric Products, Waltham, Mass.

‡ Note that the same technique can also be used to increase the signal beamwidth of the serial feeds of Fig. 63.

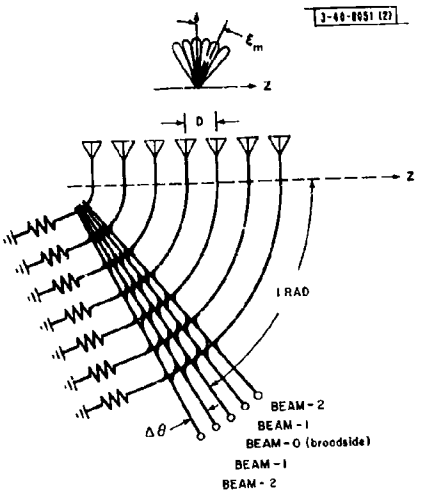

Fig. 72. Brigham's delayed array adaptation of Blass' matrix.

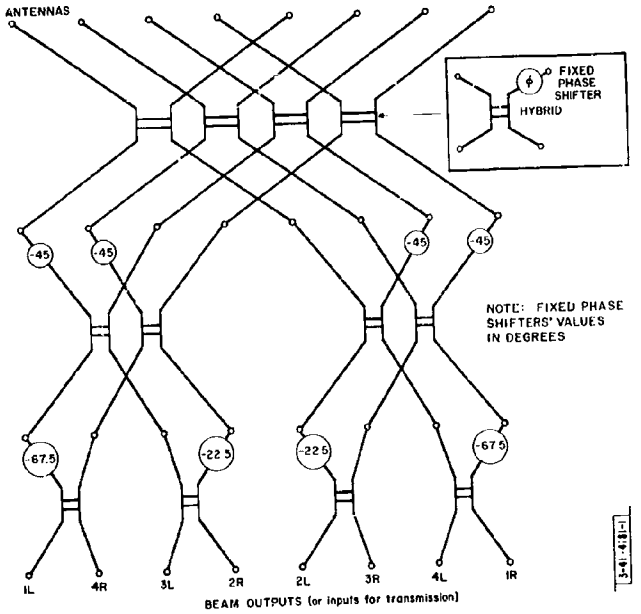

Fig. 73. 8-element parallel beam-forming matrix.

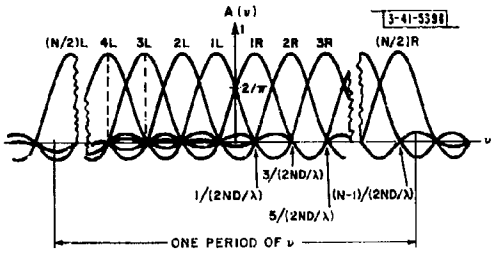

Fig. 74. Family of array functions generated by parallel beam-forming matrix.

A signal injected at any of the bottom terminals excites all antennas equally in amplitude, with phase differentials of odd multiples of 180°/N. No energy comes out any of the lower terminals; consequently, the device must be ideally lossless.

The array functions of the beams generated are of the form $\sin Nx/\sin x$, since the amplitude taper is uniform. Specifically, they are

$$A_m(v) = \frac{\sin\frac{N}{2}\left[kDv - (2m+1)\frac{\pi}{N}\right]}{\sin\frac{1}{2}\left[kDv - (2m+1)\frac{\pi}{N}\right]} \quad , \tag{90}$$

as indicated in Fig. 74, with the N main beams completely covering one period of v. It can be shown† that any beam shape realizable from an N-element array can be realized by properly weighting and summing each beam. The beams specified by Eq. (90) cross over at a relative amplitude of $2/\pi$ ($\approx$4 db).

The construction of the parallel multiple-beam configuration is not so straightforward as the construction of the serial type, because of the large number of transmission line crossovers required. However, for medium and low power applications, the device can be compactly constructed in solid dielectric strip transmission lines.‡

The parallel device uses fewer couplers for a given number of elements than the serial feed, if it is desired to form a large number of beams. If N is the number of antennas and B is the number of beams required, the serial configuration requires NB couplers while the parallel configuration requires essentially $(N/2)\log_2 N$ couplers regardless of the number of beams required (for the straightforward application of the parallel method, it is required that N be a binary number; therefore, $\log_2 N$ is an integer).

A Limitation on Beam Shape and Spacing in Multibeam Arrays:– The beam shapes and beam spacings obtainable, in general, from any multiple-beam-forming feed in a lossless manner are not completely arbitrary. It has been shown[69] that the array functions of the beams formed by any such device that has defined input and output ports§ (is representable by a scattering matrix) must be orthogonal over a period of the array function:

† Woodward and Lawson (Ref. 70) essentially prove this statement for the appropriate form of Eq. (90) for line sources; in array notation, the proof can be found in Ref. 14, pp. 221-227.

‡ Delaney (Ref. 71), summarized in Ref. 10. This reference also thoroughly examines the theoretical and practical properties of such arrays.

§ White (Ref. 72) has extended this proof to apply to any multiple-beam system.

$$\int_{-[1/(2D/\lambda)]}^{1/(2D/\lambda)} A_\ell(v)\, A_k^*(v)\, dv = \begin{cases} \frac{1}{D/\lambda} \sum_n |i_n|^2 & , \quad \ell = k \\ 0 & , \quad \ell \neq k \end{cases} \tag{91}$$

where $A_\ell(v)$ and $A_k(v)$ are the array functions associated with the ℓ^{th} and the k^{th} beam terminals, as defined by Eq. (5), and the asterisk denotes the complex conjugate.

To obtain a qualitative feeling for the significance of this orthogonality requirement, let us examine the implication on the spacing of adjacent beams. We shall assume the array illumination to be of the form $i_n \exp[-jknDv_o]$ (the i_n's may still be complex, but the steering phase term will be explicitly stated):

$$A_\ell(v) = \sum_m i_m \exp[jkmD(v - v_\ell)]$$

$$A_k^*(v) = \sum_n i_n^* \exp[-jknD(v - v_k)] \quad ,$$

where v_ℓ and v_k are the pointing direction of the ℓ^{th} and k^{th} beams. Applying the orthogonality criterion yields the result, for $k \neq \ell$,

$$\sum' |i_n|^2 \exp[jknD(v_\ell - v_k)] = 0 \quad . \tag{92}$$

The equation indicates that the beams of any lossless multibeam array must be separated far enough so that the difference in angle between the peaks of adjacent beams is equal to the difference between the peak and the first null of an array function which would be generated by an illumination function, which is the squared magnitude of the illumination actually used. Since squaring a tapered illumination produces a more tapered illumination, it is apparent that beams from illuminations tapered to yield first sidelobes lower than uniform illumination must have crossovers at still lower levels than the 4 db associated with the uniform amplitude case from the previous section, or incur an amount of loss proportional to the extent one departs from orthogonality.

For the parallel configuration of the previous section, a direct and quantitative interpretation of the orthogonality criterion is possible. It was previously pointed out that any realizable shape from an N-element array can be obtained by weighting and summing the beams given by Eq. (90). This can be done by the use of additional passive circuitry, as shown in Fig. 75. Any such

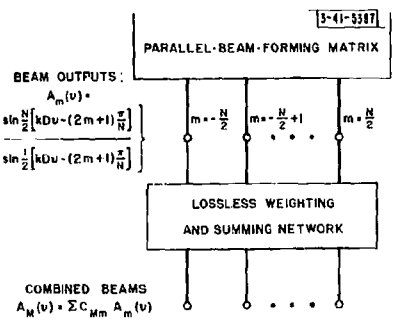

Fig. 75. Method of realizing other beam shapes from a parallel beam-forming matrix.

"composite" array function $A_M(v)$ can then be expressed as the sum of the functions of Eq. (90):

$$A_M(v) = \sum_m C_{Mm} \frac{\sin\frac{N}{2}\left[kDv - (2m+1)\frac{\pi}{N}\right]}{\sin\frac{1}{2}\left[kDv - (2m+1)\frac{\pi}{N}\right]} ,$$

where the C_{Mm}'s may be complex. Application of Eq. (91) yields the requirement that, to within a constant, the weighting coefficients for two such "composite" beams $A_M(v)$ and $A_N(v)$ satisfy

$$\sum_m C_{Mm} C^*_{Nm} = \begin{cases} 1 , & M = N \\ 0 , & M \neq N \end{cases} , \qquad (93)$$

For the important case where it is desired that all the C_m's be real and positive, this equation states that the combined beams can share no common C_m's; that is, the number of beams formed must be reduced from the N possible by the factor of the number of beam outputs combined to make up the composite beams. However, the possibility of using the same beams combined with the C_m's that are either complex or alternating in sign remains. For example, Fig. 76 shows a simple combining network for the parallel feed system which produces N/2 sum beams and a similar number of difference beams.[71]

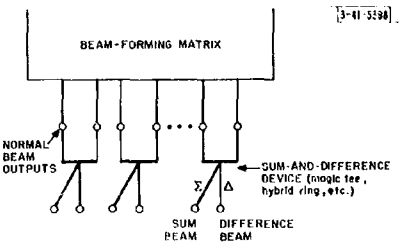

Fig. 76. Combining method for obtaining cosine (sum) and sine (difference) tapers.

Another corollary of the orthogonality criterion is that a device losslessly forming multiple beams which are stationary with changing frequency is, strictly speaking, unrealizable,† since orthogonality requires that the spacing between beams be a constant when measured in terms of beamwidths, which varies with frequency. Thus the matrix of Fig. 72, which obviously maintains a pointing angle independent of frequency, must have a varying loss with frequency, but this can be kept small if one does not attempt excessive overlap in beams.

Multiple Beams by "Optical" Techniques:– In addition to the matrix of Fig. 72, delayed arrays can be realized by a use of optical techniques, such as the pillbox antenna with multiple feeds radiating directly into space, discussed in Sec. III-B-1, and other "geodesic" techniques.[73]

One can also make use of dielectric lens techniques for wide-angle beam forming such as the Luneburg lens.[43] This lens is characterized by a radial variation of relative dielectric constant such that a plane wave impinging on the lens from any angle is focused to a point on a diameter opposite the tangent point of the wave front, as shown in Fig. 77. Thus, by an array of multiple feeds as shown in the figure, a multiple-beam array with pointing direction independent of frequency is realizable.

† First pointed out by Norman Miller, then of HRB-Singer, in a private communication.

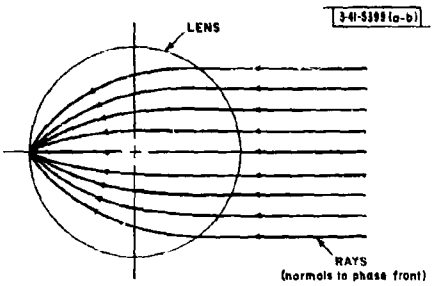

(a) Focusing action of lens.

(b) Array configuration.

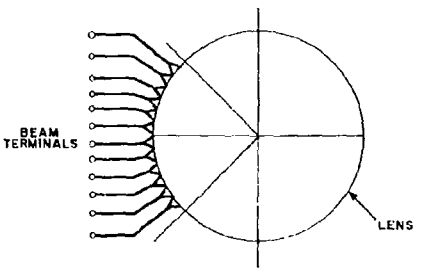

Fig. 77. Multibeam array using Luneburg lens.

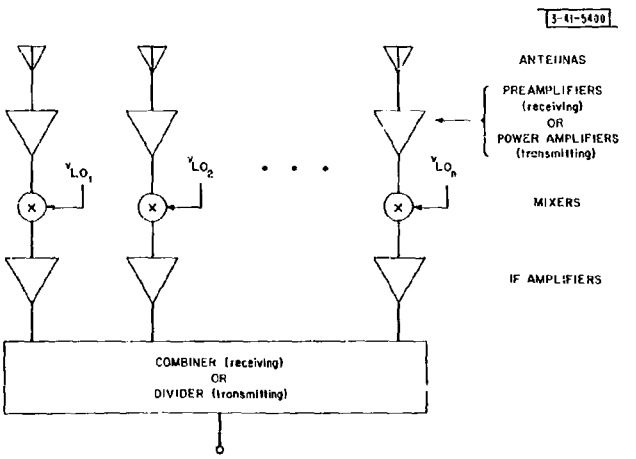

Fig. 78. Beam steering by use of phased local-oscillator signals.

An advantage of the optical techniques over the transmission line beam-forming system is one of simplicity. Again as with the single-beam configurations, significant disadvantages of such techniques are the surrender of some freedom in amplitude tapering and resultant beam shaping and, in some cases, the dielectric loss of the lens itself. In addition, some geodesic feeds incur a phase error limitation on the number of beamwidths from broadside at which beams with good patterns can be formed.[73]

Some Methods of Utilizing Passive-Element Multiple-Beam-Forming Techniques:— As with passive-element beam-steering techniques, the multiple-beam-forming techniques described in this section are adaptable to active-element systems in the straightforward manner. When used in active-element systems, a small amount of loss can be tolerated, and the orthogonality criterion may be departed from in order to realize more freedom in beam shape and spacing.

3. Active-Element Beam-Steering Systems

In this section, we shall discuss beam-steering techniques which require the use of active electronics with each element, due to the use of a frequency conversion for injection of steering signals.

The basis of most such systems is shown in Fig. 78; the key to the operation is the mixer in each element. In an array receiver, the mixer may be preceded by an RF amplifier to minimize the noise figure degradation of the mixer. For transmitters, the amplifiers are "turned around," with the RF amplifier now becoming a power amplifier.

Beam steering is accomplished by phased local oscillator (LO) signals. The n^{th} mixer is fed with an LO signal v_{LO_n} which has been phase shifted to be of the form

$$v_{LO_n} = \exp[j(\omega_{LO}t - n\alpha)] \quad , \quad \alpha = -kD\nu_o \quad .$$

If the output of the n^{th} RF amplifier for a plane wavefront arriving from ν is

$$v_{RF_n}(t) = A \exp[j(\omega t + knD\nu)] \quad ,$$

then the output of the n^{th} IF strip will be of the form

$$v_{IF_n}(t) = A \exp[j(\omega - \omega_{LO})t]\{a_n \exp[jnkD(\nu - \nu_o)]\} \quad ,$$

where a_n is a voltage gain of the n^{th} IF amplifier. The sum of these outputs is then of the form of the array function of Eq. (8) for a linear array. For transmission, the sign of the LO phase shift must be reversed, if the sum of LO frequency and driver frequency is transmitted.

If it is desired to use such a system in a planar array configuration, double-frequency conversion with two mixers can be used, with the α phase (in the nomenclature of Fig. 31) information inserted in one set of mixers and the β phase shift information in a second set.

Conceptually, this method of beam forming is a constant-phase type, and is intrinsically capable of signal bandwidths of several percent, as discussed in Sec. II-A-3. However, certain practical difficulties arise in handling broad bandwidth due to the frequency conversion. These are component limitations caused by the fact that a relatively modest percentage bandwidth at RF can become a large percentage bandwidth after frequency conversion.

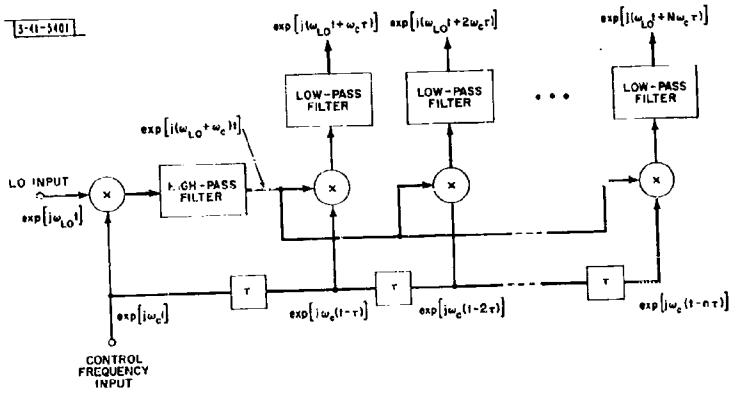

Fig. 79. Delay-line phase shifter.

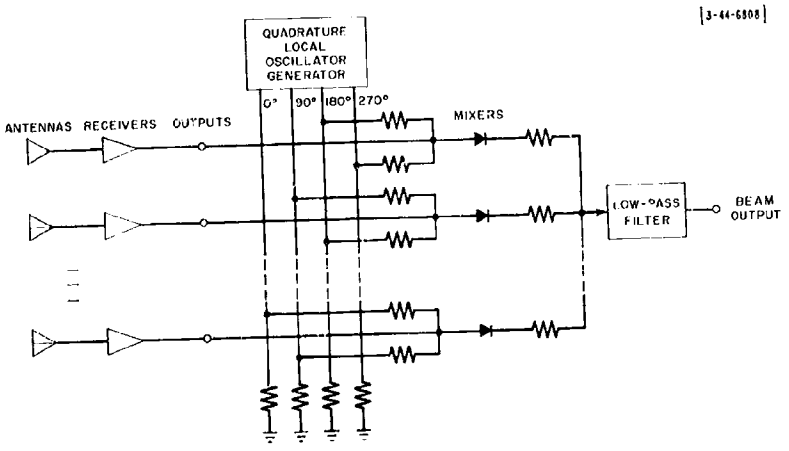

Fig. 80. IF beam-forming system.

The configuration of Fig. 78 is also prone to certain practical difficulties which should be considered in the design of such a system. First, high frequency mixers generally have complex conversion gains which vary both in phase and amplitude with the amplitude of an LO drive signal. For this reason, it is desirable to use a constant amplitude LO generator, and an LO phase shifting technique which does not affect the absolute amplitude of the LO signal. Second, since microwave mixers usually couple some of the incoming signal into the LO line (thus constituting another form of mutual coupling between elements), some form of isolation should be provided in the LO distribution. Finally, care should be taken in filtering the LO signal to remove any components of noise existing at the signal frequency. Even if relatively small amounts of noise at the signal frequency are present, the mixing operation can produce a component of noise at the output frequency which will be at least partially coherent among the channels of the array. Any coherence among these noise inputs can result in a much higher noise output (called "common LO noise") from the combining network than would be the case if all the noises were independent, as is the case with the receiver noise in each channel.†

The techniques of Secs. III-B-1 and III-B-2 are adaptable as LO distribution systems. With the methods of Sec. III-B-2, the LO signal is switched into the appropriate beam terminal. Even the frequency scan technique of Fig. 67 is adaptable to the LO feed problem with some modification. The basic adaptation is shown in Fig. 79, and is generally referred to as the delay line phase shifter or scanner. A CW control signal of frequency ω_c is fed down the delay line, and is also mixed with the LO frequency. The result of this mixing operation is filtered to select one of the sidebands (the upper sideband indicated in Fig. 79). The resulting frequency is then mixed with the output of the various taps of the delay line, and the opposite sideband selected to yield outputs of the form

$$v_n(t) = \exp[j\omega_{LO}t] \exp[-j\omega_c n\tau] \quad .$$

It is seen that the output of the delay line scanner, in the form shown in Fig. 79, always produces lagging phases. To scan both sides of broadside, one must compensate the phase of each channel so that, for some nonzero ω_c, all elements are actually in phase.

4. Active-Element Multiple-Beam-Forming Systems

In addition to adapting the multiple-beam-forming techniques of Sec. III-B-2 to active-element arrays, certain techniques exist which, because of such factors as high losses or adaptability only to low-frequency techniques, are primarily considered as multiple-beam-forming systems to be used only after amplification of the signal (in the case of reception) or prior to high power stages (in the case of transmission). These techniques are the topic of discussion in this section.

A multiple-beam-forming system using fixed phase-shifted LO inputs usable at IF frequencies is shown in Fig. 80.‡ The basis of this system is as follows: coherent LO signals are supplied with relative phases of 0°, 90°, 180°, and 270°. By resistively summing any two oscillator signals, a resulting LO signal at any phase angle can be obtained within an amplitude variation of 3 db. This amplitude variation can be eliminated in the mixing process following a resistive summation if the signal amplitude remains much smaller than the LO amplitude.

† A method of minimizing such noise is discussed in Ref. 10, Part 2, Ch. III, Sec. D.

‡ Described in detail in Ref. 11, pp. 51-76.

A difficulty with this system lies in mutual coupling between the LO lines, and it is desirable to make the LO line impedance as low as possible. As the number of elements and number of beams formed becomes large, however, it becomes difficult to maintain sufficiently low impedance. One could, of course, compute these effects and compensate for them in advance.

Another class of techniques involves putting the fixed phase shifters in the signal channels. Conceptually, such a system might consist of a set of tapped delay lines following the amplifiers, as shown in Fig. 81. Unless the delay lines are very loosely coupled to the output lines, one again finds that second-order effects must be carefully taken into account. On the other hand, if the coupling is very loose, large losses result.

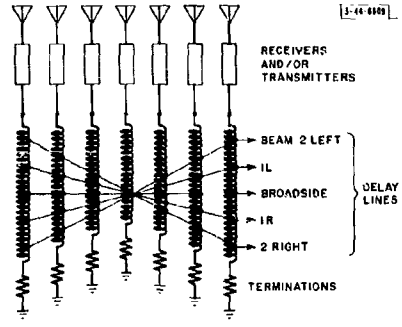

Fig. 81. Beam forming by tapped signal delay line.

Still another method is analogous to that of Fig. 80. Instead of providing quadrature LO signals, quadrature signal outputs are provided for each channel, and these quadrature signals are then combined through passive lumped circuitry to form the desired beam. Again, the matrix must be carefully calculated, taking all the loading effects into account, if very good performance in terms of antenna patterns is desired. The losses are usually large, since the matrix driving impedance must be very low for small errors.

Although small losses are usually not as important in active-array beam-forming systems as in passive-array types, it should be pointed out that one pays a manyfold price in the individual element amplifiers for large losses in the beam-forming system. For example, if for some reason it is elected to use a beam-forming system with 10-db more losses than in another possible type, it should be realized that the cost of this choice will be the necessity of providing 10-db more stable gain in each of the N array channels, if noise figure degradation is not allowable.

5. Summary of Array Beam-Forming and Beam-Steering Techniques

The techniques outlined in the previous sections certainly do not exhaust all possibilities in this field. Rather, the methods presented outline some typical examples of the various types of techniques. Not only are many interesting and worthwhile refinements of the basic techniques possible, but also a marriage of different techniques in hybrid systems can produce interesting and useful results.

REFERENCES

1. H. T. Friis and C. B. Feldman, "A Multiple-Unit Steerable Antenna for Short-Wave Reception," Proc. IRE 25, 841-917 (1937).

2. C. S. Lerch, Jr., "Phased Array Radars for Satellite Tracking," presented at the annual meeting of the American Society of Mechanical Engineers, New York, N. Y., 26-30 November 1961.

3. J. L. Allen, "Array Radars -- A Survey of Their Potential and Their Limitations," Microwave J. 5, 67 (1962).

4. S. Silver, Microwave Antenna Theory and Design, Radiation Laboratory Series, M. I. T. (McGraw-Hill, New York, 1949).

5. S. A. Schelkunoff, "A Mathematical Theory of Linear Arrays," Bell System Tech. J. 22, 80 (1943).

6. R. W. P. King, The Theory of Linear Antennas (Harvard University Press, Cambridge, 1949).

7. J. D. Kraus, Antennas (McGraw-Hill, New York, 1950).

8. H. Unz, "Linear Arrays with Arbitrarily Distributed Elements," Report Number 56, Electronics Research Laboratory, University of California (2 November 1956).

9. D. D. King, et al., "Unequally-Spaced, Broad-Band Antenna Arrays," Trans. IRE, PGAP AP-8, No. 4, 380-384 (1960).

10. J. L. Allen, et al., "Phased Array Radar Studies, 1 July 1960 to 1 July 1961," Technical Report No. 236 [U], Lincoln Laboratory, M. I. T. (13 November 1961), Part 3, Ch. III, DDC 271724.

11. _____ and W. P. Delaney, "On the Effect of Mutual Coupling on Unequally Spaced Dipole Arrays," Trans. IRE, PGAP AP-10, 784-785 (1962).

12. _____, et al., "Phased Array Radar Studies, 1 July 1961 to 1 December 1962," Technical Report No. 299 [U], Lincoln Laboratory, M. I. T. (20 February 1963), DDC

13. A. Ksienski, "Equivalence Between Continuous and Discrete Arrays," Scientific Report 3508/7, Hughes Research Laboratory, Hughes Aircraft Company, Malibu, Calif. (15 April 1960); also Canadian J. Phys. 39, 335-349 (1961).

14. J. L. Allen, et al., "Phased Array Radar Studies, 1 July 1959 to 1 July 1960," Technical Report No. 228 [U], Lincoln Laboratory, M. I. T. (12 August 1960), pp. 162-170, DDC 249470, H-335.

15. H. E. King, "Directivity of a Broadside Array of Isotropic Radiators," Trans. IRE, PGAP AP-7, No. 2, 197-201 (1959).

16. L. Brand, Advanced Calculus (Wiley, New York, 1955), p. 535.

17. T. T. Taylor, "Design of Line-Source Antennas for Narrow Beamwidth and Low Sidelobes," Trans. IRE, PGAP AP-3, 16-28 (1955).

18. _____, "One Parameter Family of Line Sources Producing Modified sin $\pi u/\pi u$ Patterns," Technical Memorandum 324, Microwave Laboratory, Hughes Aircraft Company, Culver City, Calif. (4 September 1953).

19. C. L. Dolph, "A Current Distribution for Broadside Arrays Which Optimizes the Relationship Between Beamwidth and Sidelobe Level," Proc. IRE 34, 335-348 (1946).

20. L. B. Brown and G. A. Scharp, "Tchebycheff Antenna Distribution, Beamwidth and Gain Tables," NAVORD Report 4629 (NOLC Report 383), Naval Ordnance Laboratory, Corona, Calif. (1958).

21. L. L. Bailin, et al., "Empirical Approximations to the Current Values for Large Dolph-Tchebycheff Arrays," Technical Memorandum 328, Hughes Aircraft Company, Culver City, Calif. (6 October 1953).

22. T. T. Taylor, "Dolph Arrays of Many Elements," Technical Memorandum 320, Hughes Aircraft Company, Culver City, Calif. (18 August 1953).

23. R. C. Hansen, "Gain Limitations of Large Antennas," Trans. IRE, PGAP AP-8, No. 5, 490-495 (1960).

24. R. E. Willey, "Space Tapering of Linear and Planar Arrays," Trans. IRE, PGAP AP-10, No. 4, 369-377 (1962).

25. J. Ruze, "Physical Limitations on Antennas," Technical Report 248, Research Laboratory of Electronics, M.I.T. (30 October 1952); also "The Effect of Aperture Errors on the Antenna Radiation Pattern," Nuovo Cimento (Suppl.) 9, No. 3, 364-380 (1952).

26. I. Wolff, "Determination of the Radiating System Which Will Produce a Specified Directional Characteristic," Proc. IRE 25, 630-643 (1937).

27. P. M. Woodward, "A Method of Calculating the Field Over a Plane Aperture Required to Produce a Given Polar Diagram," J. IEE 93, Part IIIA, 1554 (1947).

28. A. S. Dunbar, "On the Theory of Beam Shaping," J. Appl. Phys. 23, 847-853 (1952).

29. H. E. Shanks, "A Geometrical Optics Method of Pattern Synthesis for Linear Arrays," Trans. IRE, PGAP AP-8, 485-490 (1960).

30. A. Ksienski, "Maximally Flat and Quasi-Smooth Sector Beams," Trans. IRE, PGAP AP-8, 476-484 (1960).

31. D. R. Rhodes, Introduction to Monopulse (McGraw-Hill, New York, 1959).

32. O. R. Price and R. F. Hyneman, "Distribution Functions for Monopulse Antenna Difference Patterns," Trans. IRE, PGAP AP-8, 567-577 (1960).

33. R. W. Bickmore, "A Note on the Effective Aperture of Electronically Scanned Arrays," Trans. IRE, PGAP AP-6, 194-196 (1958).

34. W. H. Von Aulock, "Properties of Phased Arrays," Proc. IRE 48, No. 10, 1715-1727 (1960).

35. E. D. Sharp, "A Triangular Arrangement of Planar-Array Elements That Reduces the Number Needed," Trans. IRE, PGAP AP-9, 126-129 (1961).

36. J. S. Honda and E. D. Sharp, "Investigation of Methods of Scanning the Beam of Large Antennas," Scientific Report 8, Stanford Research Institute (June 1959).

37. E. Jahnke and F. Emde, Tables of Functions (reprinted by Dover Publications, New York, 1943).

38. T. T. Taylor, "Design of Circular Apertures for Narrow Beamwidth and Low Sidelobes," Technical Memorandum 372, Hughes Aircraft Company, Culver City, Calif. (30 August 1954); also Trans. IRE, PGAP AP-8, No. 1, 17-23 (1960).

39. R. C. Hansen, "Tables of Taylor Distributions for Circular Aperture Antennas," Technical Memorandum 587, Hughes Aircraft Company, Culver City, Calif. (1959); also Trans. IRE, PGAP AP-8, No. 1, 23-27 (1960).

40. J. E. Walsh, "Radiation Patterns of Arrays on a Reflecting Cylinder," Proc. IRE 39, 1074-1081 (1951).

41. J. R. Wait and J. Housholder, "Pattern Synthesis for Slotted-Cylinder Antennas," J. Research 63D, No. 3, 303-313 (1959).

42. R. H. DuHamel, "Pattern Synthesis for Antenna Arrays on Circular, Elliptical and Spherical Surfaces," Electrical Engineering Laboratory, University of Illinois (1952).

43. E.H. Braun, "Radiation Characteristics of the Luneberg Lens," Trans. IRE, PGAP AP-4, 132-138 (1956).

44. A.O. Richardson, "Direction-Finding Antennas," Chapter 28 of Antenna Engineering Handbook, H. Jasik, Editor (McGraw-Hill, New York, 1961).

45. C.P. Clasen, et al., "A Radial-Waveguide Antenna and Multiple Amplifier System for Electronic Scanning," RCA Review 22, 541-554 (1961).

46. L.J. Ricardi, "Pattern Analysis of a Circular Array of Isotropic Radiators," G-Report 36-8 [U], Lincoln Laboratory, M.I.T. (15 June 1958), not generally available.

47. R.H. DuHamel and I.R. Ore, "Logarithmically Periodic Antenna Designs," Technical Report 198, Collins Radio Company (1958). Also IRE International Convention Record, Vol. 6, Part 1, 139-151 (1958).

48. J.D. Dyson, "The Conical Log-Spiral Antenna in Simple Arrays," Abstract of the Eleventh Annual Symposium on USAF Antenna Research and Development Program, University of Illinois (16-20 October 1961).

49. G.E. Mueller and W.A. Tyrrell, "Fixed Beam Antennas," Bell System Tech. J. 26, 837-851 (1947).

50. L.L. Parad and R.W. Ercolani, "Mutual Effects Between Circularly Polarized Elements," Antenna Arrays Section of the Abstracts of the Eleventh Annual Symposium on USAF Antenna Research and Development Program, University of Illinois (16-19 October 1962).

51. S.J. Rabinowitz, "The Conductance of a Slot in an Array Antenna," Technical Report No. 192 [U], Lincoln Laboratory, M.I.T. (31 December 1958), DDC 209908.

52. B.M. Oliver, "Directional Electromagnetic Couplers," Proc. IRE 42, 1686-1692 (1954).

53. W.E. Rupp, "Coupled Energy as a Controlling Factor in the Radiation Patterns of Broadside Arrays," Abstract of the Eleventh Annual Symposium on USAF Antenna Research and Development Program, University of Illinois (16-20 October 1961).

54. J.L. Allen, "Gain and Impedance Variation in Scanned Dipole Arrays," Trans. IRE, PGAP AP-10, 566-572 (1962).

55. S. Edelberg and A.A. Oliner, "Mutual Coupling Effects in Large Antenna Arrays II: Compensation Effects," Trans. IRE, PGAP AP-8, 360-367 (1960).

56. L. Stark, "Radiation Impedance of a Dipole in an Infinite Array," Formal Technical Document, Hughes Aircraft Company, Culver City, Calif. (1 May 1960).

57. H.A. Wheeler, "The Radiation Resistance of an Antenna in an Infinite Array or Waveguide," Proc. IRE 36, No. 4, 478-487 (1948).

58. F.W. Hannan, "The Element-Gain Paradox for a Phased Array Antenna," Report 1161, Wheeler Laboratories, Great Neck, N.Y. (25 June 1963).

59. R.S. Elliott, "Mechanical and Electrical Tolerances for Two-Dimensional Scanning Antenna Arrays," Trans. IRE, PGAP AP-7, 114-120 (1958).

60. L.A. Rondinelli, "Effects of Random Errors on the Performance of Antenna Arrays of Many Elements," IRE National Convention Record, Part 1, 174-189 (1959).

61. M. Peckham, "Beam Pointing Errors of Long-Line Sources," Trans. IRE, PGAP AP-5, No. 3, 268-270 (1957).

62. H.H. Gerrish, "Noise Computations in Array Antenna Receiving Systems," Microwave J. 5, 69-74 (1962).

63. L.A. Kurtz and R.N. Lodge, Jr., "Systematic Errors Caused by the Scanning of Antenna Arrays - Phase Shifters in the Branch Lines," Technical Memorandum 359, Hughes Aircraft Company, Culver City, Calif. (1 May 1953).

64. E. J. Wilkinson, "An N-way Hybrid Power Divider," Trans. IRE, PGMTT MTT-8, No. 1, 116-118 (1960).

65. W. Rotman, "Wide Angle Scanning with Microwave Double-Layer Pillboxes," Trans. IRE, PGAP AP-6, No. 1, 96-106 (1958).

66. J. Blass, "The Multi-Directional Antenna: A New Approach to Stacked Beams," IRE Convention Proceedings, Vol. 8, Part 1, 48-51 (1960).

67. J. Butler and R. Lowe, "Beam Forming Matrix Simplifies Design of Electronically Scanned Antennas," Electronic Design 9, No. 7, 170-173 (12 April 1961).

68. J. P. Shelton and K. S. Kelleher, "Multiple Beams from Linear Arrays," Trans. IRE, PGAP AP-9, 154-161 (1961).

69. J. L. Allen, "A Theoretical Limitation on the Formation of Multiple Beams in Linear Arrays," Trans. IRE, PGAP AP-9, 350-352 (1961).

70. P. M. Woodward and J. D. Lawson, "The Theoretical Precision with Which an Arbitrary Radiation Pattern May Be Obtained with a Source of Finite Size," J. AIEE 95, Part III, 362-370 (1948).

71. W. P. Delaney, "An RF Multiple Beam Forming Technique," G-Report 41G-0012 [U], Lincoln Laboratory, M.I.T. (9 August 1961), DDC 262017, II-334.

72. W. D. White, "Pattern Limitations in Multiple-Beam Antennas," Trans. IRE, PGAP AP-10, No. 4, 430-436 (1962).

73. S. B. Myers, "Parallel Plate Optics for Rapid Scanning," J. Appl. Phys. 18, 221-229 (1947).

ADDITIONAL REFERENCES

S. Edelberg and A. A. Oliner, "Mutual Coupling Effects in Large Antenna Arrays: Part I – Slot Arrays," Trans. IRE, PGAP AP-8, No. 3, 286-298 (1960).

J. N. Hines, et al., "On the Design of Arrays," Proc. IRE 42, 1262-1267 (1954).

R. Manasse, "Maximum Angular Accuracy of Tracking a Radio Star by Lobe Comparison," Trans. IRE, PGAP AP-8, No. 3, 306-308 (1960).

A. R. Stratoti and E. J. Wilkinson, "An Investigation of the Complex Mutual Impedance Between Short Helical Array Elements," Trans. IRE, PGAP AP-7, 279-280 (1959).